Variable-Impedance-Based Human-Machine Control for Docking of Manufacturing Fixtures

Walter A. Piaskowy

A thesis submitted
in partial fulfillment of the
requirements for the degree of

Master's of Science in Mechanical Engineering

University of Washington

2016

Reading Committee:

Joseph Garbini, Co-Chair

Santosh Devasia, Co-Chair

James Buttrick

Program Authorized to Offer Degree:
Mechanical Engineering

University of Washington

Abstract

Variable-Impedance-Based Human-Machine Control
for Docking of Manufacturing Fixtures

Walter A. Piaskowy

Co-Chairs of the Supervisory Committee:
Professor Joseph Garbini
Mechanical Engineering

Professor Santosh Devasia
Mechanical Engineering

Assembly fixtures that are much smaller than the structure being manufactured, such as an aircraft, must routinely be positioned and docked against the structure on which they act. Here, docking implies physical contact between the fixture and the structure. The major contribution of this thesis is to develop a variable-impedance-based human-machine control for the docking process. The major issues investigated are: (i) impedance control to facilitate intuitive human force input; (ii) utilizing variable damping to aid docking and safeguard both the fixture and structure; and (iii) apply a dock force while preserving human control for undocking. A single-degree-of-freedom experimental test bed is used to simulate docking using the proposed controller, and to explore how controller parameter choices impact overall performance.

TABLE OF CONTENTS

LIST OF FIGURES

ACKNOWLEDGMENTS

This work was made possible by the support of Boeing Research and Technology (BR&T) and The Boeing Advanced Research Center (BARC) at the University of Washington in Seattle, WA. Special thanks to James Buttrick, a Boeing Technical Fellow, for his engineering insights and ability to forge academic opportunities in industry, as well as Professor Joseph Garbini and Professor Santosh Devasia for their generous patience and invaluable guidance throughout the project.

DEDICATION

I dedicate this work to my parents, Walter and Margarita, and sister, Lisa, for their continued support of my academic career, and always reminding me not to lose sight of what is important. I could not have done it without them.

Chapter 1

INTRODUCTION

This thesis investigates docking control of an automated mobile assembly fixture against a rigid structure for aerospace manufacturing. In this manufacturing environment, relatively small fixtures perform processes in a variety of locations on a large structure, and often many agents traverse a large structure simultaneously. In order to complete the work each fixture must frequently approach and dock with the structure, avoiding any obstacles or other agents in the work space — commonly inhabited at different times by mechanics, tools, carts, and parts. Hence the implementation of a fully automated docking system can be challenging due to the required complex programming, scheduling of numerous unique processes, and additional sensors to survey the work space for unforeseen obstacles. Alternatively, incorporating a human operator brings to bear decades of experience in performing complex manipulation and path planning, multifaceted task execution, and incorporating rich sensory feedback. This is a resource currently used in this manufacturing environment, however, as task complexity grows, so do the fixtures, and frequently relocating a large heavy fixture can be too taxing on human strength alone.

This thesis proposes a variable-impedance-based human-machine control scheme to enable the capabilities of the human operator for intuitive manipulation and docking, regardless of fixture dynamics. This approach provides the operator control over a desired system impedance, namely mass and damping, rather than the actual impedance using servo motor generated force input [10]. Additionally, as the fixture comes close to an obstacle or the structure, short-range distance measurements are used to vary impedance parameters to mitigate impact and complete docking with applied dock force [8].

1.1 Interaction Control

Interactions between an automated fixture and its environment, like docking, are growing in importance as manufacturing automation becomes more ubiquitous, bringing humans and automated fixtures into the same work space. Position sensing and control alone often fail to adequately meet these new demands of industry, where automated fixtures now operate in a much more uncertain environment due to potentially unpredictable human actions when sharing the same work space. Active global mapping of all agent locations within a work space would be required to integrate these new uncertainties. Dealing with these uncertainties, while ensuring human safety, is a major challenge for such increasingly autonomous manufacturing systems.

There are several control approaches for dealing with unexpected interactions. Modal or State Machine based controllers make use of predefined logic applied to various sensor data to switch fixture behavior mid-process to different operating modes depending on the specific interaction [5]. Hybrid position/force control blends both position and force commands to control fixture position and force applied to its environment, eliminating excess applied forces during motion and thereby ensures safety of humans sharing the work space [14, 15, 17, 18]. Impedance control customizes the system response from external forces by manipulating its natural impedance, achieving safe human-fixture interactions in the work space [1–3, 6, 9, 12].

1.2 Docking Control Selection

For the application in this thesis neither fixture nor rigid structure localization information are available to the controller. Therefore, the proposed approach will use human observations of the fixture's position and work space environment to provide position feedback for control. For expedited positioning, in lieu of a jog pendant (that achieves a commanded change in position), this thesis proposes that the operator interacts with the fixture like any accustomed hand tool—directing motion by apply forces with their hands. Therefore, the selected controller does not attempt to command a position, but rather appear to directly control the

fixture motion based on interaction forces. However, the fixture can be heavy and difficult to move by human generated forces alone. Therefore, impedance control, e.g. [13], [4], is proposed to augment the human force and thereby modify the operator perceived mass and damping of the fixture.

Impedance control has been applied in this capacity for applications such as medical rehabilitation and spacecraft docking. To modify the impedance of these systems, actuators produce additional forces to alter the dynamics of the system. In the rehabilitation application, using a highly accurate model of the mechanical system and user force input, the controller commands torques to the actuators to amplify operator forces and effectively modify system impedance. This method unfortunately includes inherent difficulties of system identification and model accuracy [13]. In the spacecraft application, the response of an ideal system is calculated for human force input to determine desired velocities of each degree of freedom [4]. This controller uses force inputs and a reference model in conjunction with a classic controller closing a velocity loop, such as proportional-integral (PI), in order to prescribe dynamics of the reference model to the actual plant [11] This removes the high accuracy constraint of the previous method, but relies on sufficient controller-plant bandwidth in order to keep up with the reference model. In both applications the position of the mechanism was not considered for the controller, position was governed by the human in the loop. More importantly, these controllers were designed to accept interaction forces and delivering the set impedance behavior or velocities of the desired system.

A challenge of using a force input controller for docking against a rigid structure is the potential for contact instabilities (such as repeated rebounding against the structure) arising forces applied to the fixture by the docking counterpart. Often this is solved via compliant surfaces or compliant fixtures [9]. The use of series elastic actuators have been successful in reducing impact loads via a compliant intermediary (such as an elastomer) between the actuator and the controlled device, but sacrifices joint stiffness [7]. In the proposed method, the contact instability is mitigated by altering the desired impedance parameters when close to docking. In particular, the damping is increased as the sensors on the fixtures detect the

rigid structure, to slow the contact velocity and avoid the instability.

To further guarantee docking between the fixture and structure, a dock force will be maintained via the fixture force sensor once contact is made. This dock force will allow the fixture's controller to reject any minor disturbances that will act to separate the two objects. It is important that the dock force be great enough to adequately reject erroneous inputs, but small enough to allow human intervention when fixture manipulation and undocking are desired.

Chapter 2

APPLICATION

In the aerospace application being considered, a beam-like fixture, mounted on a mobile platform, is to be positioned against a rigid structure. Fig. 2.1 illustrates the fixture, which is 0.5 m wide and supported roughly 1 m off the floor by the mobile platform, and the rigid structure, approximately 0.3 m tall, 15 m long, and 3 m wide, similarly supported 1 m off the ground. Controller inputs are generated by human hand applying forces, F_h, directly onto the fixture. Once the fixture is docked a dock force, F_d, must be generated against the structure to secure its position, which the operator must be able to overcome for undocking.

To simulate the application, a single degree of freedom test bed was developed to evaluate controller concepts. Fig. 2.2 & 2.3 show the test bed consisting of: a mobile base driven by a servo motor on a rack and pinion and guided by a linear rail, aligned to a hard stop simulating the rigid structure, and a force input device with a beam-like fixture, housing a limited range optical distance sensor to measure fixture-structure proximity, $\tilde{x}(t)$, between the fixture and the rigid structure. Where F_h and F_m are operator and motor forces applied, M is the lumped mass of the plant, B is the lumped damping of the plant, and $x(t)$ is the position of the fixture relative to the hard stop (rigid structure). [1]

[1] See Appendix A

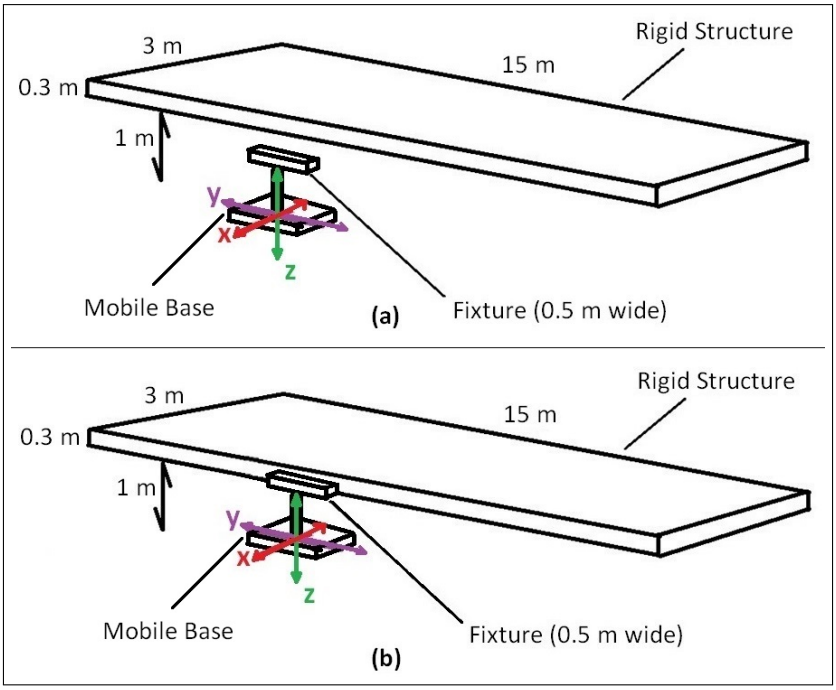

Figure 2.1: Illustration of the application analyzed in this thesis. The fixture is approximately 0.5 m wide and supported roughly 1 m above the ground by a mobile platform. The structure is approximately 0.3 m tall by 15 m long and 3 m wide held 1 m off the ground.(a) Rigid structure and fixture in arbitrary starting locations. (b) Fixture docked against the rigid structure.

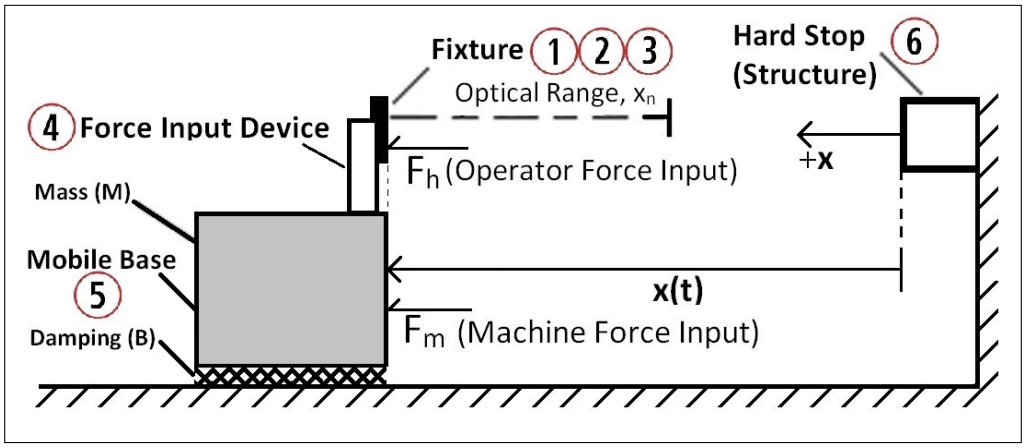

Figure 2.2: One dimensional impedance control test bench setup. Where M is lumped mass, B is lumped damping, and F_h and F_m are operator and machine force inputs, respectively. A fixture ① that houses two optical sensors ② and contact bumpers ③, is mounted onto a force input device ④ which is attached to a mobile base ⑤ supported by a linear guide rail, and driven by a motor on a rack and pinion. The optical distance sensors have limited range, $x_n \approx 0.030m$. The fixture and optical sensors are aligned to a hard stop ⑥ to simulate fixture-structure interaction and measured proximity, $\tilde{x}(t)$, when $x(t) \leq x_n$.

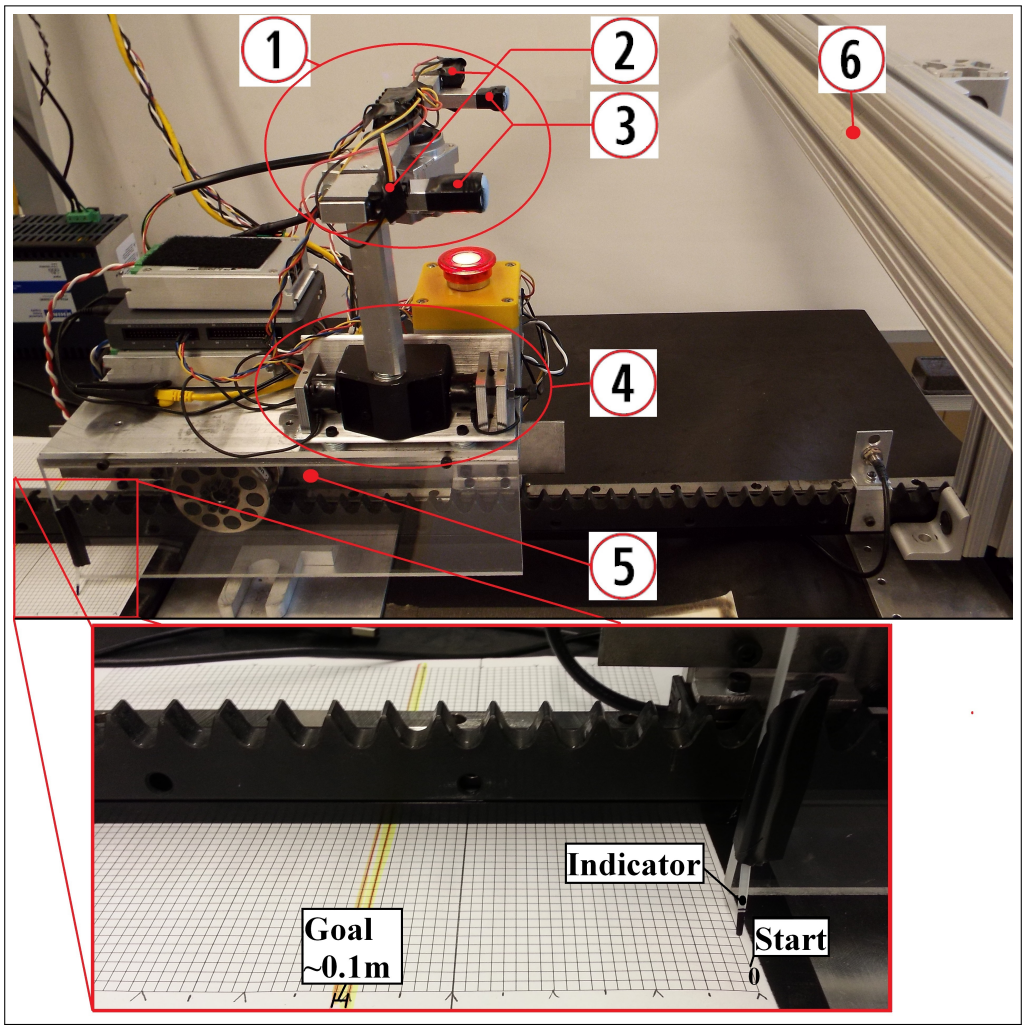

Figure 2.3: *Top*: Laboratory Test Bed, build from the design shown in Fig. 2.2. ① Fixture - Emulating the tool, ② Optical Sensors - Two optical sensors' data are blended in order to improve accuracy, ③ Stiff Bumpers - To ensure contact points with the hard stop, ④ Force Input Device - Handle-mount assembly supported by a short linear rail guiding contact with two strain-type force sensors preloaded to give a differential yielding an accurate force input, ⑤ Mobile Base - Aluminum angle mounted to a linear rail with rack and pinion drive, housing drives and other electronics, ⑥ Hard Stop - Stiff Structure built from 80/20 to simulate a rigid body. *Bottom*: The lower left hand corner of the base was used to test positional accuracy; see section 5.1.

Chapter 3

CONTROL APPROACH

The proposed control approach uses impedance control to tailor fixture interactions, and measured structure proximity to vary the desired impedance parameters thereby achieving safe and controlled contact. The operation can be characterized as having two regimes: (i) a far-regime, where impedance control is used to enable rapid manipulation of the fixture using human force input, and (ii) a near-regime, where fixture-to-structure distance sensing is available — i.e., beginning at the optical sensors' maximum range, $x_n \approx 0.030m$ — and variable damping is used to enable low-impact docking and to avoid contact instabilities . Fig. 3.1 illustrates these regimes defined by distance from the fixture, x.

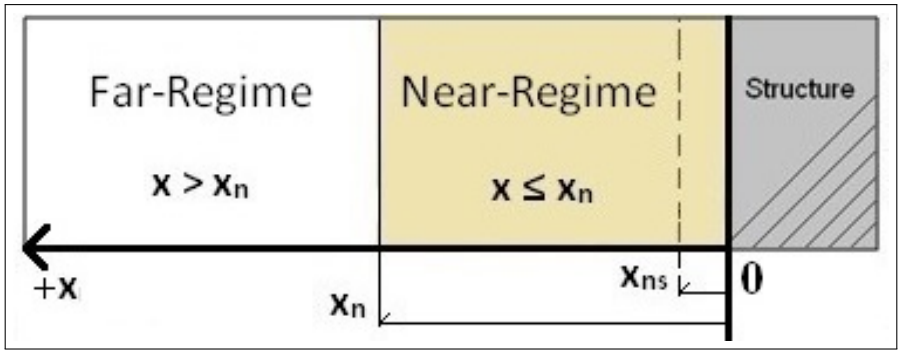

Figure 3.1: Operating regimes defined as a function of distance from structure, x. At or below x_n, the optical sensors become reliable and fixture-structure proximity, $\tilde{x}(t)$, acts on system damping. This defines the near-regime. Within the near-regime, a saturation damping occurs when the measured distance $\tilde{x}(t)$ is below x_{ns}.

3.1 Far-Regime

Due to the unknown starting position of the fixture relative to the structure, the proposed solution utilizes feedback control via the human operator to achieve the required accuracy. This may be difficult for the human if the mass or damping of the system are too high. Applying impedance control to the system allows the user to set and adjust an apparent mass and damping of a system to tailor the resulting motions from their force input. The intention will be to manipulate the fixture with natural forces produced by a human, akin to manipulating a shop cart—pushing or pulling to position the device.

3.2 Near-Regime

As the fixture approaches the structure sensors become reliable and can measure the fixture-structure proximity, $\tilde{x}(t)$. In this near-regime, the controller varies the impedance and dock force to achieve controlled docking. Specifically, damping is increased as a function of fixture-structure proximity, $\tilde{x}(t)$. This is done in order to prevent the human from commanding high fixture velocity when making contact with the rigid structure, thereby attenuating impact forces and potential contact damage. Similarly, dock force, F_d, is also increased as a function of fixture-structure proximity, $\tilde{x}(t)$, in order to only apply the dock force close to the structure.

3.3 Impedance Control

Fig. 3.2 shows the control block diagram of the proposed impedance controller. In this approach, desired velocity, $v_d(t)$, is calculated using filtered measurement of operator input force, $\hat{F}_h(t)$, summed with the dock force, F_d, to yield input force, F_i, which is used to solve the differential equation describing the desired system dynamics

$$\hat{F}_h(t) + F_d(\tilde{x}(t)) = F_i(t) = M_d\dot{v}_d(t) + B_d v_d(t), \tag{3.1}$$

where M_d is the desired mass, B_d is the desired damping, and $v_d(t)$ is the desired velocity,

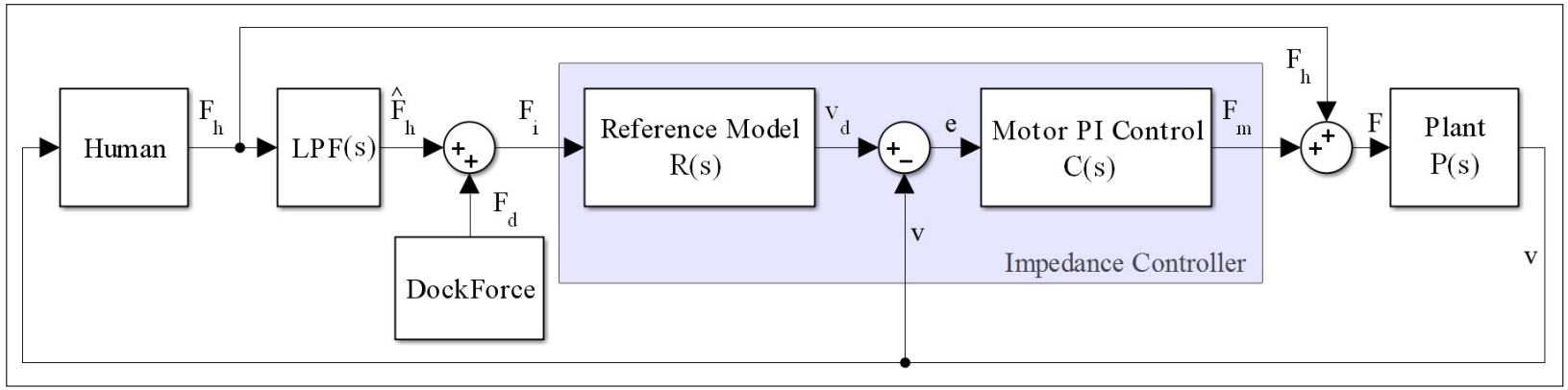

Figure 3.2: Block diagram of impedance controller creating the desired plant dynamics from human force input, F_h, using a reference model with custom set mass, M_d, and damping, B_d, parameters. The human force input, F_h, is put through a low pass filter (LPF), the filtered human force input, $\hat{F}_h$, is then added to dock force, F_d, to yield force input, F_i, that drives the reference model. This model estimates ideal system dynamics and outputs desired velocity, v_d, commands to the motor controller. The motor's proportional-integral (PI) controller then works on the error, e, between desired velocity, v_d, and actual plant velocity, v, in order to produce motor force, F_m. By the design of the application the human force input, F_h, is also applied directly on the fixture/plant. This will be treated as a disturbance force attempting to disrupt the reference tracking of the motor's PI loop.

defined as $v_d(t) = \dot{x}(t) = \frac{dx(t)}{dt}$. The calculated desired velocity, $v_d(t)$, is then passed to the motor's controller as a velocity command. At this point the impedance control relies on the motor's encoder feedback and proportional-integral (PI) controller in order to keep the plant velocity, $v(t)$, close to the desired velocity, $v_d(t)$. [1]

The desired mass M_d and the desired damping B_d affect the apparent response of the fixture to the input force F_i. For example, in the far-regime, with a fixed desired damping, B_d, constant force input, F_i, and no dock force, $F_d = 0$, the transient solution of the the fixture dynamics (1) is

$$v_d(t) = \frac{F_i}{B_d}\left(1 - e^{-t/\tau}\right) \tag{3.2}$$

where $\tau = M_d/B_d$ is the time constant, and the steady state solution is

$$v_d(t \to \infty) = \frac{F_i}{B_d}. \tag{3.3}$$

This shows that the maximum velocity is governed by F_i/B_d, and the acceleration by the time constant $\tau = M_d/B_d$.

The combined system behavior will only approach the desired velocity, v_d, generated by (3.1), if the motor's controller has sufficient bandwidth to achieve. For the test bed, the motor's proportional-integral (PI) controller, C(s), was tuned with proprietary Elmo software for a velocity feedback loop. Fig. 3.3 shows the resulting response for the motor-plant dynamic. For adequate control, the input for the motor-plant loop should be at least a decade lower than its bandwidth frequency of 1393 rad/s, e.g. input bandwidth should be equal to or less than 139 rad/s. Shown in Fig. 3.2, desired velocity, v_d, is the motor-plant loop input, which is produced by the output our reference mass-damper model. Therefore the response of our reference model must have a maximum bandwidth that preserves control authority. The Laplace transformation of (3.1) is used to yield the reference model's transfer function, $R(s)$, below,

---

[1] See Appendix B

$$R(s) = \frac{V(s)}{F_i(s)} = \frac{1/B_d}{\tau s + 1} \tag{3.4}$$

where s is a complex frequency, τ is the time constant, and B_d is the desired damping. Furthermore, this mass-damper system will have a bandwidth frequency, ω_{bw}, defined by

$$\omega_{bw} = 1/\tau = B_d/M_d, \tag{3.5}$$

in rad/s, where τ is the time constant, B_d is the desired damping, and M_d is the desired mass.

Fig. 3.3 demonstrates the time constant, τ, to bandwidth relationship in (3.5). Although this can preserve controllable bandwidth for the reference system, it is not guaranteed. Values for desired mass, M_d, and desired damping, B_d, are investigated in section 4 in regards to the control constraint from our motor-plant loop.

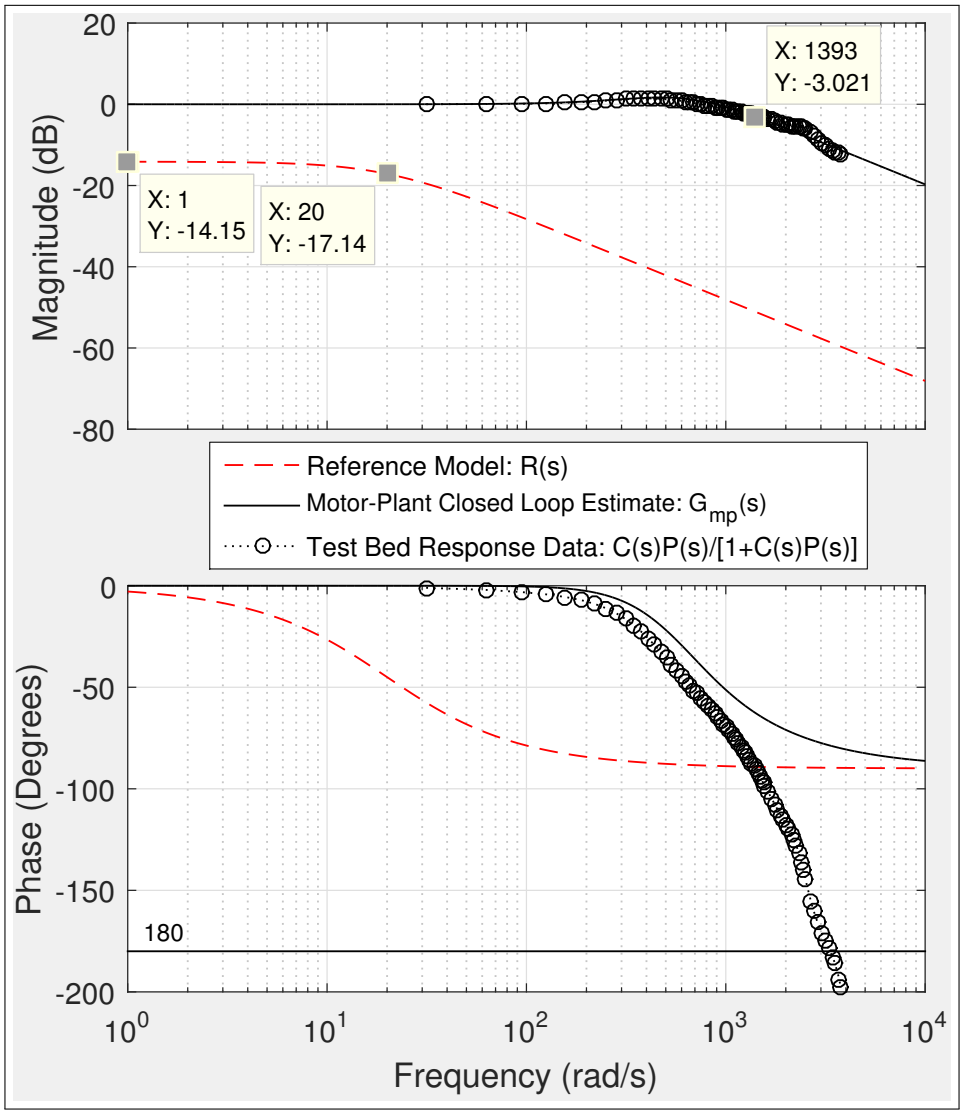

Figure 3.3: Bode plot showcasing the responses of: Reference Model, $R(s)$, Motor-Plant Closed Loop Estimate, $\approx C(s)P(s)/[1 + C(s)P(s)]$, Test Bed Closed Loop Response: $C(s)P(s)/[1 + C(s)P(s)]$, and Motor-Plant Sensitivity to Disturbances: $1/[1 + C(s)P(s)]$. Note the reference model is using a desired mass, M_d, of 10 kg, and desired damping, B_d, of 200 N-s/m, therefore the bandwidth frequency, ω_{bw}, is observed at 20 rad/s; well below the motor-plant bandwidth of 1393 rad/s. The test bed data was obtained using Elmo software for system identification, and a transfer function estimate was formulated using the motor tuning parameters and measured test bed mass and damping.

3.4 Variable Damping and Dock Force

Recall that the fixture is driven to the desired position by a mobile base, which is commanded by any force applied to the fixture. Ideally this would be purely human force input, F_h, however extraneous force inputs need to be accounted for. In this application, the fixture-structure interaction is an expected, but unspecified, source of force inputs. Our method to minimize contact force interference with the desired docking behavior is to vary the reference model impedance when nearing contact in order to limit base velocity and create an greater insensitivity to high frequency inputs, like contact forces.

Fig. 3.4 illustrates the mobile base overshooting the fixture-structure contact position due to a high incoming velocity. The fixture yields with some stiffness, k, storing energy and resulting in a reaction force, F_r, between the fixture and the structure. Assuming the structure and base are rigid, any overshoot will produce a net force away from structure as the reaction force, F_r, which can be defined as

$$F_r = F_h + k \cdot d_{os}, \tag{3.6}$$

a sum of human force input, F_h, and the energy stored via fixture stiffness, k, and base overshoot distance, d_{os}, assuming no dock force, F_d. Since the reaction force, F_r, is opposite in direction as human force input, F_h, the net force input, F_i, to the reference model will be only from energy stored in the fixture stiffness, $(k \cdot d_{os})$. The result is a command for base velocity away from the structure. As the base moves away from the structure the overshoot is corrected, however if the system is under-damped the reaction force, F_r, will cause the base to overshoot the fixture-structure contact position. When the fixture leaves the structure surface, the reaction force, F_r, becomes zero, and the human force input, F_h, is again the governing input for the reference model and can command the base towards the structure and the overshoot cycle can begin once again.

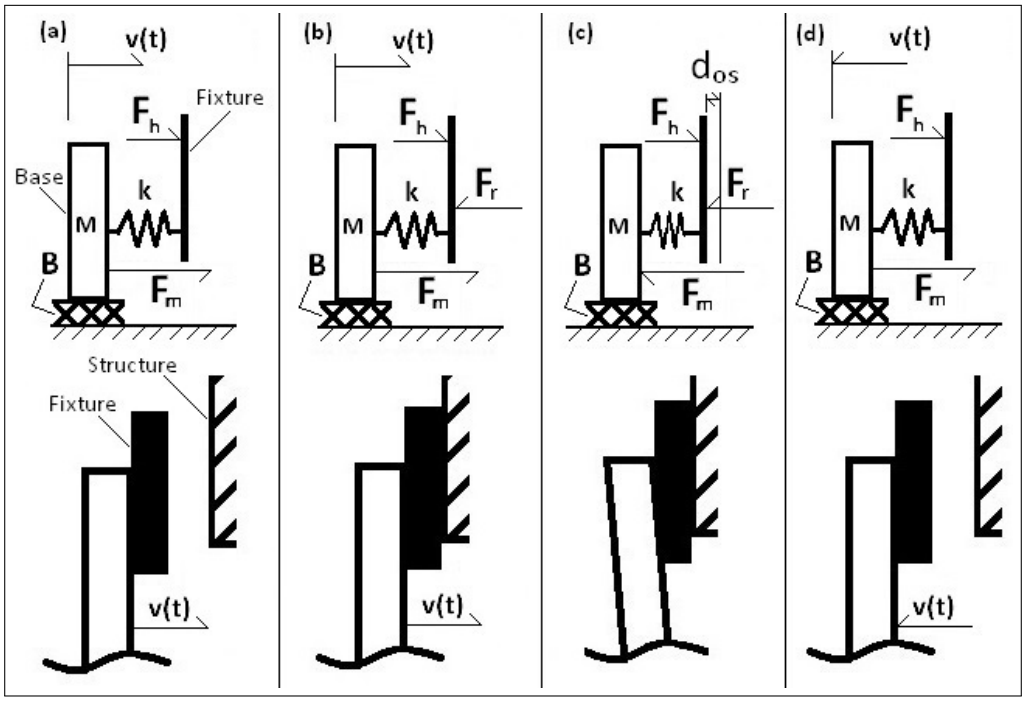

Figure 3.4: Diagram of dock rebound due to the reaction force from the structure once the fixture makes contact. Assuming the fixture is a massless device, with a constant human operator force, F_h, applied to it, no dock force, $F_d = 0$, and is attached to a base by some stiffness, k. The fixture's base has mass, M, damping, B, and motor force, $F_m(t)$, applied to it. **(a)** Before contact: the fixture of mass, M, is traveling at steady state velocity $v(t) = \hat{F}_h/B_d$. **(b)** Contact: The fixture makes contact with structure, deflecting the fixture, and generating a reaction force, F_r, canceling human force input, F_h, and commanding an opposing acceleration from the reference model causing the motor to decelerate the fixture mass, M. **(c)** Docked: The mass, M, is at zero velocity and the fixture is in contact with the structure, however energy may have been stored in the fixture stiffness, k, due to the mobile base overshooting the fixture-structure contact position by some distance, d_{os}, resulting in a residual force, F_r. **(d)** Rebound: when in fixture-structure contact the reaction force, F_r, will be greater than or equal to human force input, F_h, and commands a velocity away from the structure. Once separated from the structure, the reaction force, F_r, becomes zero and the human force input, F_h, once again commands the base towards the structure.

To manage the velocity and response of the fixture near docking, variable damping is used in the near-regime to slow the base velocity and deliver an over damped system. A dock force, F_d, can also be applied to allow for some residual reaction force, F_r, and producing a threshold for force inputs in order to achieve fixture-structure separation. Together these successfully achieving a proper docking routine — swift far regime manipulation, avoid base overshoot, mitigating reaction forces' effects, and preserving dock contact.

For ideal docking, the mobile base would reach zero velocity as the fixture comes into contact with the structure—eliminating spikes in reaction force, F_r. The proposed controller increases damping as a function of distance from the structure to minimize velocities near contact (the near-regime). Conversely, when chance of contact is low, (the far-regime) swift manipulation is desired and therefore flexibility in producing a low damped system is necessary. A desired transition is a smooth, intuitive, and highly customizable function for the operator and process requirements. To facilitate these needs, a logistic function—developed to capture population growth in nature [16]—was used in (3.7) in an attempt to create a highly customizable "natural" growth from the desired damping, B_d, to maximum machine damping, $(B_m)_{max}$.

The machine damping, B_m, design was broken down into three regions when approaching the structure: (1) constant desired damping, B_d; (2) transition to maximum machine damping, $(B_m)_{max}$; and (3) constant machine damping, B_m, near contact. The proposed controller integrates this variable damping by replacing the desired damping, B_d, with variable machine damping, $B_m(\tilde{x}(t))$, defined as,

$$B_m(\tilde{x}) = \begin{cases} B_d, & \tilde{x} \geq x_n \\ \left(\dfrac{2\left[(B_m)_{max} - B_d\right]}{1 + e^{[\tilde{x} - x_{ns}]/r_B}} \right) + B_d, & x_{ns} \leq \tilde{x} < x_n \\ (B_m)_{max}, & \tilde{x} < x_{ns}, \end{cases} \tag{3.7}$$

where $B_m(\tilde{x}(t))$ is machine damping, $(B_m)_{max}$ is maximum machine dampening, B_d is desired damping, r_B is the machine damping distance constant, $\tilde{x}$ is the measured distance between

the fixture and structure, x_n is the near-regime transition point, and x_{ns} is the near-regime saturation point. The shape of the machine damping, B_m, curve is illustrated in Fig. 3.5.

To be sure sure that the damping transition adequately occurs within a prescribed range away from the saturation point of the near-regime, x_{ns}, the machine damping distance constant, r_B, is used. Fig. 3.5 shows that at 7 distance constants, r_B from saturated machine damping or maximum, $(B_d)_{max}$, we will achieve 99.8% of our transition to desired damping, B_d. Note that this is not 100%, and therefore will produce a small discontinuity at the near-far regime transition distance, x_n. As long as there are at least 7 distance constants within the transition zone this discontinuity is kept small, $\leq 0.2\%$ of the maximum machine damping, $(B_d)_{max}$, attenuating it's impact when switching to constant desired damping, B_d.

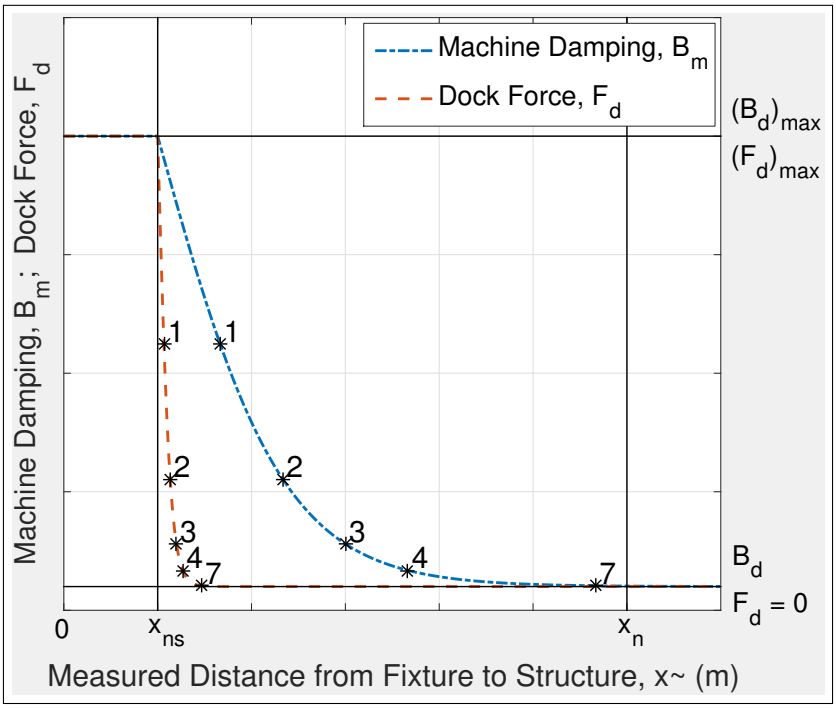

Figure 3.5: An illustration of the machine damping, B_m, and dock force, F_d. Highlighted design parameters: $(B_m)_{max}$, the maximum damping set, B_d, the desired damping set by operator, $(F_d)_{max}$, the maximum dock force, $x_n = 0.030m$, the maximum distance of near-regime, and $x_{ns} = 0.005m$, the damping saturation distance. Not explicitly shown, but used in demonstrating the shape are: machine damping distance constant, $r_B = 0.0033m$, and dock force distance constant, $r_F = 0.00033m$. Points, $*^n$, where $(\tilde{x} - x_{ns}) = nr_B$ or nr_F, n-multiples of the distance constants, r_B or r_F, demonstrate the exponential transition between maximum machine damping, $(B_d)_{max}$, or maximum dock force, $(F_d)_{max}$, and desired damping, B_d, or zero dock force, $F_d = 0$, respectively. When the fixture is n distance constants, r_B or r_F, away from the saturation point, x_{ns}, the transition completion is: 46.2%, 76.2%, 90.5%, 96.4%, and 99.8% at $n = 1, 2, 3, 4,$ & 7, respectively.

Similarly the dock force, F_d, can be prescribed using the same form as machine damping, B_m, defined as the following

$$F_d(\tilde{x}) = \begin{cases} 0, & \tilde{x} \geq x_n \\ \left(\dfrac{2(F_d)_{max}}{1 + e^{[\tilde{x} - x_{ns}]/r_F}} \right), & x_{ns} \leq \tilde{x} < x_n \\ (F_d)_{max}, & \tilde{x} < x_{ns}, \end{cases} \tag{3.8}$$

where $F_d(\tilde{x}(t))$ is the applied dock force, $(F_d)_{max}$ is the maximum dock force, r_F is the dock force distance constant, $\tilde{x}$ is the measured distance between the fixture and structure, x_n is the near-regime transition point, and x_{ns} is the near-regime saturation point. Once again this equation allows for a highly customizable shape that can be molded to meet control and process needs. Dock force, $F_d(\tilde{x}(t))$, is illustrated in Fig. 3.5.

3.5 Feedforward Human Force

Fig. 3.2 shows that the human force input, F_h, is applied to the controller as well as directly onto the plant as a feedforward input. This feedforward force applied to the plant could modify the reference model behavior. However, the feedforward human force input, F_h, passes through the motor with a 100:1 gearbox in the testbed. The mechanical (dis)advantage and losses associated with the gearbox reduces the impact of the feedforward action of the human force input, F_h, on the plant dynamics. Therefore, the effect of the feedforward term is not as significant as the effect of the closed-loop control input F_m, and is neglected in the analysis.

Chapter 4

PARAMETER SELECTION

To tune the performance of the proposed controller, this thesis investigates seven parameters:

ω_c	Low Pass Filter (LPF) Cutoff Frequency
M_d	Desired Mass
B_d	Desired Damping
$(B_m)_{max}$	Maximum Machine Dampening
r_B	Machine Damping Distance Constant
$(F_d)_{max}$	Maximum Dock Force
r_F	Dock Force Distance Constant

4.1 Low Pass Filter Cutoff Frequency, ω_c

Using Fig. 3.3, the upper control limit of our reference model bandwidth is set at 139 rad/s, a decade below the motor-plant bandwidth of 1393 rad/s. Note this upper limit is also the lower limit when setting the LPF cutoff frequency, $omega_c$, for filtering force input, F_h, to avoid setting the filter as the dominant response of the cascaded filter-reference model system. Therefore for our test bench a cutoff frequency, ω_c, of 139 rad/s was used in order to attenuate as much high frequency noise as possible without causing problems in performance. A first order filter was used in this application, as shown below,

$$LPF(s) = \frac{1}{s/\omega_c + 1}. \tag{4.1}$$

4.2 Desired Mass, M_d

From the analysis in section 3, the desired mass, M_d, adjusts system accelerations, more specifically is in the numerator of the reference model's time constant. By increasing this parameter, the time constant is also increased, which means the system will require more time to accelerate, or respond, to force inputs. This can allow for improved stability when the controller is confronted with noisy force inputs, acting as a filter, however this can also lead to a sluggish response, not ideal for the operator in the far-regime. Decreasing this parameter yields a faster reaction, but can lead to jerky behavior with only small force inputs relative to an operator's strength.

Desired mass, M_d, must be selected along with desired damping, B_d, in order to keep the bandwidth below the motor-plant control criteria derived in section 3. For this application the bounds will be placed on the desired damping, B_d, term, and the determined appropriate range for fixture mass is

$$10kg \leq M_d \leq 100kg. \tag{4.2}$$

Note that this mass, while seemingly heavier than conventional hand-operated tools, is neutrally balanced by neglecting the force due to gravity in the reference model input.

4.3 Desired Damping, B_d

From the analysis of (3.1), the desired damping, B_d, will effect accelerations and steady state velocity. Desired damping, B_d, is in the denominator of the time constant, which means by increasing this parameter, or reducing the time constant, the system responds more quickly to inputs, but sets a lower limit to steady state velocity or slow manipulation speeds. Decreasing this parameter, or increasing the time constant, reduces resistance and raises maximum positioning speed, but increases the time for damping deceleration potentially causing overshoot without operator training.

Once the desired mass, M_d, is set, the relationship between bandwidth frequency, ω_{bw},

and time constant, τ, (3.5) can be used to limit desired damping, B_d. Since a reduction of desired mass, M_d, will increase the bandwidth of our reference model system, we must relate the upper limit of desired damping, B_d, as a function of desired mass, M_d, in order to preserve our bound on bandwidth of 139 rad/s set in section 3. Desired damping, B_d, can now be defined as

$$B_d \leq \left(139\frac{N \cdot s}{m \cdot kg}\right) M_d \ . \tag{4.3}$$

4.4 Maximum Machine Dampening, $(B_m)_{max}$

Maximum machine dampening, $(B_m)_{max}$, will dictate the shape and saturation of machine damping, B_m, of the system damping near contact. As before with desired damping, B_d, maximum machine damping, $(B_m)_{max}$, will modify velocities and accelerations when $x \leq x_n$, and most notably when $x \leq x_{ns}$ to aid in managing fixture-structure contact as shown in Fig. 3.1. If fixture-structure rebound occurs, the maximum machine damping, $(B_m)_{max}$, can be increased to reduce velocity at the point of contact. However, too large of a $(B_m)_{max}$ will create very sluggish fixture manipulation close to the structure, so a balance must be met with the machine damping distance constant, r_B, in order to allow for proper manipulation.

4.5 Machine Damping Distance Constant, r_B

The shape of the machine damping, B_m, is adjusted by the machine damping distance constant, r_B. This governs how quickly the desired damping, B_d, ascends to the maximum machine damping, $(B_m)_{max}$. The machine damping distance constant, r_B, can be designed similar to a traditional exponential time constant, giving a relationship of transition completion over a distance away from saturation, $x_n s$. A large machine damping distance constant, r_B, will produce a wider transition region, while a smaller value will narrow the transition approaching a step function. This parameter should be large enough to avoid a jarring change in damping, but must ensure the damping transition is adequately achieved within

the near-regime in order to avoid exhibiting discontinuities at the near-far regime boarder, $x = x_n$. As discussed in 3.4, when the transition area is greater than or equal to 7 times the distance constant the damping is 99.8% transitioned, adequate for the machine damping, B_m, function (3.7) and therefore sets an upper bound of,

$$r_B \leq \frac{(x_n - x_{ns})}{7} \tag{4.4}$$

where x_n is the near-regime starting distance and x_{ns} is the saturation distance. In our case, the transition region or near-regime has a distance of $(x_n - x_{ns}) = 0.030m - 0.005m = 0.025m$. This is governed by the optical distance sensors' range, $x_n = 0.030m$, and the saturation region, x_{ns}, selected in this thesis as $0.005m$ to include potential fasteners protruding from the docking surface. These can also be changed with new hardware or software to suit the needs of the process, although not further investigated here. For the presented test bench setup, (4.4) yields $r_B \leq 0.0036$ which does indeed successfully transition our machine damping, B_m, in Fig. 3.5.

4.6 Maximum Dock Force, $(F_d)_{max}$

The maximum magnitude of dock force, F_d, the fixture applies to the structure is set by the maximum dock force parameter, $(F_d)_{max}$, setting the threshold of force required to separate the two. Process requirements and human factors are considered for this parameter in order to balance an increase in dock stability, but allow for operator override of the dock force bias when necessary.

4.7 Dock Force Distance Constant, r_F

Similar to the machine damping, B_m, equation, the dock force, F_d, includes a dock force distance constant, r_F, which modifies the distance away from the structure at which the dock force, F_d, is felt. Although the governing formula is similar to machine dampening, B_m, the dock force, F_d, translates into a fixture velocity, therefore, in regard to operator control

authority, a preference to a faster rise to saturation was found from preliminary testing. This ensures that the influence is felt only near the point of contact, preserving human force input, F_h, manipulation without a bias until the fixture is very close to the structure. Increasing this term will attract the fixture from further distances from the structure, which may not be ideal for manipulation. Alternatively, a very small dock force distance constant, r_F, will approach a step, and suggests that perhaps a binary on/off toggle for the user may meet the needs of the process and will be vetted in further design iterations. An upper bound on dock force distance constant, r_F, follows the same inequality as the machine damping distance constant, r_B, and (4.4), and is defined as

$$r_F \leq \frac{(x_n - x_{ns})}{7}. \tag{4.5}$$

where x_n is the near-regime starting distance and x_{ns} is the saturation distance.

Chapter 5

EXPERIMENTAL RESULTS

5.1 Free Space Manipulation Regime: M_d, B_d

One goal for the controller is to accurately position a fixture. The first experiment was to position the test bed fixture to a goal approximately 0.1 m away from a start position. Shown in Fig. 2.3, the test setup used the motor's encoder, and graph paper as a visual indicator, to measure 0.1m from a starting zero on the graph paper and set this as our "goal". For each trial, a randomized assignment of mass and damping was used, and the operator would begin to test by commanding a velocity towards the goal with the intent on placing the indicator within the goal area, and completed via a mouse click when satisfied in positioning the mobile base. Once a trial was complete, to ensure consistent starting position and blind assignment of control parameters, the code automatically drove the test bed back to zero and assigned a new combination of desired mass, M_d, and desired damping, B_d, for the tester to evaluate. The investigation used 300 trials, 10 runs of 30 permutations of the desired mass, M_d, and the desired damping, B_d, and recorded how those variations effected the percent overshoot, the settling time, and the steady state error, defined as,

$$\%OS = \begin{cases} \left(\frac{x_{max}}{x_g} - 1\right) 100 & \text{if } x_{max} > x_g \\ 0 & \text{if } x_{max} \leq x_g \end{cases} \tag{5.1}$$

$$T_s = t_{\pm 2\%} - t_0 \tag{5.2}$$

$$e_{ss} = |x_{final} - x_g| \tag{5.3}$$

where $\%OS$ is percent overshoot, x_{max} is the maximum position reached away from the start position, x_g is the goal position (0.1 m), T_s is settle time, $t_{\pm 2\%}$ is the time it takes to reach and stay within $\pm 2\%$ of the goal, t_0 is the time when the fixture was first moved from the start position, e_{ss} is steady state error, x_{final} is the final position of the fixture when the trail is completed. [1]

There was only one participant in the tests, and the results in Fig. 5.1 show how well different desired mass, M_d, and desired damping, B_d, combinations affected the positioning performance. Some trends that were found:

- Percent Overshoot ranged from 0% to 10%. Lower desired mass, M_d, and higher desired damping, B_d, showed reductions in this metric.

- Settling time ranged from 1.2 to 2.2 seconds, and showed better performance with a smaller desired mass, M_d, increasing acceleration, and smaller desired damping, B_d, increasing maximum speed.

- Steady State Error benefited the most from higher desired damping, B_d, minimizing velocities allowed for smaller position corrections.

Within the range of masses and dampening coefficients tested, a preference began to take shape. For this user, a desired mass of 30 kg and desired damping of 150 N-s/m yielded the best percent overshoot, $\%OS$, and steady state error, e_{ss}, and near best settling time, T_s, only 15% slower than the fastest time recorded. This type of data can be found for individual operators and the control tailor to optimize manipulation accuracy.

[1] See Appendix C

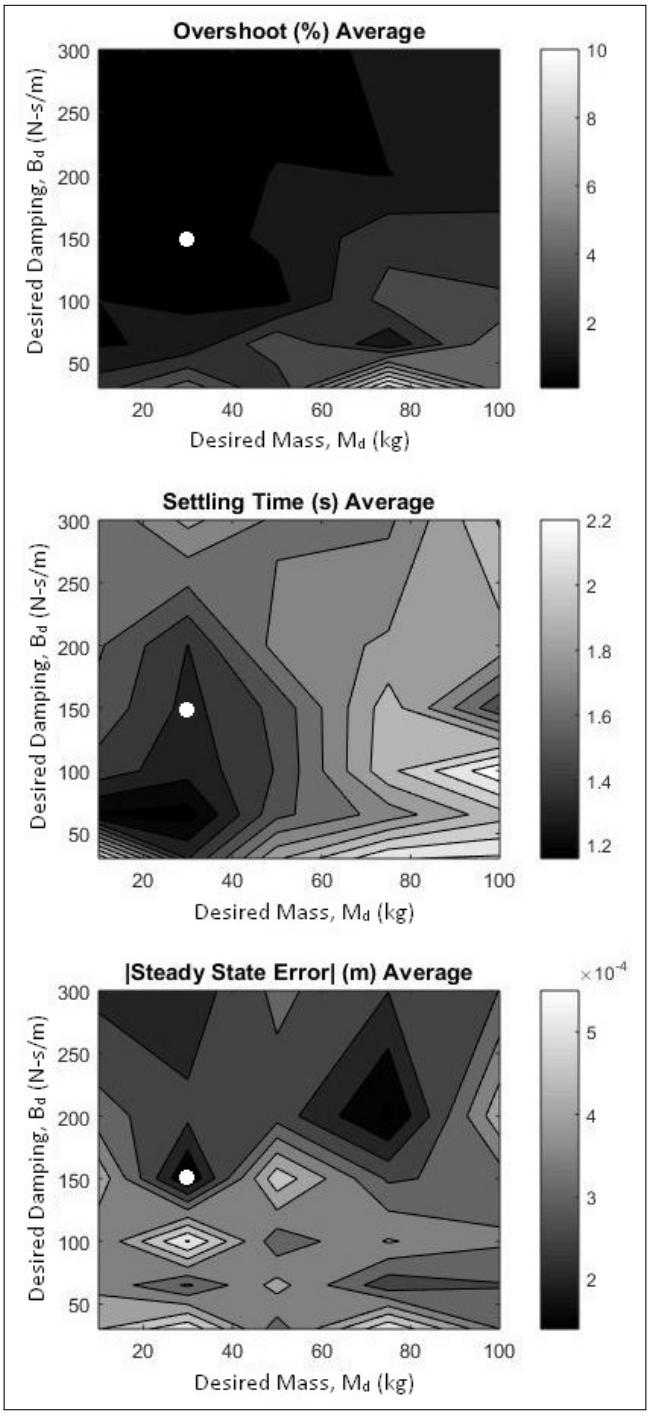

Figure 5.1: Free Space Manipulation Test Results. Heat map plots of positing accuracy in moving the test bed fixture 0.1 m away from a starting position. The plots show percent overshoot,$\%OS$, settling time, T_s, and steady state error, e_{ss}. Darker areas denote better performance. Note the points, $\circ$, that show a preference of $30kg$ and $150N \cdot s/m$ for this task.

5.2 Docking Regime: $(B_m)_{max}$

The near-regime damping parameter for docking was investigated empirically. The parameter tested was maximum machine damping, $(B_m)_{max}$. Recall this defines machine damping, B_m, in the desired reference model system (3.1) as the fixture approaches the rigid structure. As before, the time constant is a function of desired damping, B_d, or in this case machine damping, B_m, and desired mass, M_d, set by the operator. This desired mass, M_d, will play a role in system behavior even at machine damping saturation, $(B_m)_{max}$, further analysis of this relationship will be conducted in the future.

A test to measure how well the machine damping, B_m, mitigates docking rebound, trials were conducted on the test bed in Fig. 2.3. The optic sensors have a range, x_n, of 0.030 m, therefore the test was to dock the fixture to the structure from a starting position 0.035 m away to capture the entire near-regime, and used the following parameters: a constant operator force input, $F_h = -5\ N$, desired mass, $M_d = 30kg$, desired damping, $B_d = 150$ N-s/m, zero dock force, $(F_d)_{max} = 0N$, machine damping distance constant, $r_B = 30$, and a range of maximum machine damping, $(B_m)_{max}$. The results are shown in Fig. 5.2.

Without additional damping, i.e., $B_m = B_d = 150$ N-s/m, contact oscillations developed and forced the fixture off of the structure on the order of millimeters. Applying additional damping, $(B_m)_{max} = 300$, reduced the magnitude of the oscillations dramatically, however a marginally stable response was still present. Finally, at $(B_m)_{max} = 600$, the system rejected enough of the contact forces to allow the fixture to settle against the structure and successfully dock. Further testing is planned for stability criteria and machine damping distance constant, r_B.

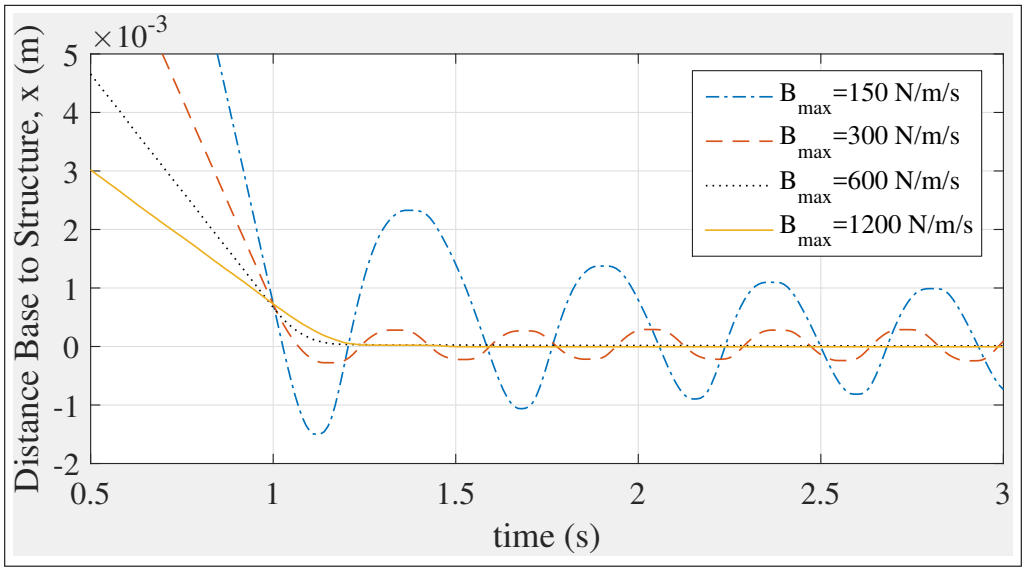

Figure 5.2: Dock attempts with a constant user input force, $F_h = -5\ N$, desired mass, $M_d = 30\ kg$, desired damping, $B_d = 150$ N-s/m, machine damping distance constant, $r_B = 0.0036m$, and varying maximum machine damping, $(B_m)_{max}$. Note: Times have altered to collocate the point of contact.

5.3 Dock Force: $(F_d)_{max}$

To select the dock force, the previous experiments for desired mass, M_d, and desired damping, B_d, were examined for their human force input, F_h, distribution. This is an attempt to characterize force inputs for control and to determine what force could influence the response, but allow the human operator to easily overcome the bias with reasonable force input. Fig. 5.3 shows a normalized histogram, or probability distribution for the magnitude of human force input, F_h, collected in section 4.4. Along with this information, a review of the application predicts at most we expect to see a force of around $4N$ from the operation. Therefore a maximum dock force, $(F_d)_{max} = 5N$, was selected and through test bench simulation the dock force distance constant, $r_F = 0.00033m$, was determined, successfully creating a more stable dock condition with the ability to easily override with operator influence. Further testing is planned for stability and dock force distance constant, r_F.

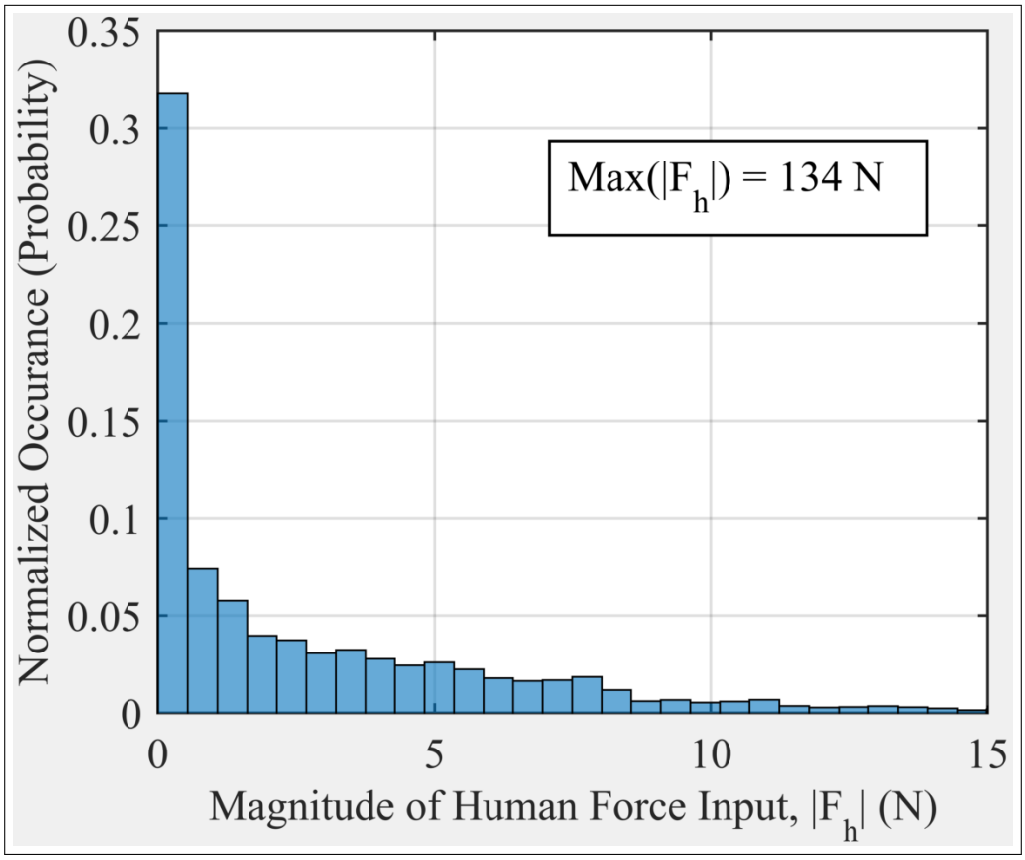

Figure 5.3: Histogram of the magnitude of human force input, F_h, during the free space manipulation trials of varying desired mass, M_d, and desired damping, B_d, from section 5.1 and shown in Fig. 5.1. Normalized to give a probability distribution. Note a maximum human force input, F_h, of 134 N.

Chapter 6

CONCLUSION

In this thesis, we proposed a variable-impedance-based human-machine control solution for docking a fixture to a rigid structure, and proved its validity. By leveraging the human element for fixture path planning and positioning, intuitive force inputs, and a variable reference model tracking impedance control, a swift robust control law was created. Varying the damping minimized the risk of unwanted movements via human force input, F_h, or reaction force, F_r, during close fixture-structure proximity and ensured controlled contact. Through experimentation, the system parameters, M_d, B_d, $(B_m)_{max}$, and $(F_d)_{max}$, were selected to successfully create: (i) intuitive, swift, and accurate operating dynamics in free space manipulation; (ii) controlled interaction behavior; and (iii) applied a dock force for stable contact. Future improvements to this controller involve evaluating various dock force, F_d, and machine damping, B_m, scenarios for manipulation and fixture-structure stability while docking.

BIBLIOGRAPHY

[1] J. Buchli, F. Stulp, E. Theodorou, and S. Schaal. Learning variable impedance control. *The International Journal of Robotics Research*, 30(7):820–833, 2011.

[2] Ricardo Carelli and Rafael Kelly. An Adaptive Impedance/Force Controller for Robot Manipulators. *IEEE Transactions on Automatic Control*, 36(8):967–971, 1991.

[3] CC Cheah and Danwei Wang. Learning impedance control for robotic manipulators. *IEEE Journal Transactions on Robotics*, 14(3):452–465, 1998.

[4] Chuanzhi Chen, Hong Nie, Jinbao Chen, and Xiaotao Wang. A Velocity-Based Impedance Control System for a Low Impact Docking Mechanism (LIDM). *Sensors*, 14(Lidm):22998–23016, 2014.

[5] Andrea Cherubini, Robin Passama, Philippe Fraisse, and André Crosnier. A Unified Multimodal Control Framework for Human-Robot Interaction. *Robotics and Autonomous Systems*, 70:106–115, 2015.

[6] Jae H Chung. Modeling and Control of a New Robotic Deburring System. *ASME Journal of Manufacturing Science and Engineering*, 129(October 2007):1–17, 2007.

[7] J. C Coulson and M. Maudsley. Playing it safe. *Journal of Epidemiology & Community Health*, 61(10):876–876, 2007.

[8] Rajiv V Dubey, Tan Fung Chan, and Steve E Everett. Variable Damping Impedance Control of a Bilateral Telerobotic System. *IEEE Control Systems Magazine*, 17(February):37–45, 1997.

[9] N. Hogan. Stable execution of contact tasks using impedance control. *Proceedings. 1987 IEEE International Conference on Robotics and Automation*, 4:1047–1054, 1987.

[10] Neville Hogan. Impedance Control: An Approach to Manipulation. *American Control Conference, 1984 IS - SN - VO -*, (March):304–313, 1985.

[11] Roman Kamnik, Drago Matko, and Tadej Bajd. Application of Model Reference Adaptive Control to Industrial Robot Impedance Control. *Journal of Intelligent and Robotic Systems*, 22(1):153–163, 1998.

[12] H. Kazerooni, P. K. Houpt, and T. B. Sheridan. Robust Compliant Motion for Manipulators, Part II: Design Method. *IEEE Journal on Robotics and Automation*, 2(2):93–105, 1986.

[13] Bongsu Kim, Aurelien Rodot, and Ashish D. Deshpande. Impedance Control Based on a Position Sensor in a Rehabilitation Robot. *ASME 2014 Dynamic Systems and Control Conference*, (1):1–7, 2015.

[14] Liang Liao, Fengfeng Jeff Xi, and Kefu Liu. Adaptive Control of Pressure Tracking for Polishing Process. *ASME Journal of Manufacturing Science and Engineering*, 132(1):011015, 2010.

[15] M. H. Raibert and J J Craig. Hybrid Position / Force Control of Manipulators. *ASME Journal of Dynamic Systems, Measurement, and Control*, 102(June 1981):126–133, 1981.

[16] Pierre-François Verhulst. Recherches mathématiques sur la loi d'accroissement de la population. *Nouveaux Mémoires de l'Académie Royale des Sciences et Belles-Lettres de Bruxelles*, 18:1–42, 1845.

[17] Y. L. Yao and S. M. Wu. Development of an adaptive force/position controller for robot-automated composite tape-layering. *ASME Journal of Manufacturing Science & Engineering*, 115(AUGUST):1–7, 1993.

[18] Jianming Zhan and Sihai Yu. A New Aspheric Surfaces Polishing by Parallel Orthogonality Movement/Force Servomechanism. *ASME Journal of Manufacturing Science & Engineering*, 133(3):31011–31015, 2011.

Appendix A

1-DOF TEST BED

A.1 Objective

To test the control scheme in this thesis, a single degree of freedom test bed was built. The test bed design should emulate the mobile base, fixture, and rigid structure shown in Fig. A.1, and should include force and proximity sensing for input and adjustment of the controller near contact.

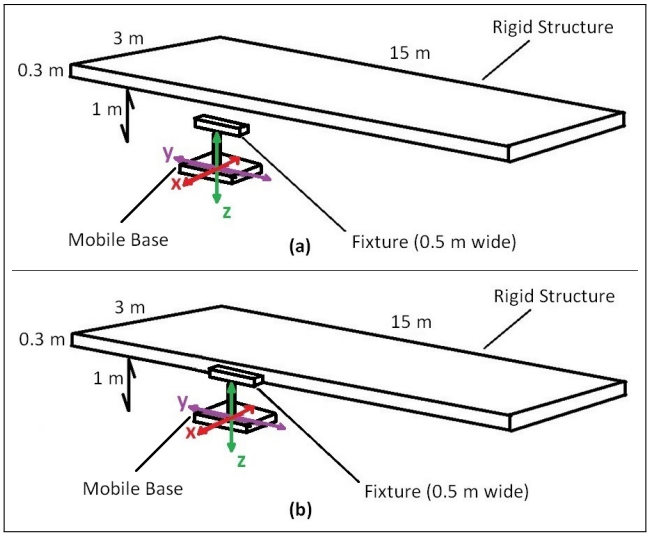

Figure A.1: Illustration of the application analyzed in this thesis. The fixture is approximately 0.5 m wide and supported roughly 1 m above the ground by a mobile platform. The structure is approximately 0.3 m tall by 15 m long and 3 m wide held 1 m off the ground.(a) Rigid structure and fixture in arbitrary starting locations. (b) Fixture docked against the rigid structure.

A.2 Test Bed Design

Fig. A.2 illustrates the test bed design. A mobile base driven by a single motor on a rack and pinion guided by a linear rail. A force input device mounted between the mobile base and fixture will allow force commands inputted directly onto the fixture. Optical sensors placed on the fixture and aimed toward the structure to feedback fixture-structure proximity.

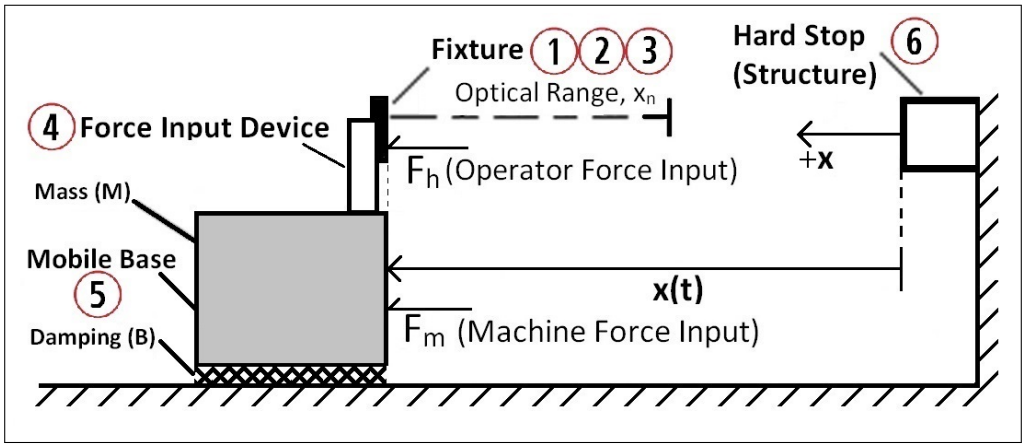

Figure A.2: One dimensional impedance control test bench setup. Where M is lumped mass, B is lumped damping, and F_h and F_m are operator and machine force inputs, respectively. A fixture ① that houses two optical sensors ② and contact bumpers ③, is mounted onto a force input device ④ which is attached to a mobile base ⑤ supported by a linear guide rail, and driven by a motor on a rack and pinion. The optical distance sensors have limited range, $x_n \approx 0.030m$. The fixture and optical sensors are aligned to a hard stop ⑥ to simulate fixture-structure interaction and measured proximity, $\tilde{x}(t)$, when $x(t) \leq x_n$.

A.2.1 Mobile Base

Fig. A.3 & A.11 show the construction of the mobile base. A piece of aluminum angle was supported by two NSK NH15AN linear guide carts, which were attached to the guide rail along a Nexen 966651 rack and driven by a Harmonic Drive FHA-11C-100-US200-E servo motor and a 2" diameter Nexen 966687 pinion. A plate was fixed atop the angle in order to yield a larger area to mount devices. The detailed drawings of the components can be found as Fig. A.4-A.10.

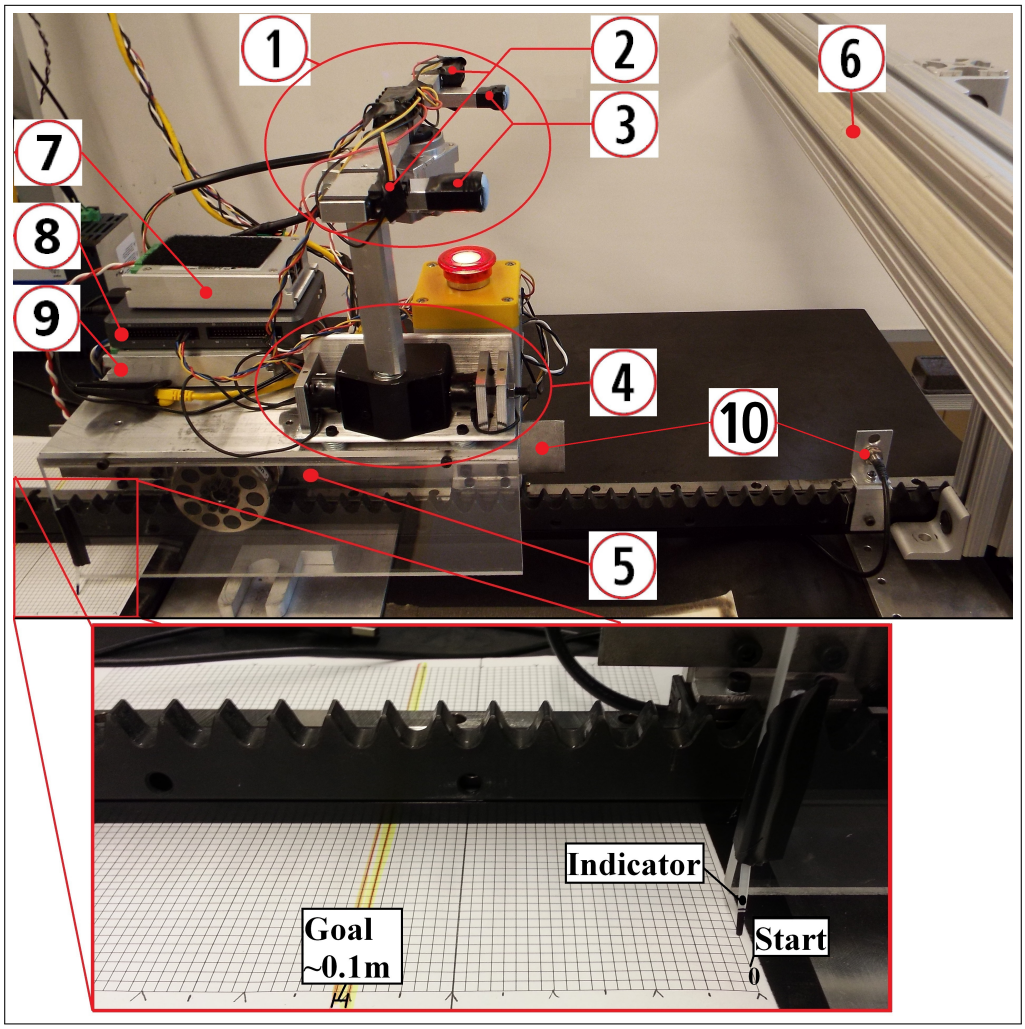

Figure A.3: *Top*: Laboratory Test Bed, build from the design shown in Fig. A.2. ① Fixture - Emulating the tool; ② Optical Sensors - Two optical sensors' data are blended in order to improve accuracy; ③ Stiff Bumpers - To ensure contact points with the hard stop; ④ Force Input Device - Handle-mount assembly supported by a short linear rail guiding contact with two strain-type force sensors preloaded to give a differential yielding an accurate force input; ⑤ Mobile Base - Aluminum angle mounted to a linear rail with rack and pinion drive, housing drives and other electronics; ⑥ Hard Stop - Stiff Structure built from 80/20 to simulate a rigid body; ⑦ Elmo Whistle Drive for Fixture Alignment Motor (A-Axis); ⑧ myRio embedded hardware device for executing LabVIEW VI; ⑨; Elmo Whistle Drive for Mobile Base Motor (Y-Axis); ⑩ Steel plate and hall effect limit sensor. *Bottom*: The lower left hand corner of the base was used to test positional accuracy.

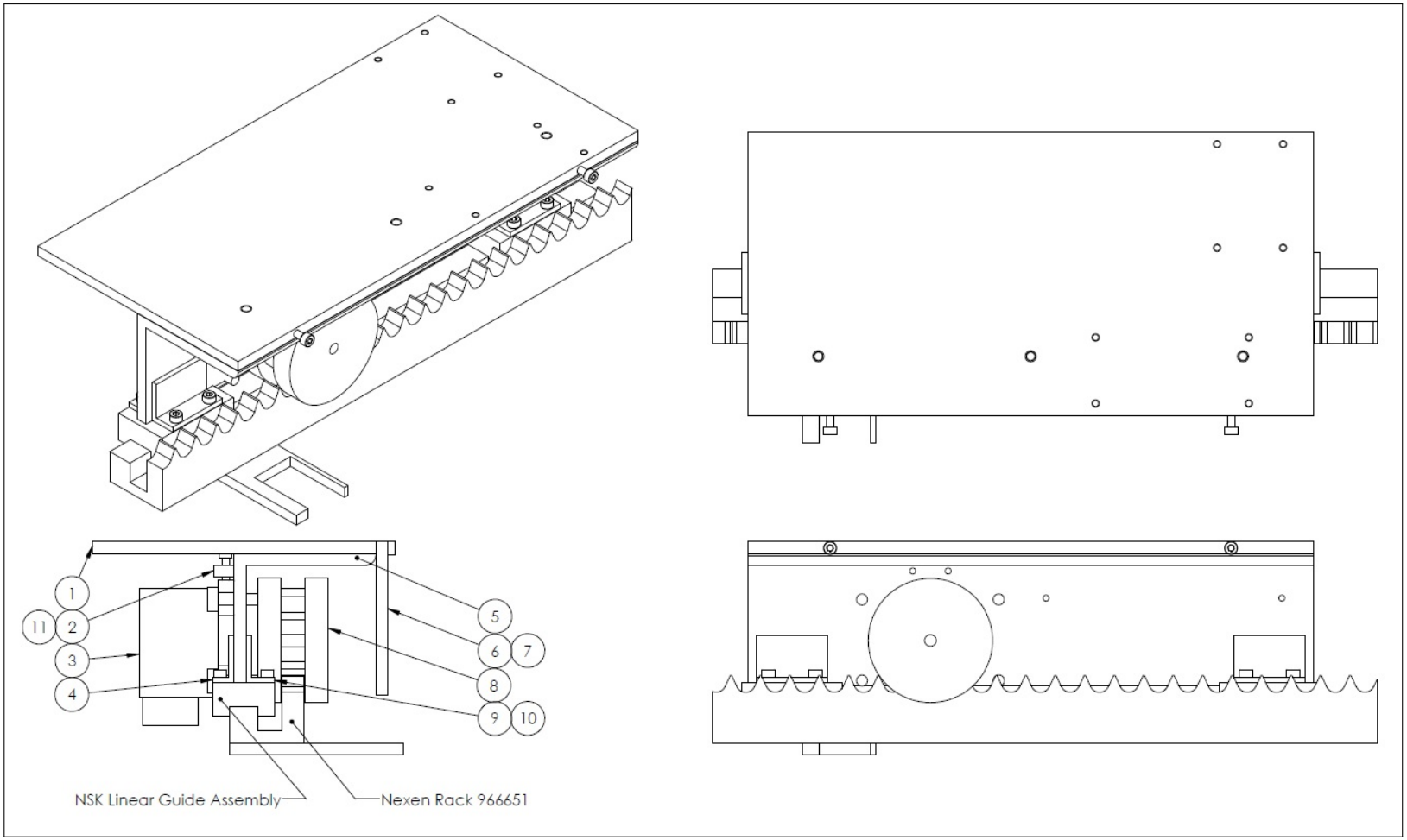

Figure A.4: Mobile Base - Overview: ① Foundation Plate, Fig. A.5; ② Pinion Adjust, Fig. A.6; ③ Harnomic Drive Servo Motor FHA-11C-100-US200-E; ④ Rear Mounting Foot, Fig. A.8; ⑤ Mounting Angle, Fig. A.7; ⑥ Pinion Cover, Fig. A.10; ⑦ M4x10mm SHCS; ⑧ Nexen Pinion 966687; ⑨ Front Mounting Foot, Fig. A.9; ⑩ M4x10mm SHCS; ⑪ M4x15mm SHCS.

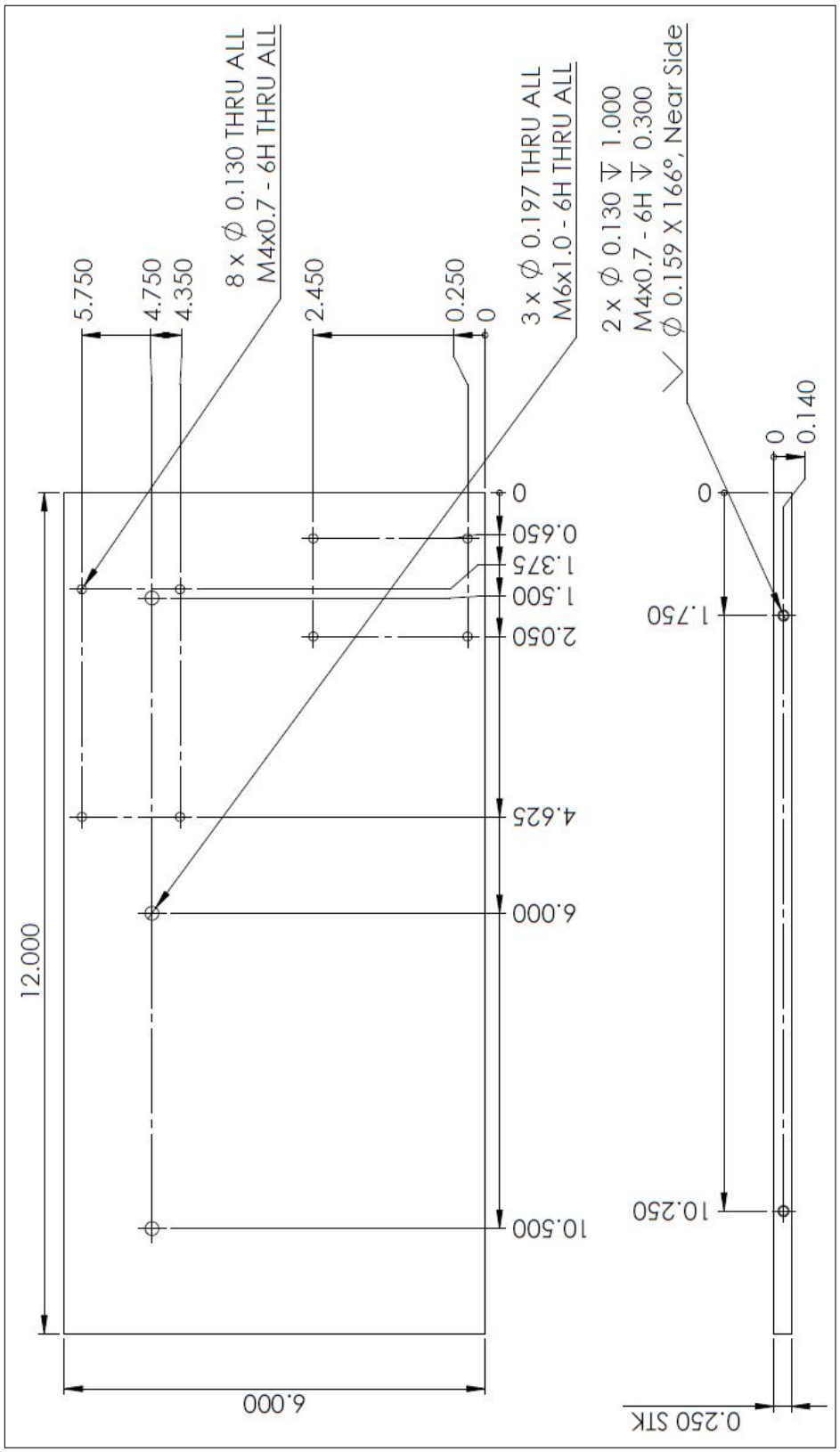

Figure A.5: Mobile Base - Foundation Plate Detail. Material: Aluminum. UNLESS OTHERWISE SPECIFIED, ALL DIMENSIONS ARE IN INCHES.

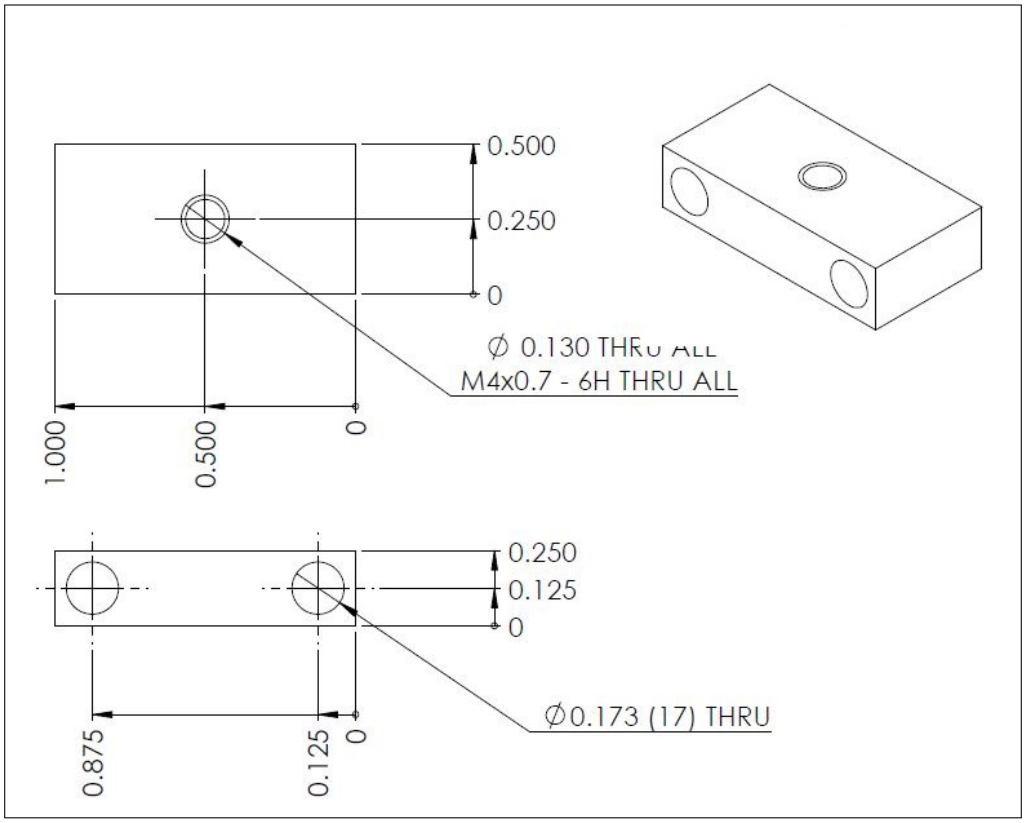

Figure A.6: Mobile Base - Pinion Adjust Detail. Material: Aluminum. UNLESS OTHERWISE SPECIFIED, ALL DIMENSIONS ARE IN INCHES.

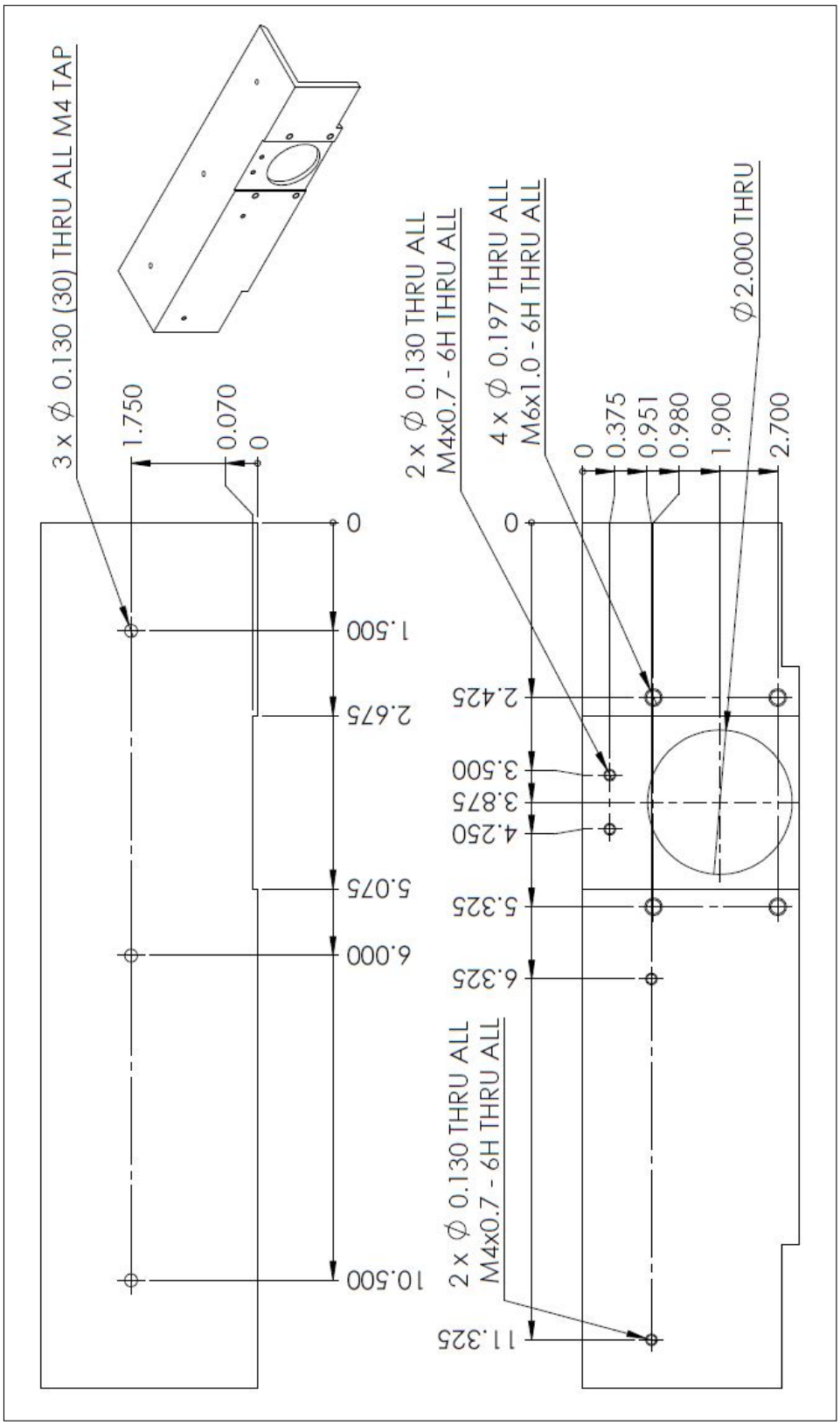

Figure A.7: Mobile Base - Mounting Angle Detail. Material: Aluminum. UNLESS OTHERWISE SPECIFIED, ALL DIMENSIONS ARE IN INCHES.

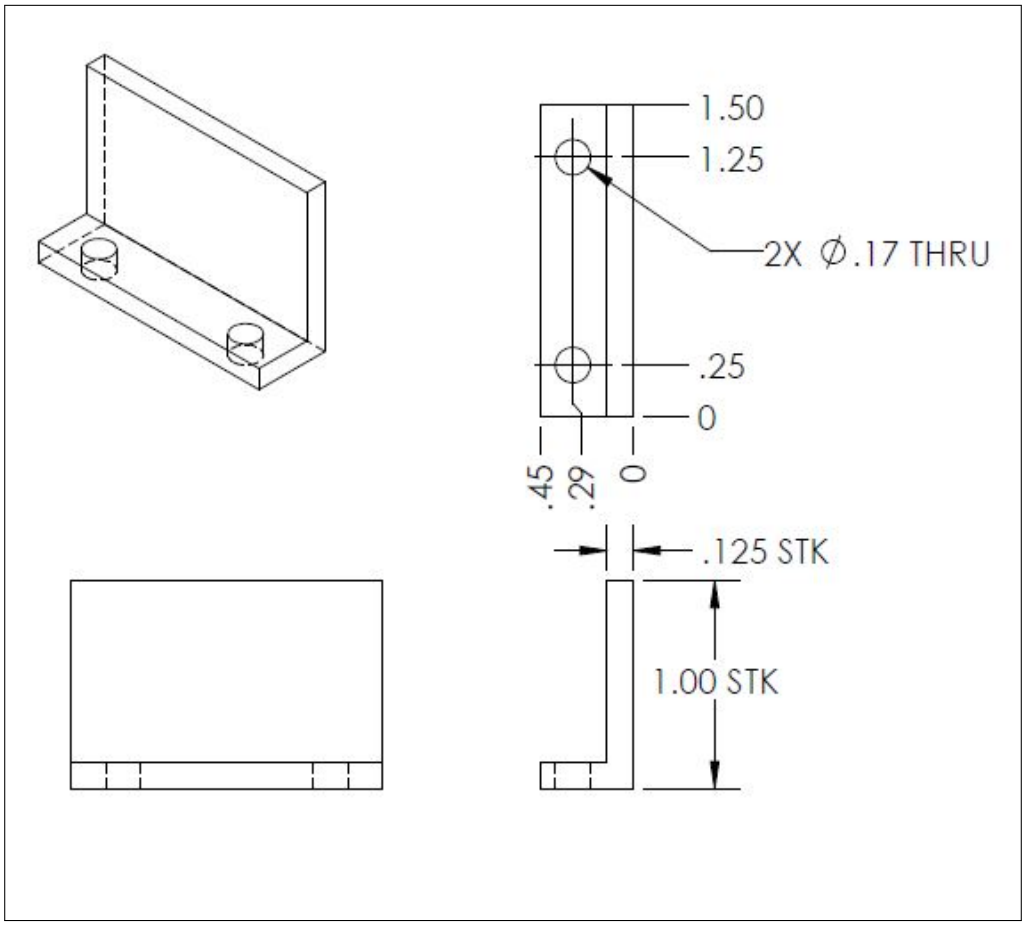

Figure A.8: Mobile Base - Rear Mounting Foot Detail. Material: Aluminum. UNLESS OTHERWISE SPECIFIED, ALL DIMENSIONS ARE IN INCHES.

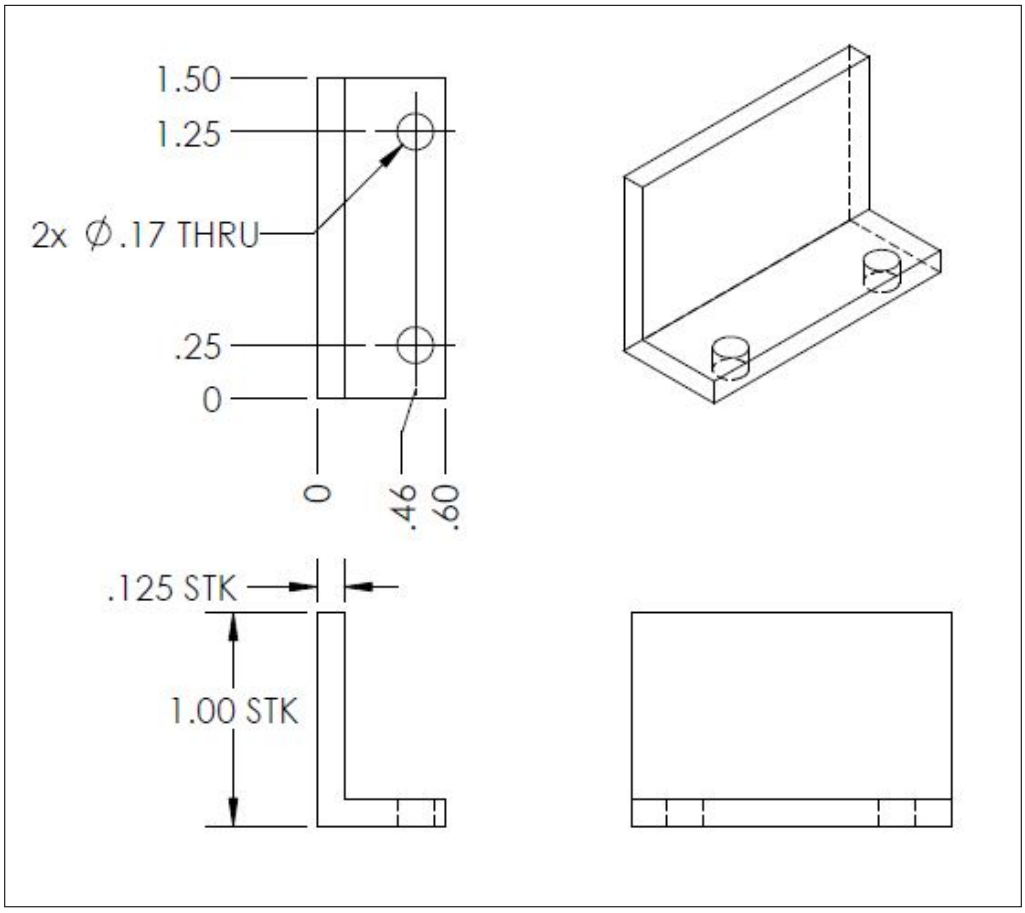

Figure A.9: Mobile Base - Front Mounting Foot Detail. Material: Aluminum. UNLESS OTHERWISE SPECIFIED, ALL DIMENSIONS ARE IN INCHES.

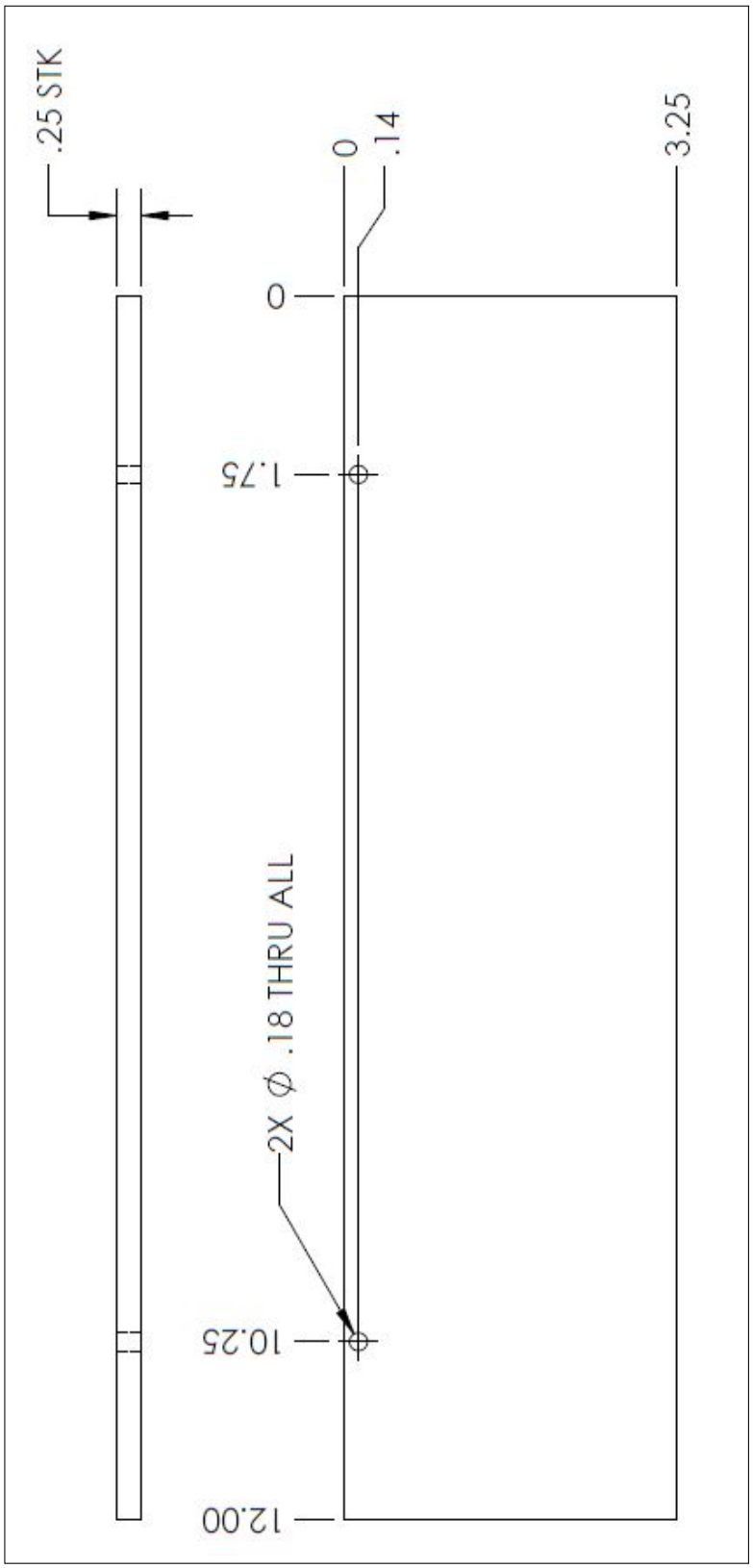

Figure A.10: Mobile Base - Pinion Cover Detail. Material: PMMA. UNLESS OTHERWISE SPECIFIED, ALL DIMENSIONS ARE IN INCHES.

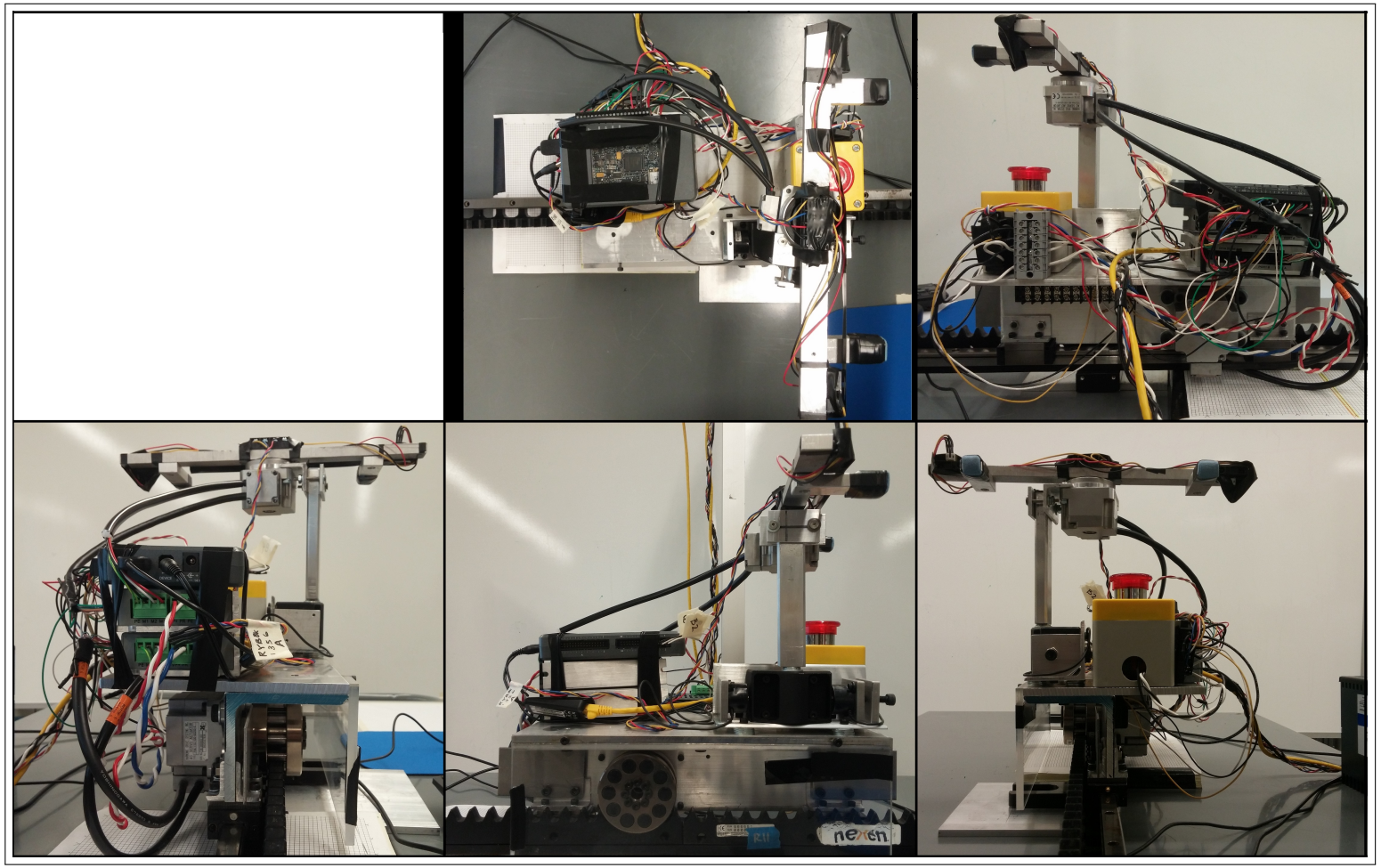

Figure A.11: Test Bed Mobile Base and Fixture build. Starting from top left and working clockwise: Blank. Top View. Back View. Right View. Front View. Left View.

A.2.2 Fixture

The fixture was constructed of 3/8" x 3/4" aluminum stock material cut to lengths for the main body and contact points, shown in Fig. A.12. The fixture was equipped with two optical sensors and was mounted to a motor in order to allow for alignment to the structure, or the A-Axis, but is not a necessary axis to demonstrate the impedance control technology.

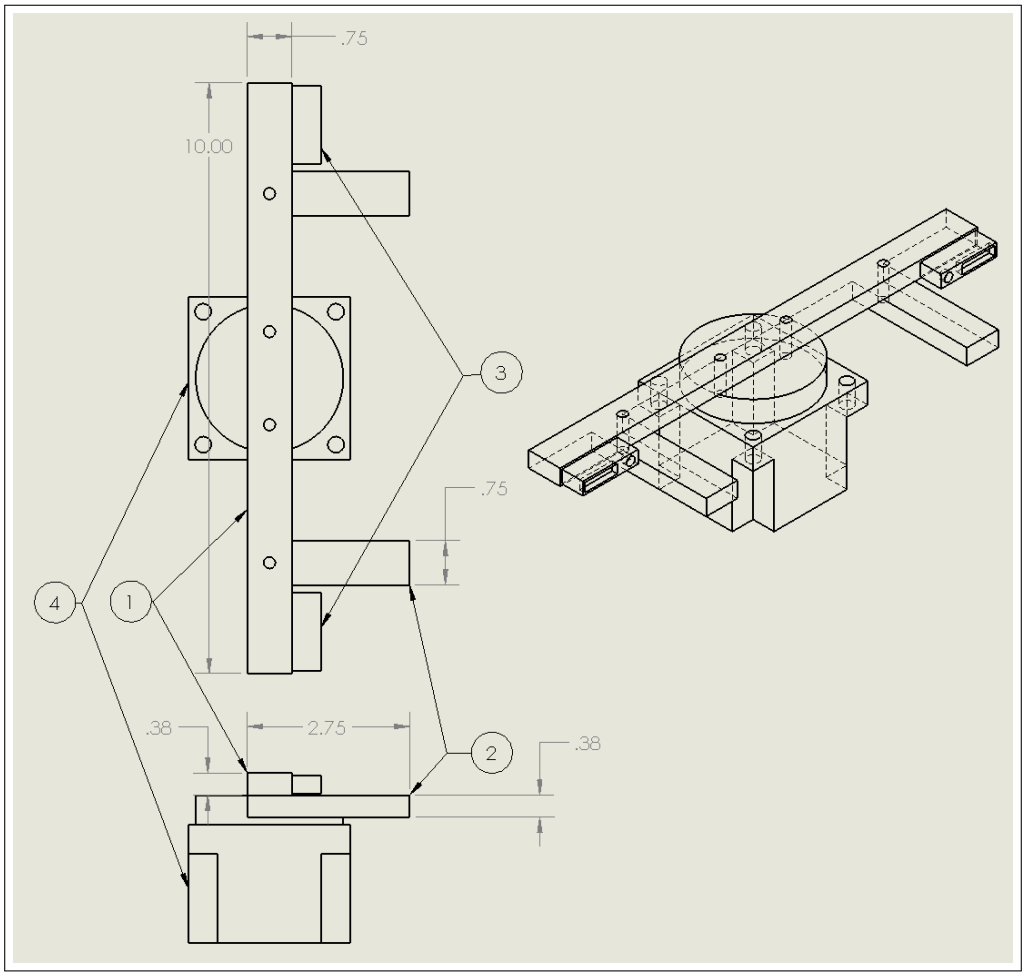

Figure A.12: Fixture Design Concept Drawing: ① Fixture Structure - 10" x 3/4" x 3/8" Aluminum; ② Contacts - 2.75" x 3/4" x 3/8" Aluminum; ③ Optical Distance Sensors; ④ Harmonic Drive Servo Motor FHA-8C-100-US200-E (A-Axis). UNLESS OTHERWISE SPECIFIED, ALL DIMENSIONS ARE IN INCHES.

Optical Sensors

Two infrared Sharp GP2Y0A41SK0F sensors were used in order to find our fixture-structure distance. With a range of 4-30 centimeters, the signal sent back to our controller was 2.8V-0.4V, respectively. Outside of this range the signal was discarded.

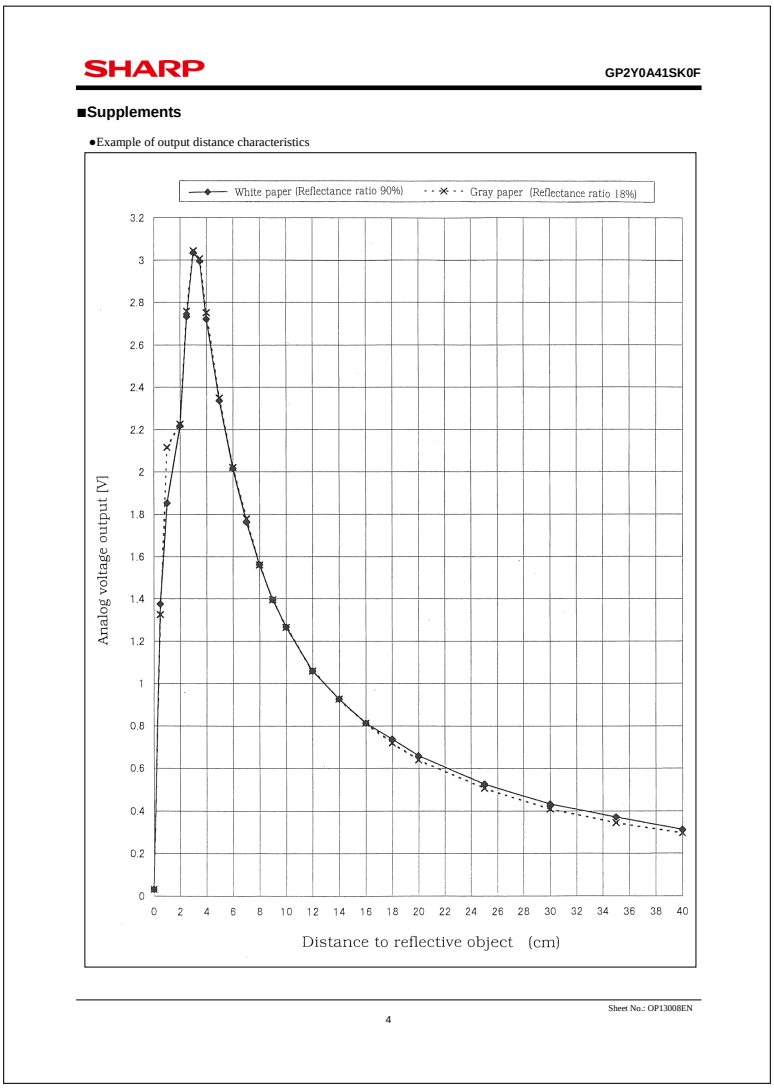

Figure A.13: Sharp GP2Y0A41SK0F IR Distance Sensor Voltage Output vs Distance Sensed.

A-Axis - Fixture Orientation

As an additional alignment tool, a Harmonic Drive FHA-8C-100-US200-E motor was fixed to the force input handle and supported the fixture centered between the two contact points. This motor was controlled in velocity mode, and operated on the error between the two optical sensor distances in order to align to the structure which the fixture is pointed towards. Fig. A.14 shows the effect the two optical sensors have on this axis. See Fig. A.31 for the software execution/command of this loop.

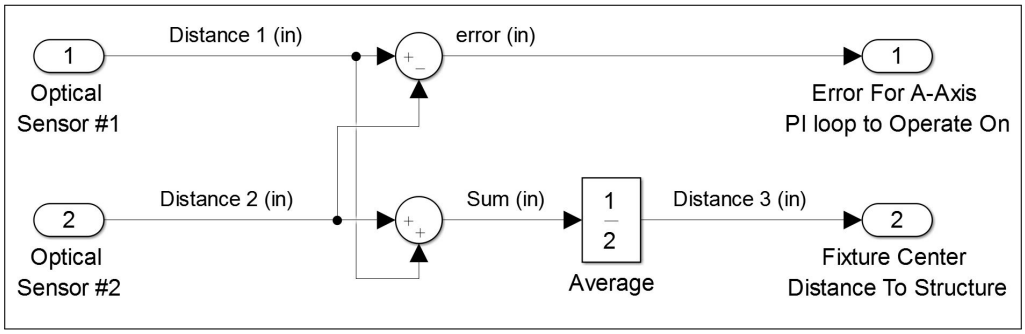

Figure A.14: Control Block Diagram showing the use of the two measured distances.

A.2.3 Force Input Device

A single degree of freedom force input was generated by taking the differential of two TE Connectivity Measurement Specialties FC2231-000-0050-L load cells opposing one another. A handle/fixture was mounted to a block guided by a NSK NH15AN linear guide cart mounted to a short linear rail. The block was the constrained to move by the two load cells and preloaded by a screw. The difference between the two load cells output was converted to a net force input and applied to the controller. The details for this device can be found the following Fig. A.16-A.20.

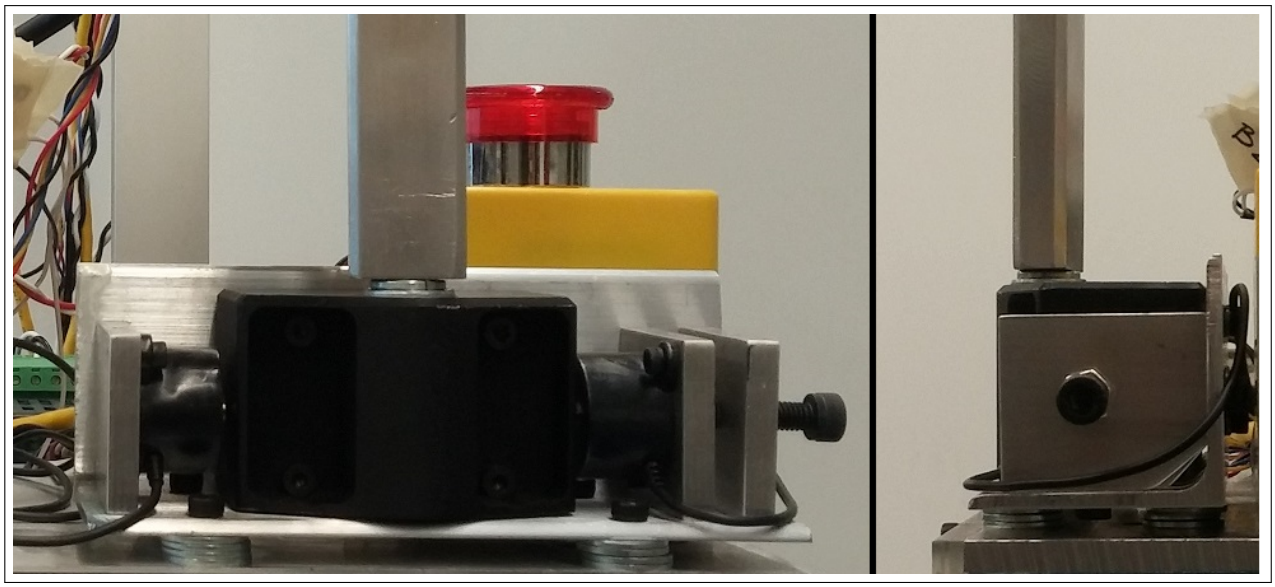

Figure A.15: Custom made force input device. See Fig. A.3 & A.11 for more views.

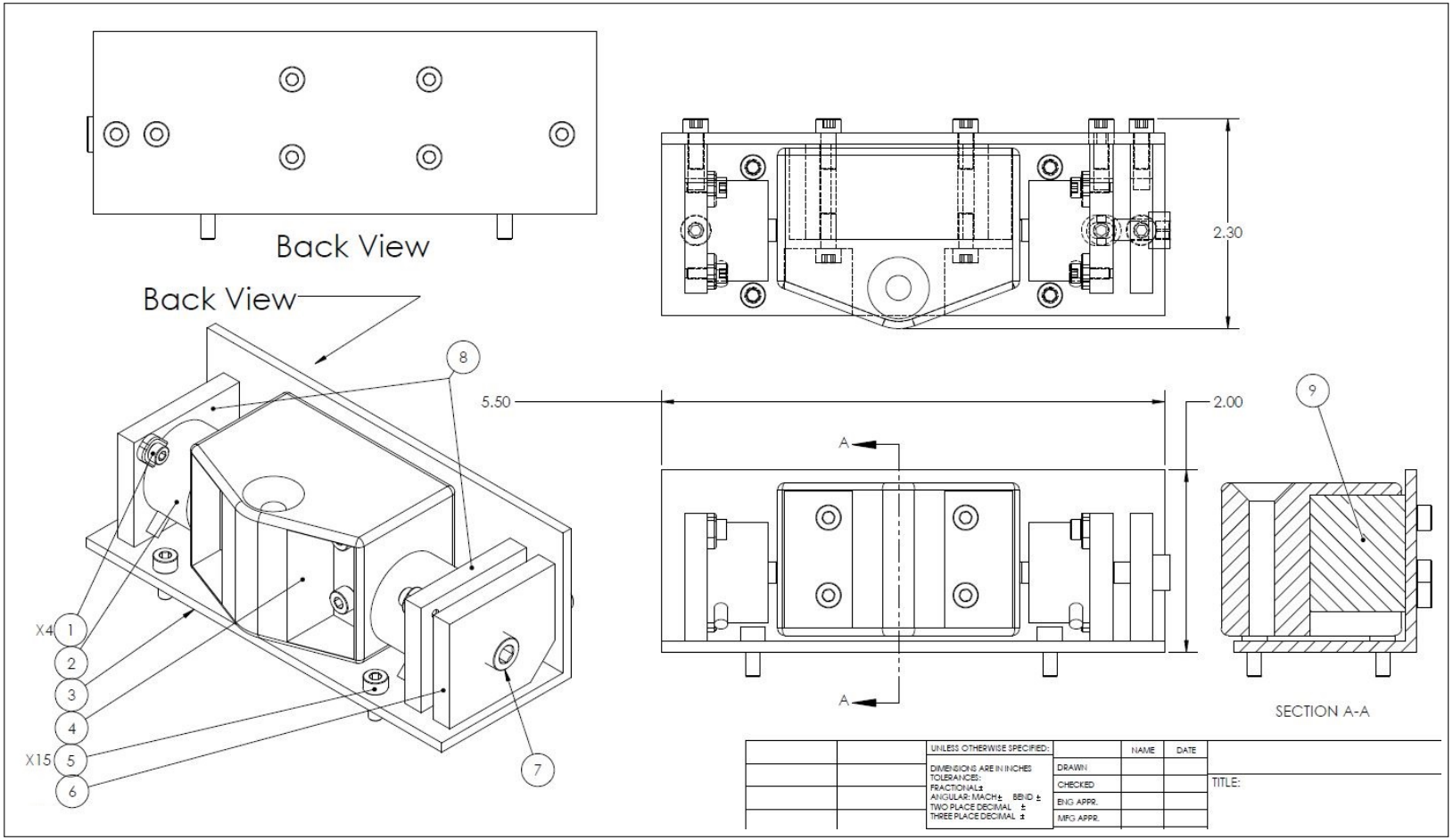

Figure A.16: Force Input Device - Overview: ① M3x10mm SHCS; ② TE Connectivity Measurement Specialties FC2231-000-0050-L Load Cell; ③ Mounting Angle, Fig. A.17; ④ Interface Block, Fig. A.17; ⑤ M4x15mm SHCS; ⑥ Preload Plate, Fig. A.19; ⑦ Foundation Plate, Fig. A.5; ⑧ Load Cell Mounting Plate, Fig. A.19; ⑨ NSK NH15AN linear guide cart and rail assembly, dimensional placeholder shown here. UNLESS OTHERWISE SPECIFIED, ALL DIMENSIONS ARE IN INCHES.

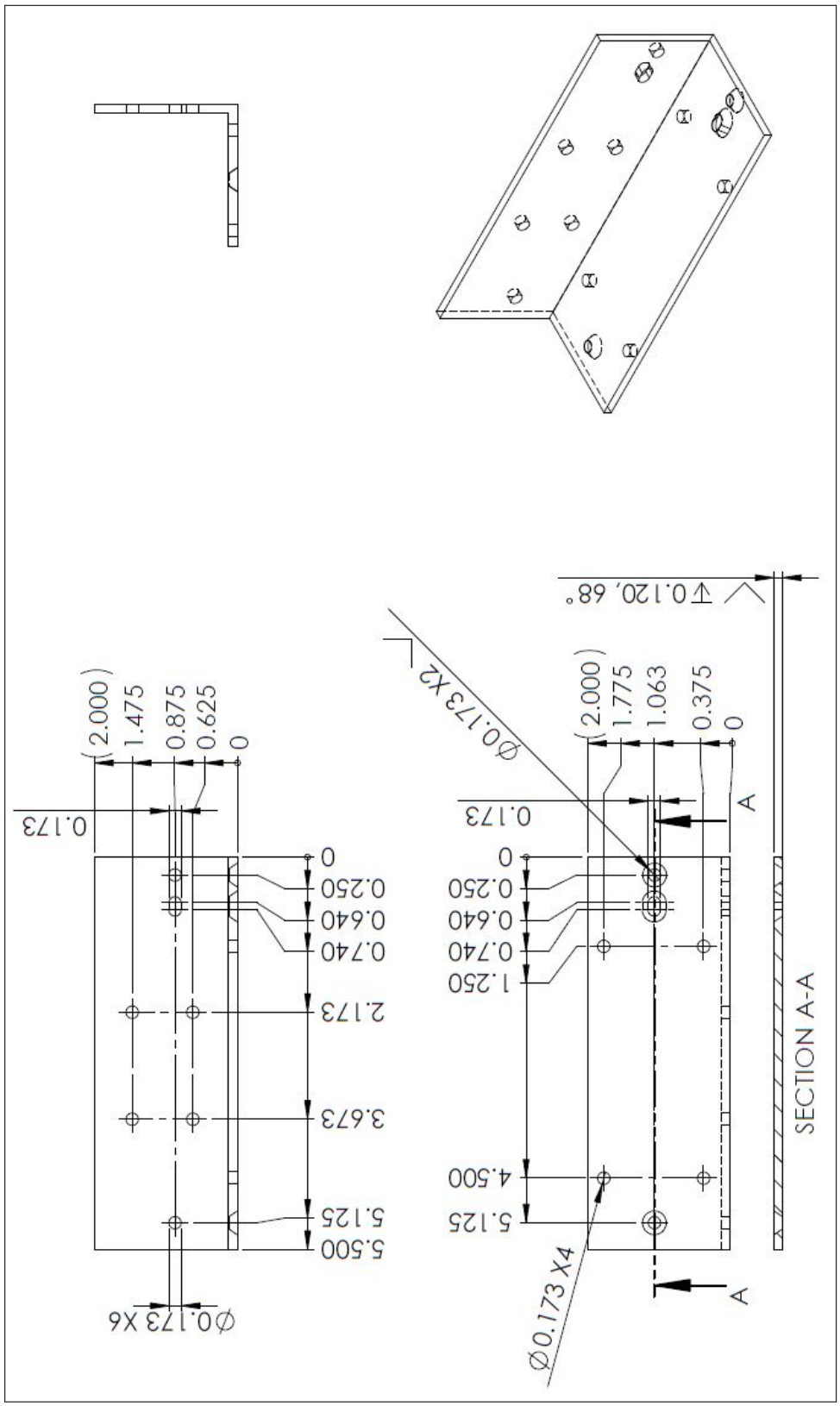

Figure A.17: Force Input Device - Mounting Angle Detail. Material: Aluminum. UNLESS OTHERWISE SPECIFIED, ALL DIMENSIONS ARE IN INCHES.

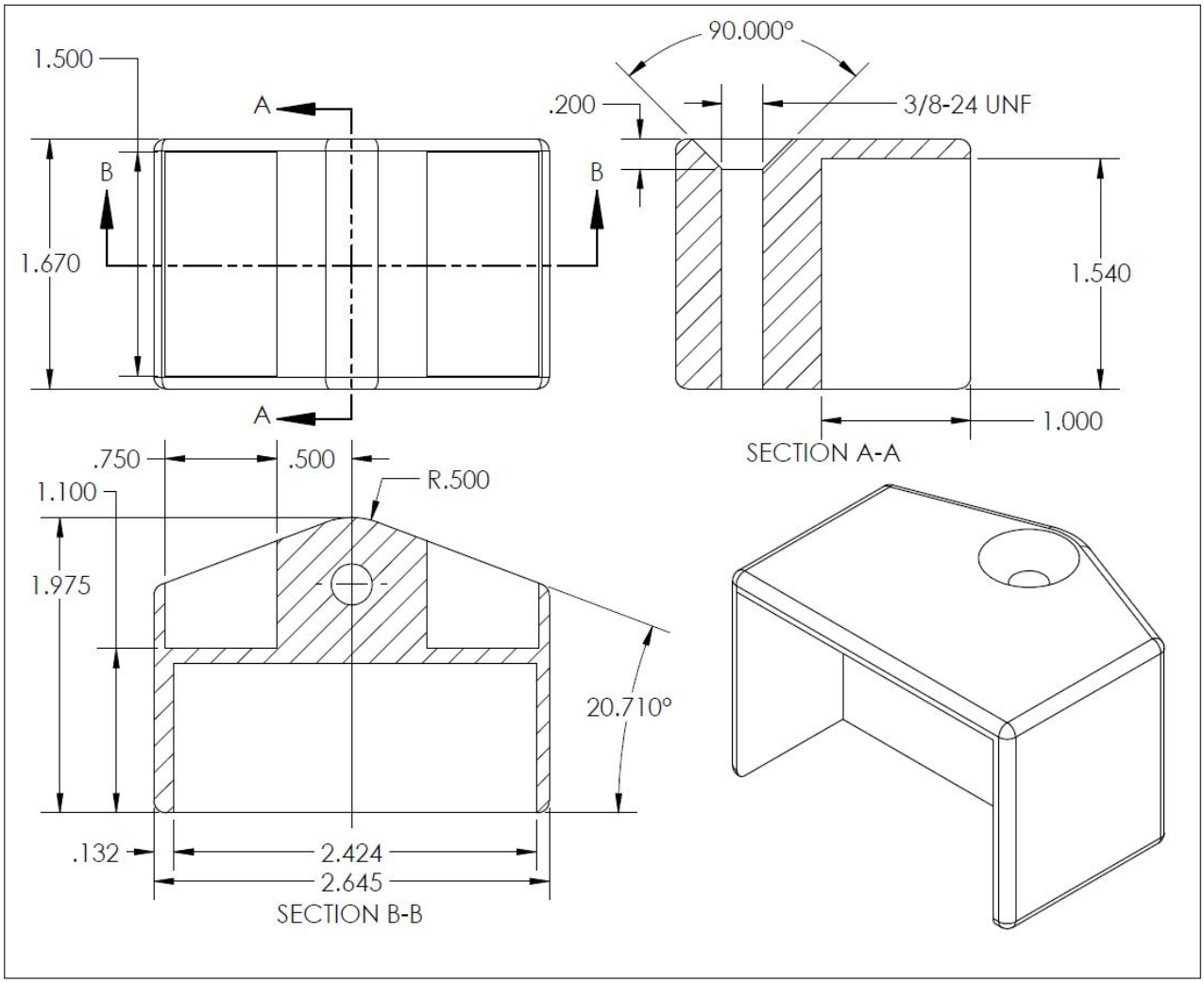

Figure A.18: Force Input Device - Interface Block Detail. Material: Aluminum. UNLESS OTHERWISE SPECIFIED, ALL DIMENSIONS ARE IN INCHES.

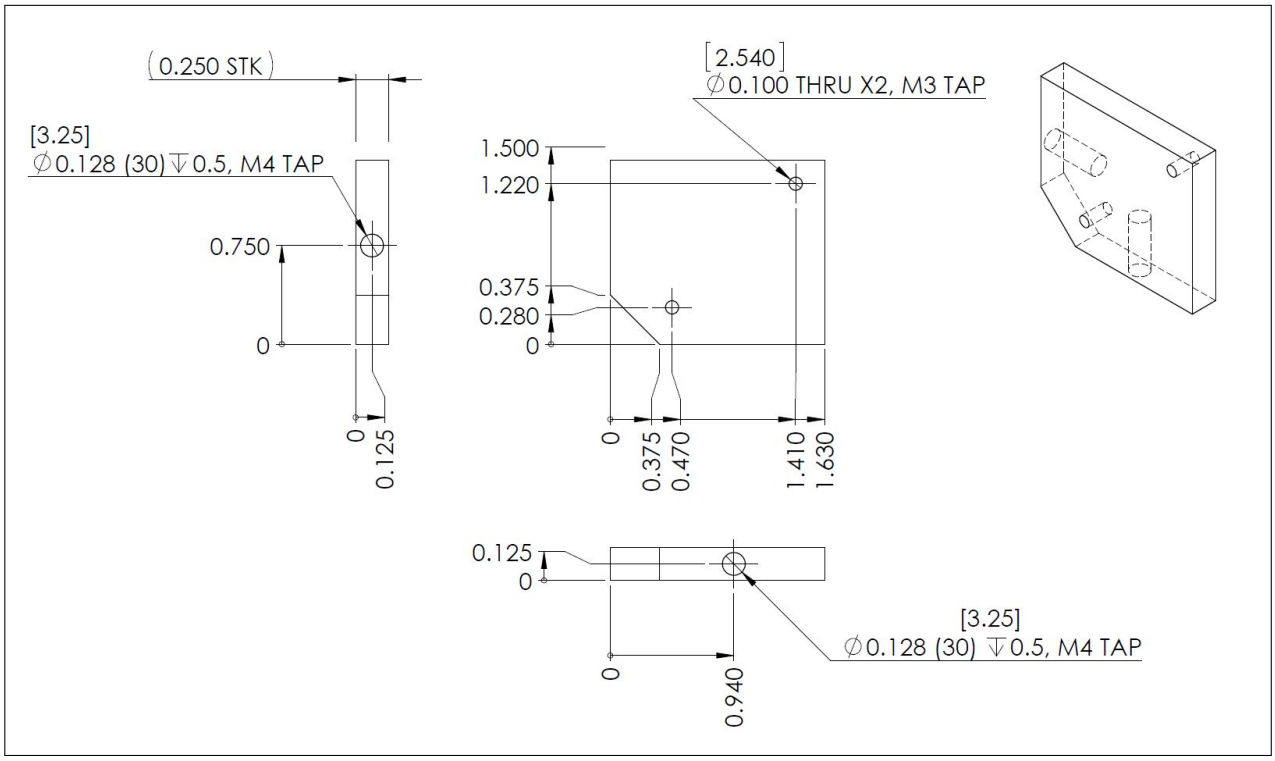

Figure A.19: Force Input Device - Load Cell Mounting Plate Detail. Material: Aluminum. UNLESS OTHERWISE SPECIFIED, ALL DIMENSIONS ARE IN INCHES.

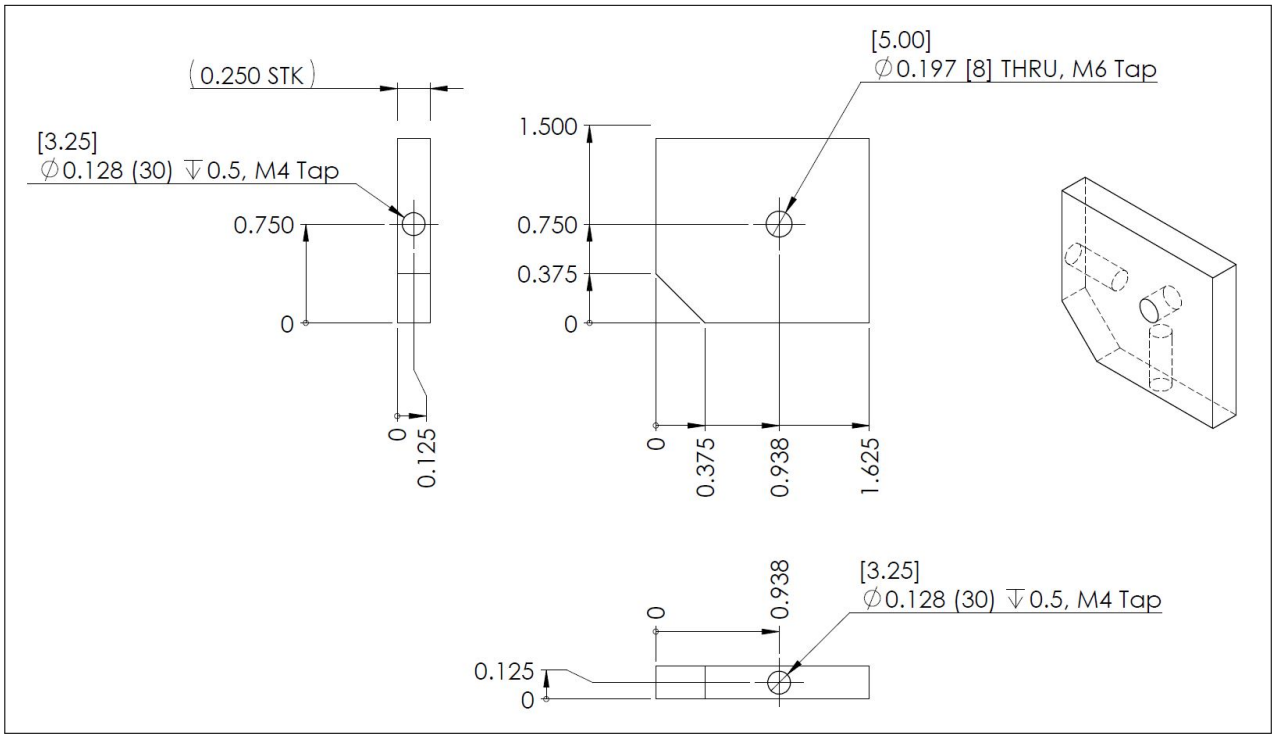

Figure A.20: Force Input Device - Preload Plate Detail. Material: Aluminum. UNLESS OTHERWISE SPECIFIED, ALL DIMENSIONS ARE IN INCHES.

A.2.4 Limit Switches

For the test bed, limit switches were placed on both extremes of travel. Fig. A.21 shows one of the two small custom brackets supporting a Keyence EZ-8M hall effect sensor installed onto the rack and aligned with steel plates (Seen in Fig. A.2) on the mobile base in order to detect the change in magnetic field.

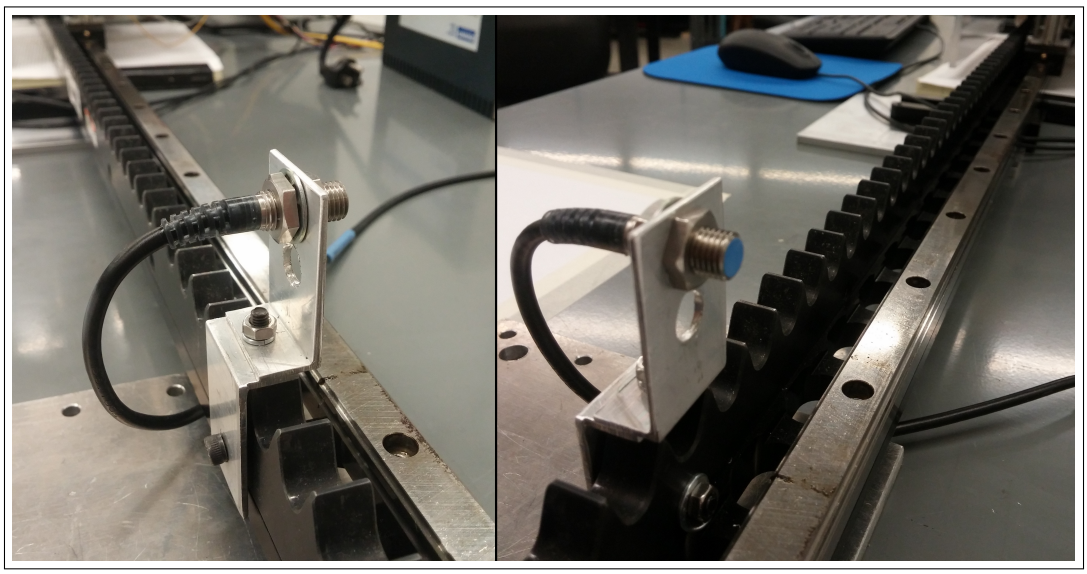

Figure A.21: Limit Switch installed on rack to detect mobile base.

A.3 Wiring Diagram

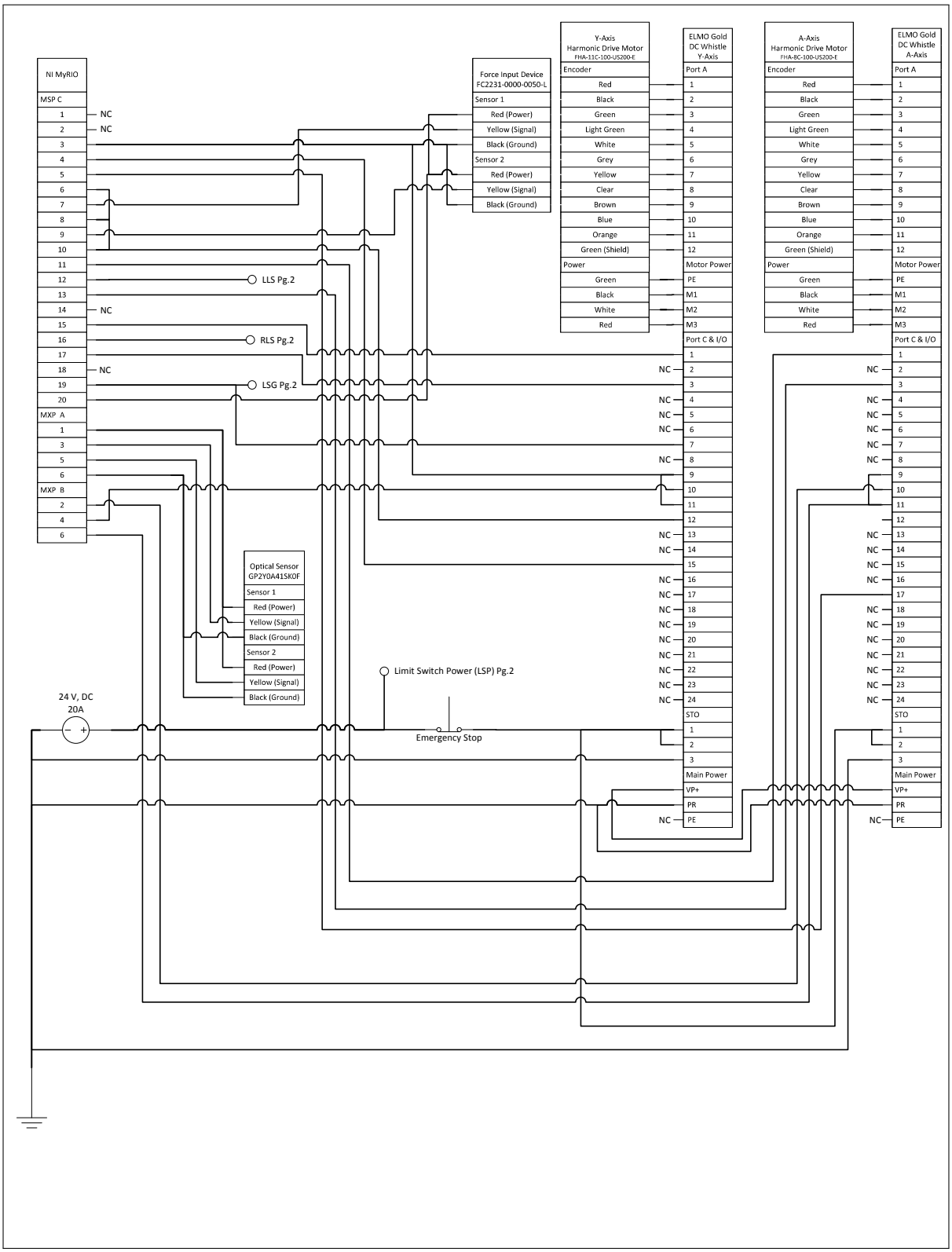

Figure A.22: Test Bed Wiring Diagram.

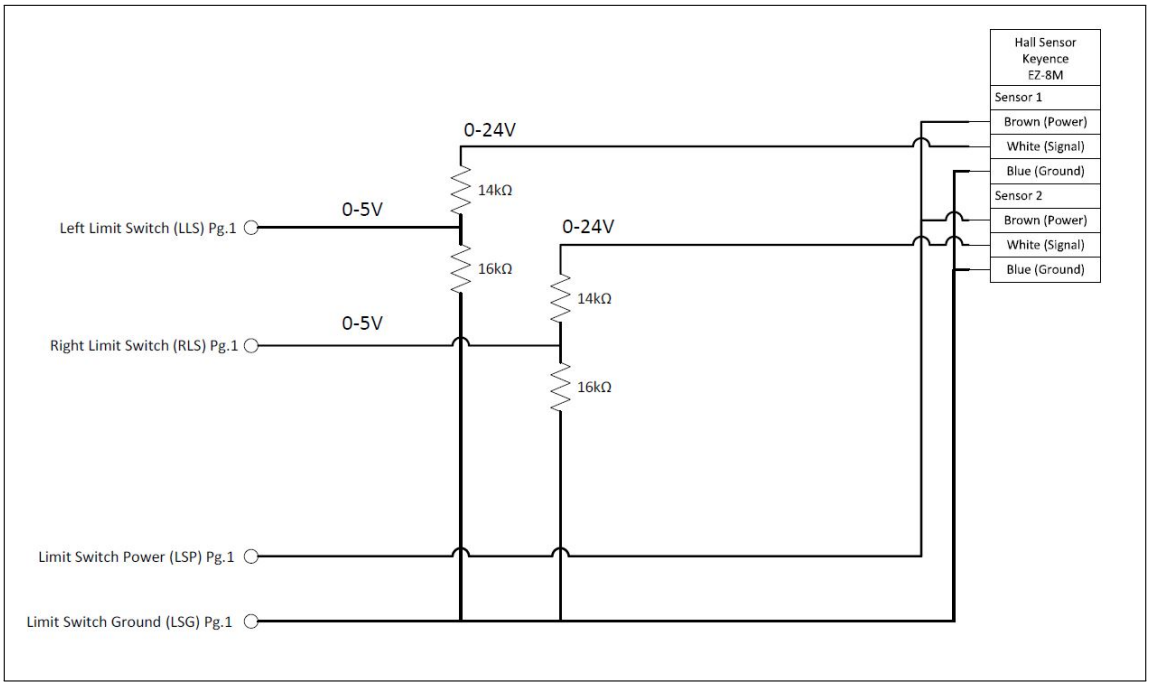

Figure A.23: Test Bed Wiring Diagram Continued - Voltage Divider for Limit Switch Circuit.

A.4 LabVIEW

A.4.1 LabVIEW Hardware and Communication

The following code was executed on a National Instruments (NI) myRIO-1900 embedded hardware device. LabVIEW 2014 64-bit software was used to program and deploy the virtual instrument (*.vi file). The myRIO used ethernet network communication with the PC and was setup with the following settings:

PC	IPv4 address:	192.168.0.80 (Static)
	Subnet Mask:	255.255.255.0
	Gateway:	192.168.0.1
	DNS Server:	0.0.0.0
myRIO	IPv4 address:	192.168.0.100 (Static)
	Subnet Mask:	255.255.255.0
	Gateway:	192.168.0.1
	DNS Server:	0.0.0.0

A.4.2 LabVIEW Software - Virtual Instruments (.vi)*

The program operating the test bed consisted of the following .vi:

Virtual Instrument (.vi) Name	**Summary**
TestBedVariableParameter.vi	Main program - Control Loop
A_ Axis_ BeamTracker.vi	Fixture-Structure Alignment Control
NearRegimeLogistic.vi	Calculates Near Regime Logistic Function
PosEst.vi	Position Estimate Based on Motor Encoder
VelEst.vi	Velocity Estimate Based on Motor Encoder
RoundTo_ 10.vi	Round input to Nearest Tenth (≈ 0.1)
RoundTo_ 1000.vi	Round input to Nearest Thousandth (≈ 0.001)
VeltoV.vi	Convert Velocity Command to Analog Voltage Signal

The following is a description of the operation of the above programs running in concert. See Fig. A.24-A.27 for highlighted areas of interest referring to the numbered points below.

1. Initialization
    (a) Identify the sample rate in milliseconds.
    (b) MyRIO samples initial force sensor voltage readings and to tear the force to zero.
2. Control Loop (Timed Loop)
    (a) A 1 kHz simulation Timing Source Clock.
    (b) Loop rate/frequency set by sample rate in (1).
3. Y-Axis Enable
    (a) Checks for Y Axis Enable Boolean
    (b) Commands the myRIO to send 0V (disable) or 10V (enable) to inhibit pin on Whistle Drive.
4. Force Input Device
    (a) Samples the two force sensors.
    (b) Subtracts the initial readings.
    (c) Takes the differential.
    (d) Passes the differential through a discrete low pass filter, with cutoff 140 rad/s. (Note: Must be recalculated with a change in sample rate.)
        i. Output Force Input voltage information to front panel.
        ii. Change voltage to force - Newton.
        iii. Display the force on front panel.

iv. Output Force Input, F (User), to the control loop.

5. Dock Force

   (a) Checks Apply Dock Force Boolean to set 0N or 5N of maximum dock force

   (b) Near-Regime behavior is applied by calculating the logistic equation [*NearRegimeLogistic.vi*]. See (13).

   (c) Outputs the force input bias, $F(dock)$, to our control loop.

6. Solve the ODE

   (a) Take the Force Input, $F(User)$, and sum it with the Variable Dock Force Output, $F(dock)$.

   (b) The ODE we want to solve for velocity, v, is :

$$F = M_d\dot{v} + B_d v. \tag{A.1}$$

   Therefore, we subtract Bv from our force, F, to yield $M_d\dot{v}$.

   (c) Once we have $M_d\dot{v}$, we can divide by the desired mass, M_d, to get $\dot{v}$.

   (d) To solve for v we must take the integral.

   (e) Before the discrete integration:

      i. A zeroing command prevents drift with small force commands, therefore a deadband is applied as a combination of force input and velocity. See (10).

      ii. An anti-windup loop is subtracted from v in order to prevent integrator windup due to the velocity saturation of 0.25 m/s. See (8).

7. Integration Approximation

   (a) We can now take the integral via discrete difference approximation

$$(\dot{v}[n] - \dot{v}[n-1])dt = v[n]. \tag{A.2}$$

(b) This result is now the calculated desired velocity, $v(cmd) = v[n]$.

8. Velocity Saturation

   (a) To keep the structure from moving too fast, a limit of 0.25 m/s was set.

   (b) A simple check to see if the $v(cmd)$ is above 0.25:

      i. if $v(cmd) \leq 0.25m/s$, send the $v(cmd)$ command through.

      ii. if $v(cmd) > 0.25m/s$, then clip the command and only send $v(cmd) = 0.25m/s$.

   (c) This however does not change v(cmd) from being well above the saturation and therefore needs to be communicated back to the loop so that there isnt lag in the system. (Integrator Windup)

9. Anti-Windup Feedback

   (a) Take the difference: $v(cmd) - v(cmd)_{sat}$.

   (b) Gain this difference and subtract it from our integrand, $\dot{v}$.

10. Anti-Creep

    (a) Because the input commands eventually resolve to being very small, but non-zero, an anti-creep keeps the velocity at zero when small inputs and velocity outputs are realized.

    (b) Round force input voltage to nearest 0.1.

    (c) Round $v(cmd)_{sat}$ to nearest 0.001.

    (d) If both force input voltage and $v(cmd)_{sat}$ round to zero, then zero the command velocity, $v(cmd)_{sat} = 0$.

11. Velocity Command to Voltage

(a) The motor drive commands a velocity based on an analog signal 0-5V.

(b) Once a desired velocity in [m/s] is found, the [*Velocity Command to Voltage.vi*] maps this to possibly 0-5V.

(c) Since the signal is more susceptible to noise at low voltage, an offset was made, making 3V as 0 m/s command, e.g.:

i. 5V is +0.25 m/s command

ii. 1V is -0.25 m/s command

12. Variable Damping Parameter

(a) Like Dock Force, F(dock), in section 4, variable damping follows similar rules.

(b) Near-Regime behavior is applied by calculating the logistic equation [*NearRegimeLogistic.vi*]. See (13).

(c) This value is fed into the control loop for calculating $B_d v$.

13. Near-Regime Behavior

(a) A value is calculating the logistic equation (shown for damping, B, but will be used for dock force too)

$$B_m(\tilde{x}) = \begin{cases} B_d, & \tilde{x} \geq x_n \\ \left(\dfrac{2\left[(B_m)_{max} - B_d\right]}{1 + e^{[\tilde{x} - x_{ns}]/r_B}} \right) + B_d, & x_{ns} \leq \tilde{x} < x_n \\ (B_m)_{max}, & \tilde{x} < x_{ns}, \end{cases} \tag{A.3}$$

based on:

x	Optical fixture-structure proximity.
r	Distance constant.
B_d or F_d	Far-Regime initial value.
$(B_m)_{max}$ or $(F)_{max}$	Maximum value at Saturation.

(b) The result is then applied to the ODE solution loop.

14. A-Axis Beam Tracker

    (a) This VI takes two optical distance measurements and outputs the distance from the center of the fixture to the structure.

        i. Takes voltage readings from two sensors.

        ii. Translates the voltages into distances.

        iii. Calculates an average between the two readings to give a center distance value.

        iv. A running average of this center distance is taken and outputted.

    (b) The output is noisy and requires filtering.

    (c) A low pass filter with approximately 5 rad/s cutoff frequency was used.

15. Encoder Feedback

    (a) For visualization purposes, the MyRIO can interpret emulated encoder signals to obtain motor position [*PosEst.vi*].

    (b) From position a differential estimator is used in order to yield a velocity as well [*VelEst.vi*].

16. Limit Switches

    (a) For safe reasons, two limits on travel were placed using Hall effect sensors.

    (b) The myRIO takes two analog signals in (Hall Sensor Output).

(c) Checks if either signal is high.

(d) If they are:

   i. Zero all commands.

   ii. Disable all motors.

   iii. Stop control loop execution.

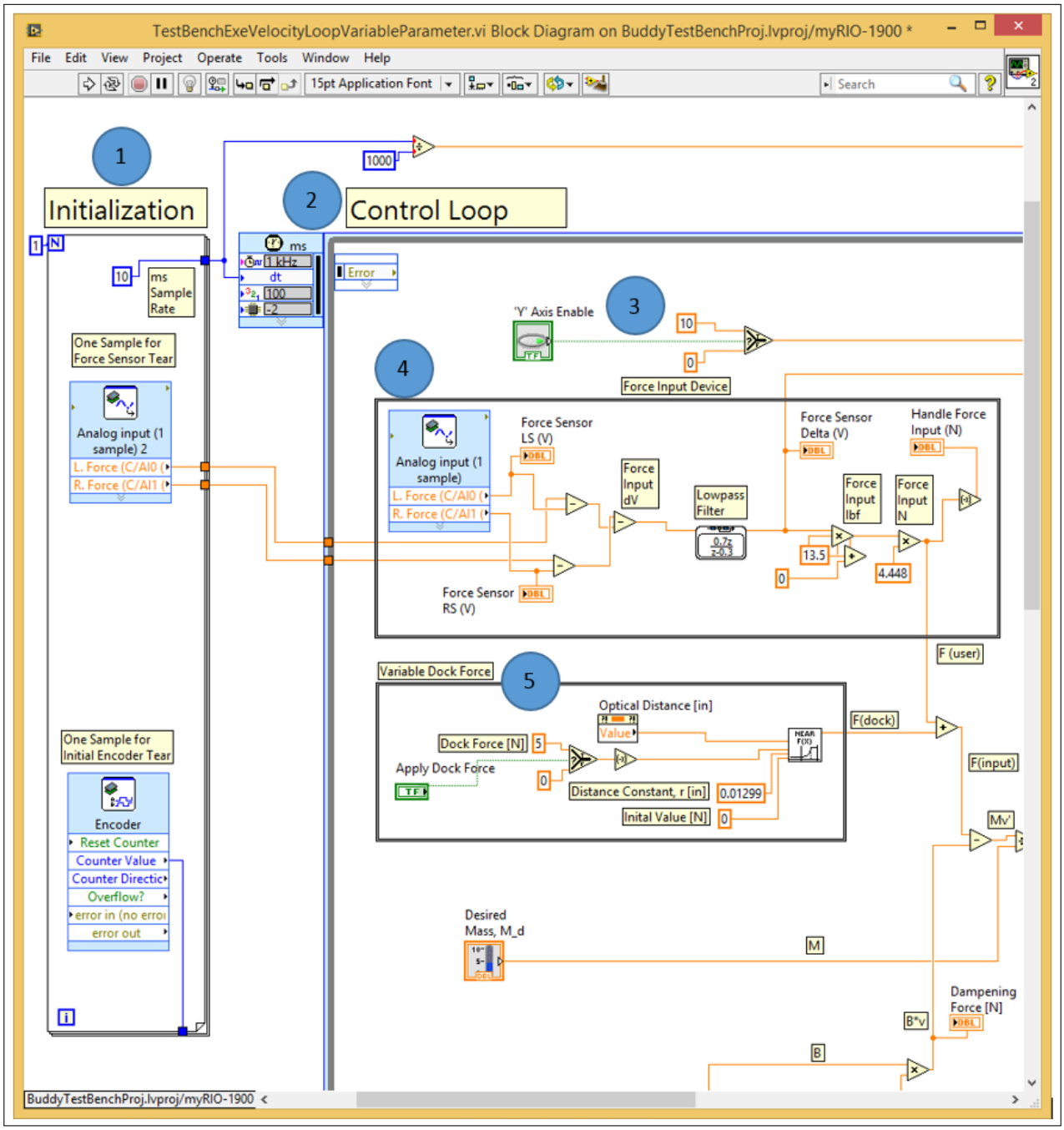

Figure A.24: LabVIEW TestBenchExeVelocityLoopVariableParameter.vi - Main control loop showing: ① Initialization; ② Control Loop; ③ Y-Axis Enable ; ④ Force Input Device; ⑤ Dock Force.

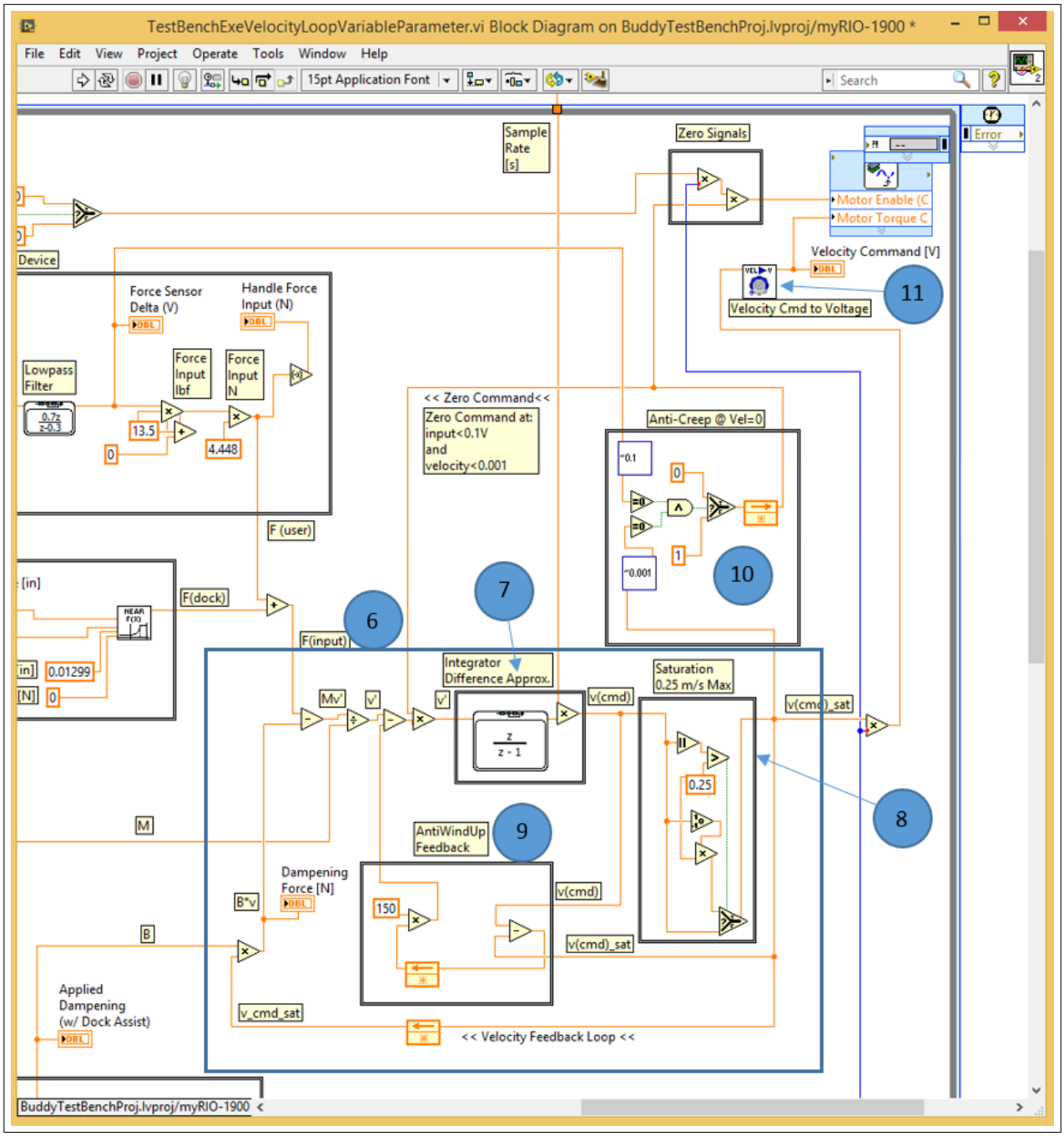

Figure A.25: LabVIEW TestBenchExeVelocityLoopVariableParameter.vi - Main control loop continued, showing: ⑥ Solving the ODE ⑦ Integral Approximation; ⑧ Velocity Saturation; ⑨ Anti-Windup; ⑩ Anti-Creep; ⑪ Command Velocity to Voltage.

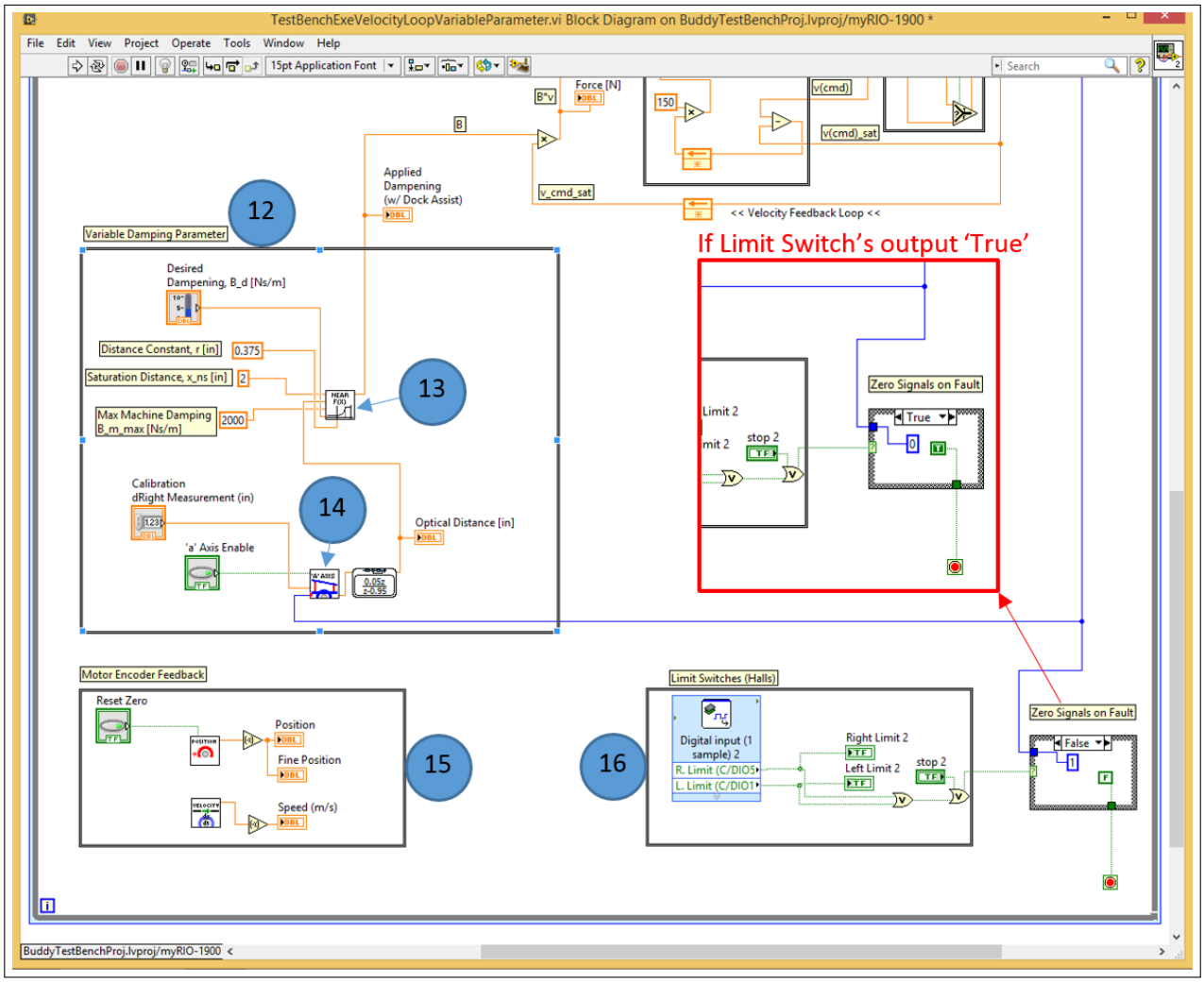

Figure A.26: LabVIEW TestBenchExeVelocityLoopVariableParameter.vi - Main control loop continued, showing: ⑫ Variable Damping; ⑬ Near-Regime Behavior; ⑭ A-Axis Beam Tracker; ⑮ Encoder Feedback; ⑯ Limit Switches.

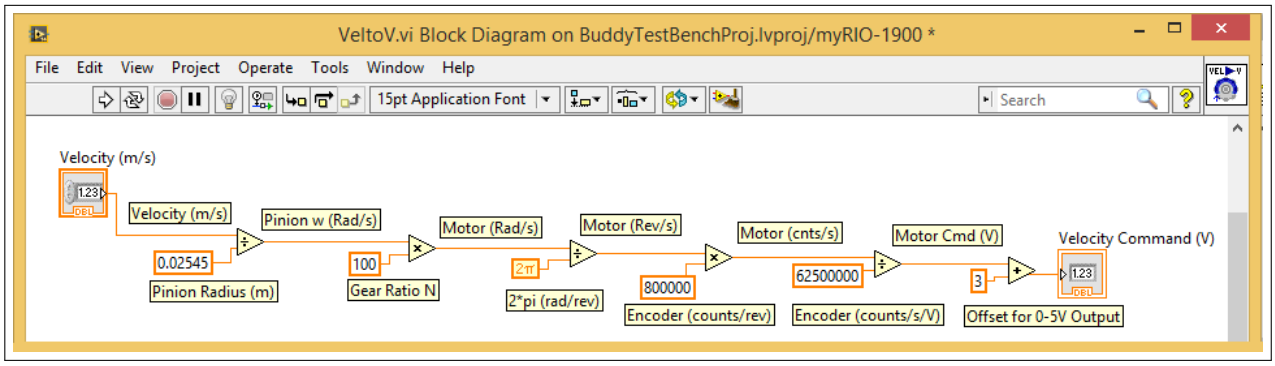

Figure A.27: LabVIEW VeltoV.vi - Velocity Command to Voltage Signal for motor drive: Steps through the math when taking the velocity commanded down through rotations, gear reductions, and encoder translations to yield a reference voltage for the motor to track.

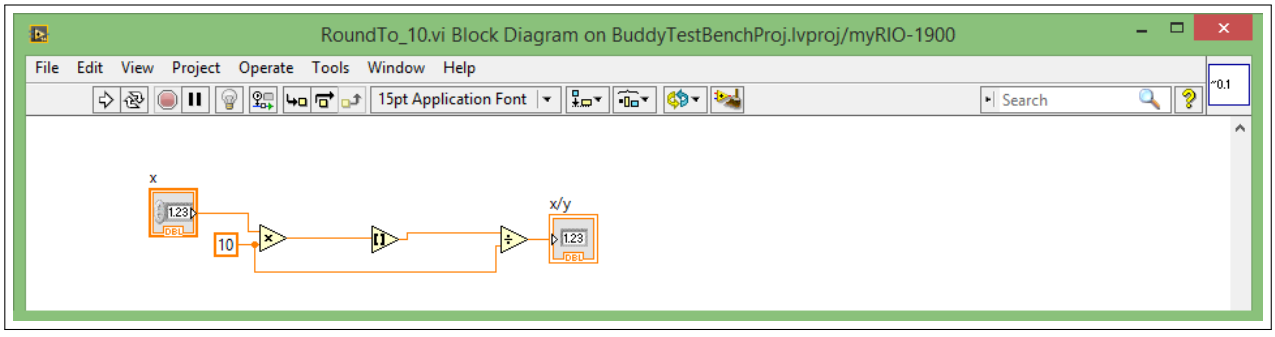

Figure A.28: LabVIEW RoundTo_ 10.vi - Custom Rounding Function: Rounds the input to the nearest 0.1.

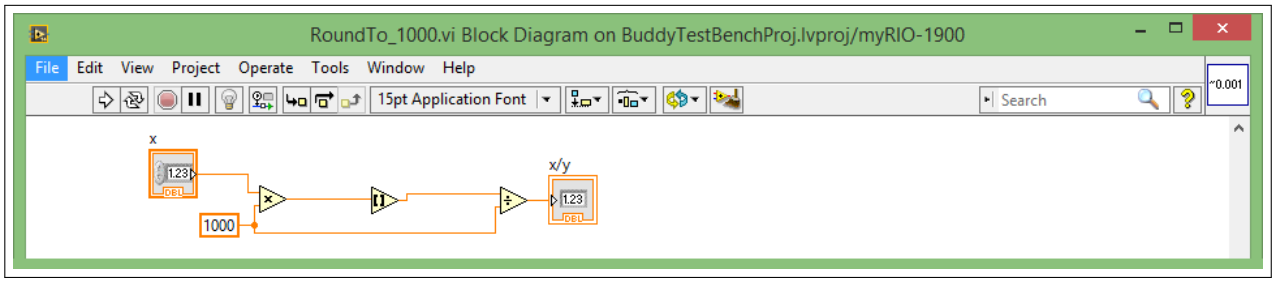

Figure A.29: LabVIEW RoundTo_ 1000.vi - Custom Rounding Function: Rounds the input to the nearest 0.001.

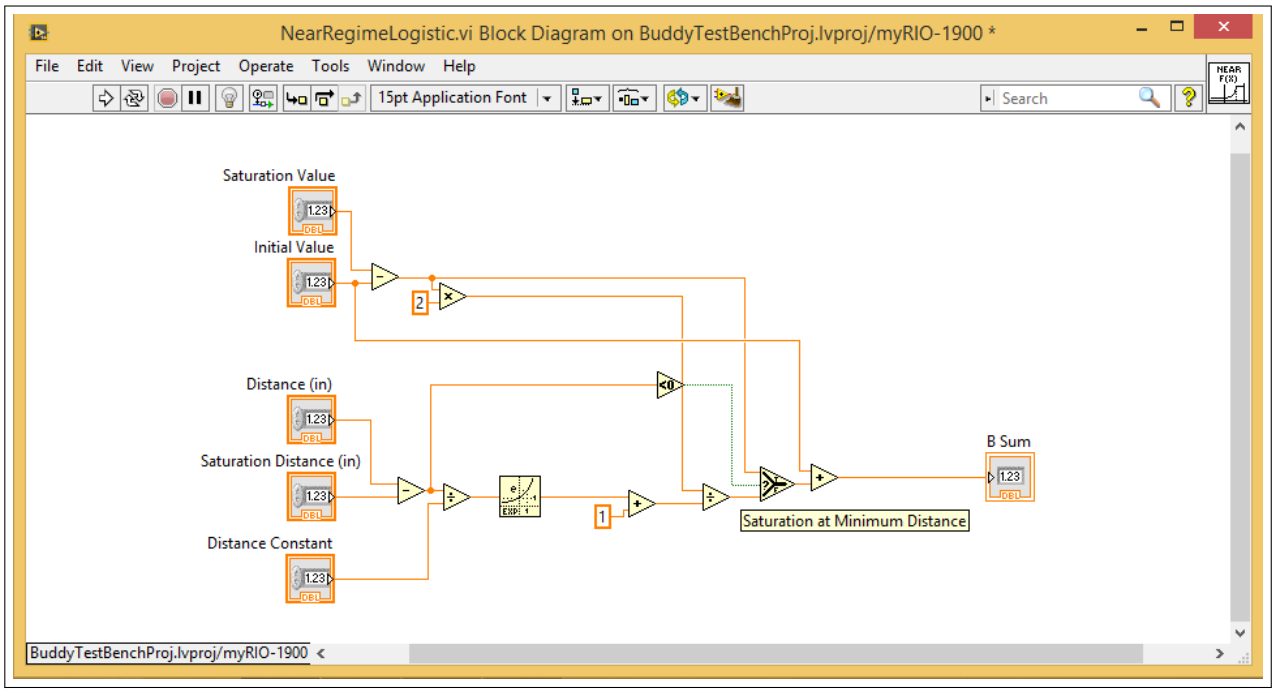

Figure A.30: LabVIEW NearRegimeLogistic.vi - Custom function to calculate the logistic function developed for variable damping and dock force.

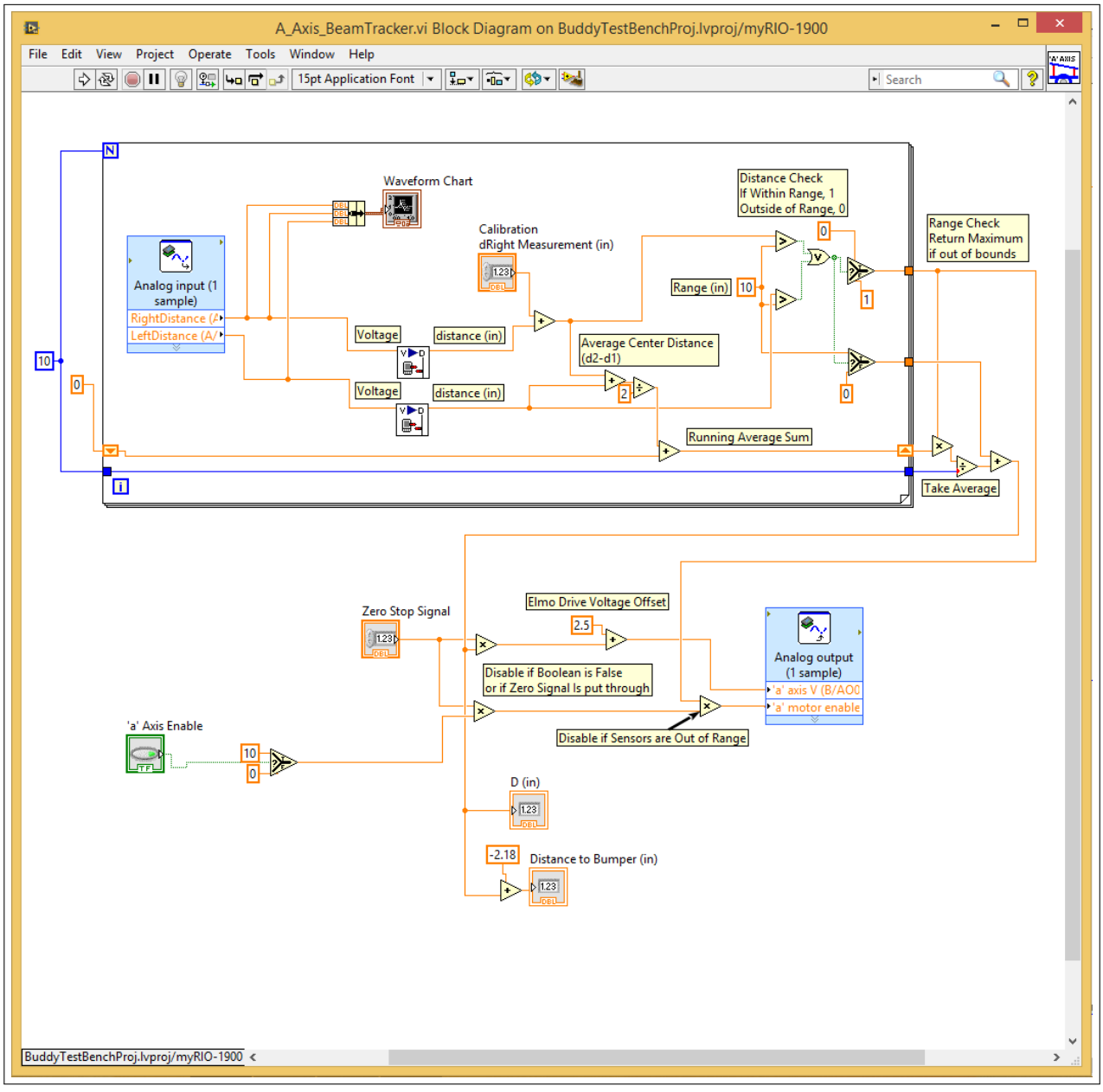

Figure A.31: LabVIEW A_ Axis_ BeamTracker.vi - Fixture Alignment Command: Reads in optical sensor information and outputs error for the alignment motor (A-Axis) to act on, as well as a center distance from the fixture to the structure in order to calculate the logistic equation. Also sets limitations on the A-Axis movements in case of insufficient sensor data or failure.

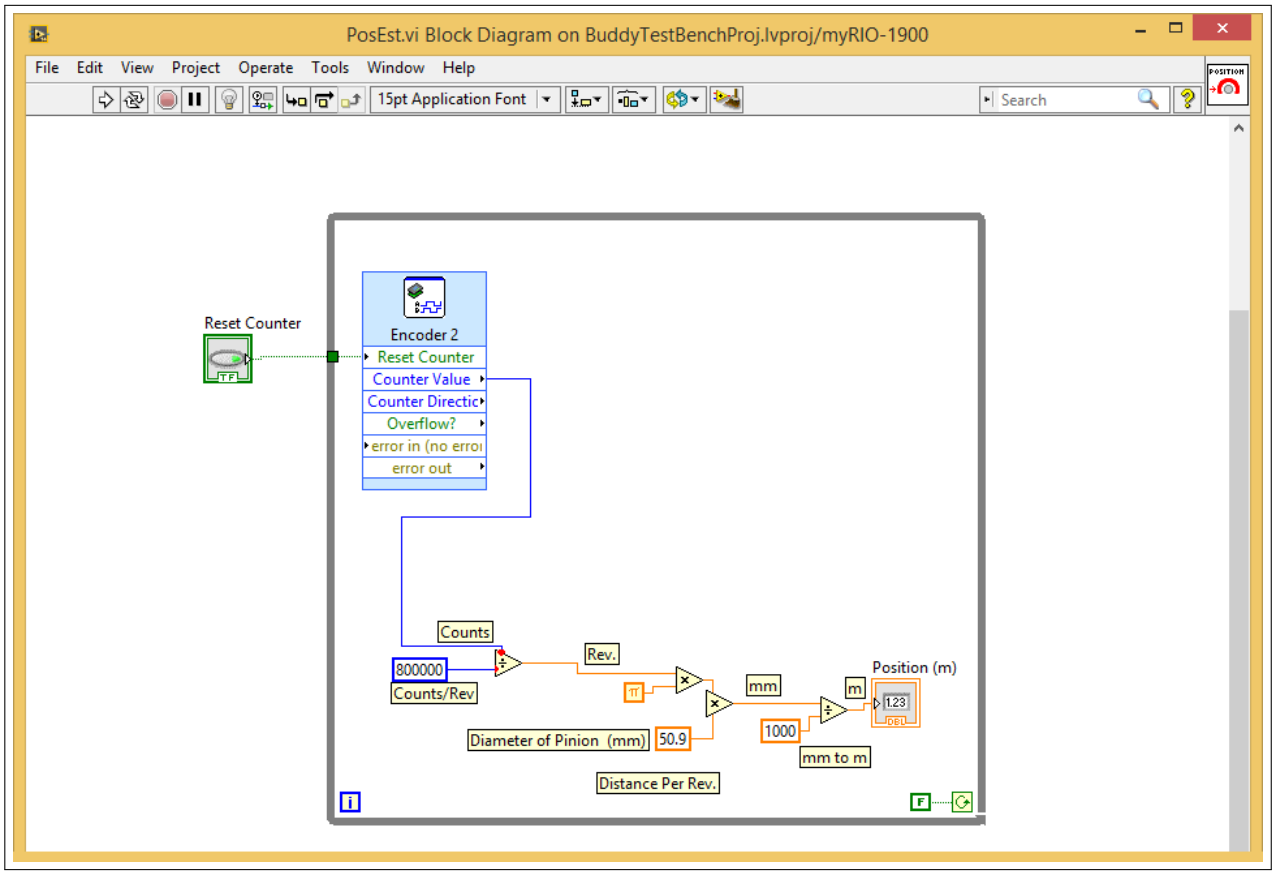

Figure A.32: LabVIEW PosEst.vi - Estimates position: Queries the motor encoder count and does the mapping to position based on counts per revolution, gearing, and pinion radius.

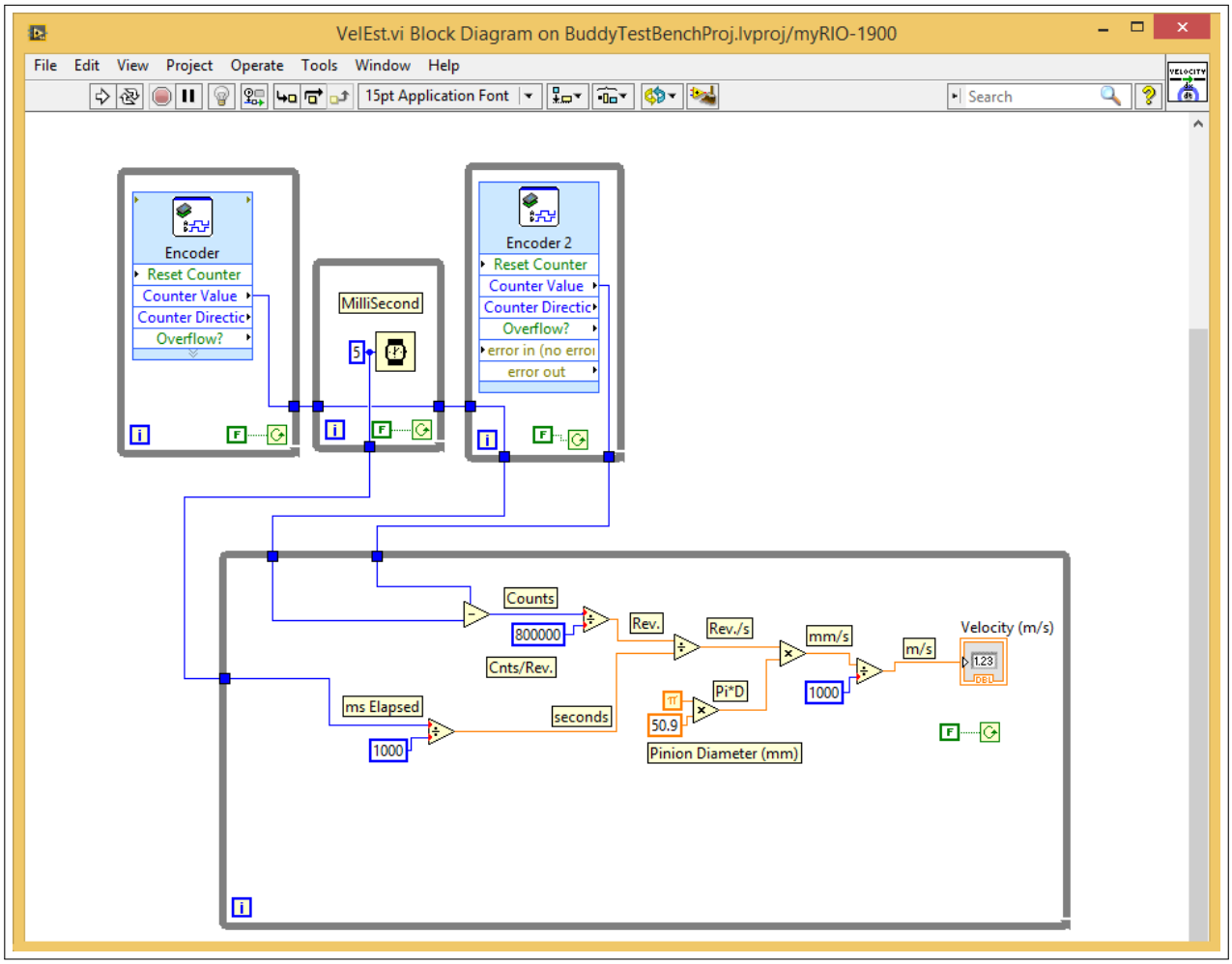

Figure A.33: LabVIEW VelEst.vi - Estimates velocity: Queries the motor encoder before and after a time step (5ms in this case) and takes this difference over the step size in order to do a estimate of velocity from position.

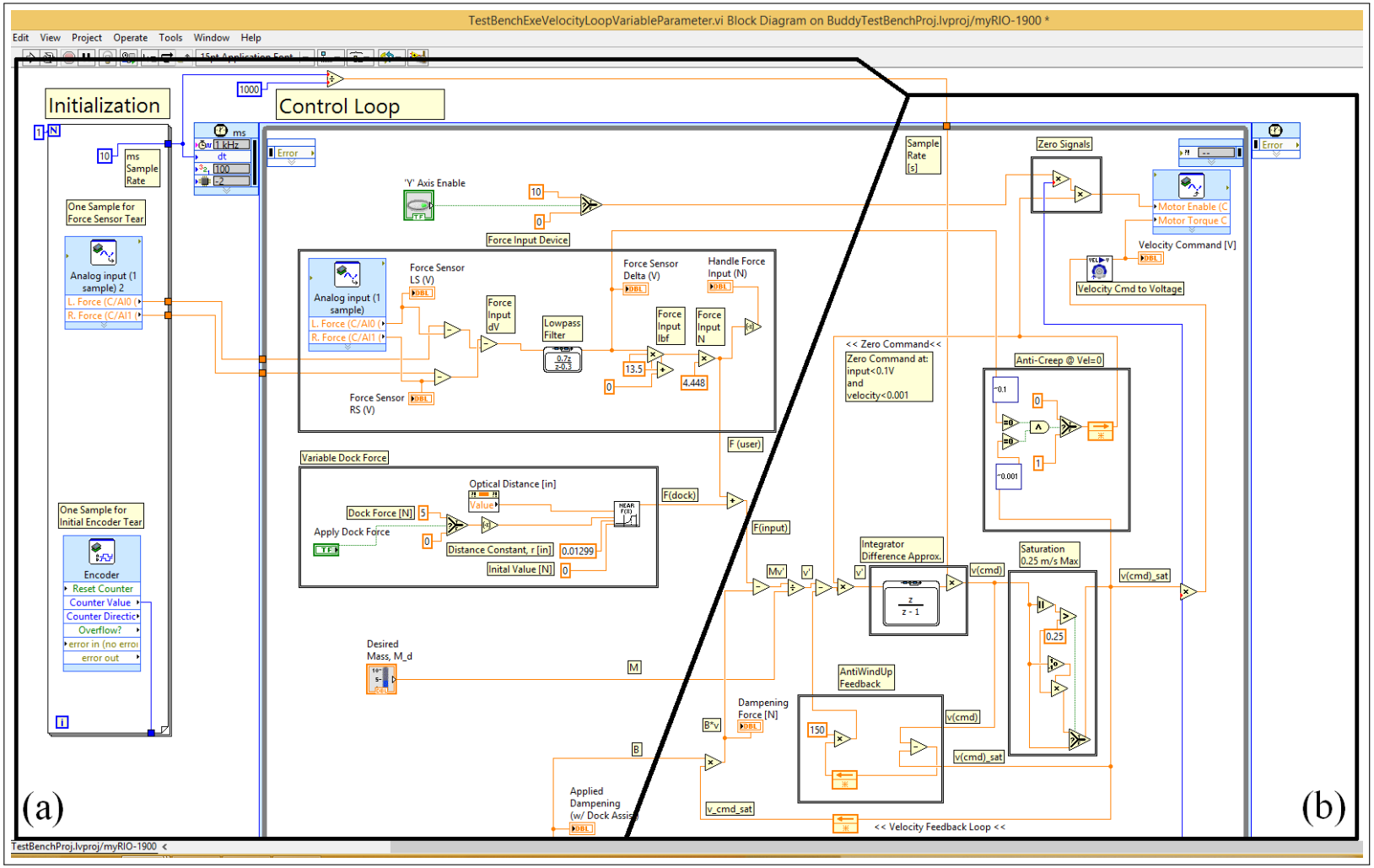

Figure A.34: LabVIEW Control Loop Overview. For more detail: (a) Fig. A.24; (b) Fig. A.25.

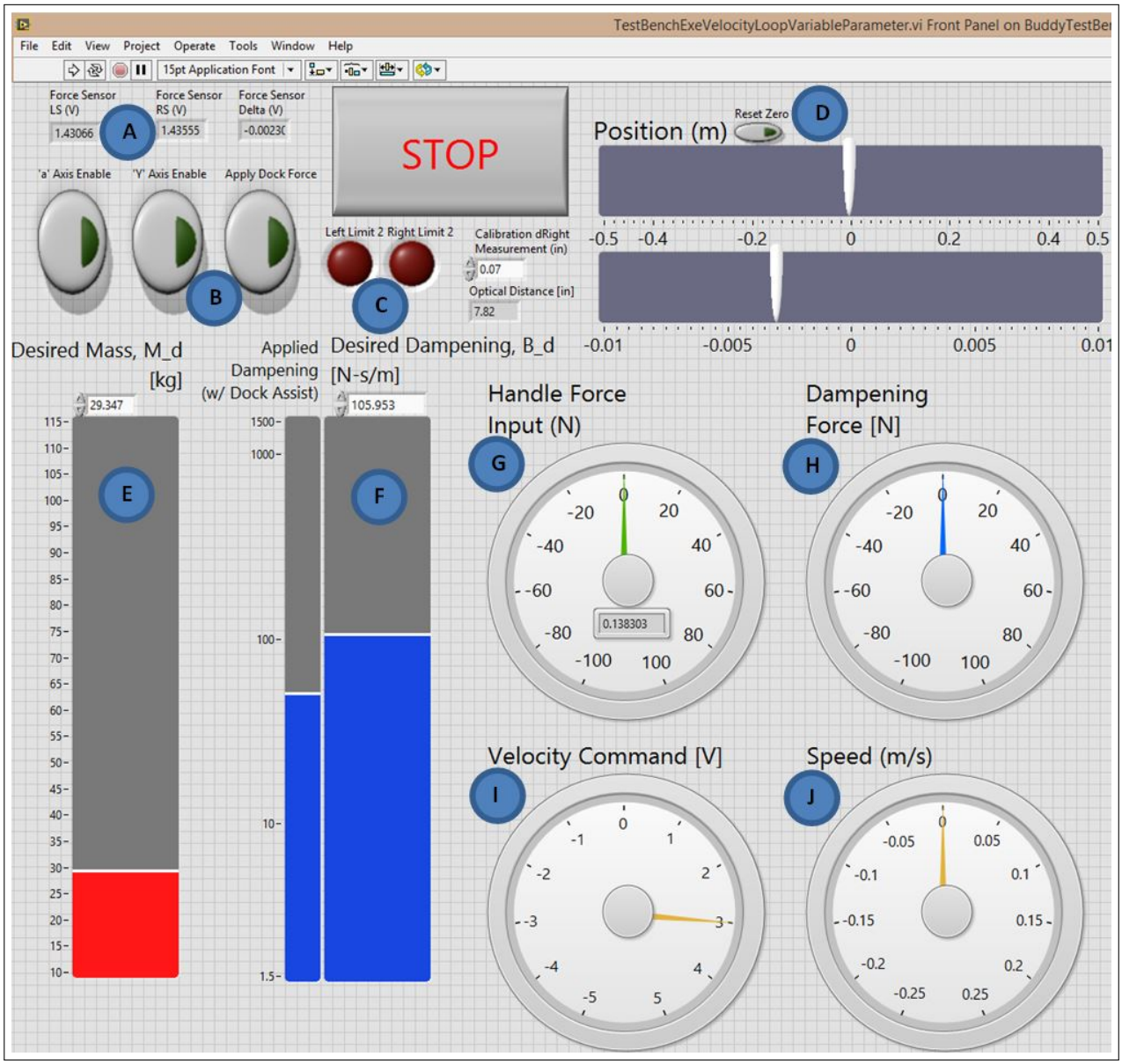

Figure A.35: Test Bed Main Program Front Panel: Ⓐ Load Cell Voltage and Difference; Ⓑ Enable Switches, Boolean Logic; Ⓒ Limit Switch LED Indicators, Optical Distance Sensor Readout, and Optical Sensor Calibration Offset; Ⓓ Motor Encoder Position Feedback - Gross and Fine Scaled Readouts; Ⓔ Desired Mass, M_d, Input; Ⓕ Desired Damping, B_d, Input and Applied or Machine Damping, B_m (left column); Ⓖ Force Measured by the Force Input Device; Ⓗ Calculated damping force from applied damping and simulated reference model velocity; Ⓘ Calculated velocity command converted into voltage output to the motor drive; Ⓙ Velocity of the fixture estimated from motor encoder position feedback and loop time step.

A.5 Elmo

A.5.1 Elmo Hardware - Whistle Drive

In order to control the two Harmonic Drive servo motors (Y-Axis Along the Rack and Guide rail and A-Axis Fixture Alignment), each utilized an Elmo G-DCWHI20/100EE Gold DC Whistle Digital Servo Drive. Fig. A.2 shows these two drives stacked with the NI myRIO. These were both 24V powered and interfaced with the other hardware via USB communication and analog signals. The software to program these drives, Elmo Application Studio (EAS) II, was supplied by Elmo and provided PI loop tuning for position, velocity, and current control of the motor using these drives.

A.5.2 Elmo Software - Elmo Application Studio (EAS) II

In order to control the motor drives, Elmo provided Elmo Application Studio II (EASII) to interface with the Whistle Drives described in the previous section. USB communication was used to program the drives, and to achieve our test bed setup the following steps were used:

1. Download and Install EASII
2. USB connection with drive - Plug and Play, Direction Communication with Software.
3. Setup a workspace and add gold drive.
4. Enter the parameters of the motor and select the mode of command operation (position, velocity, or current).
5. Enter feedback settings.
6. Automatically tune the motor.
7. Enable encoder emulation to output encoder quadrature on port A (for the myRIO).

8. Set inhibit pit to have the ability to enable/disable the motor via digital input.

9. Set ECAM and Direct Reference Command to enable analog input commanded velocity.

10. Save parameters to the drive.

11. Restart (unplug and plug back in) drive.

Fig. A.36- A.37 show these steps using EASII.

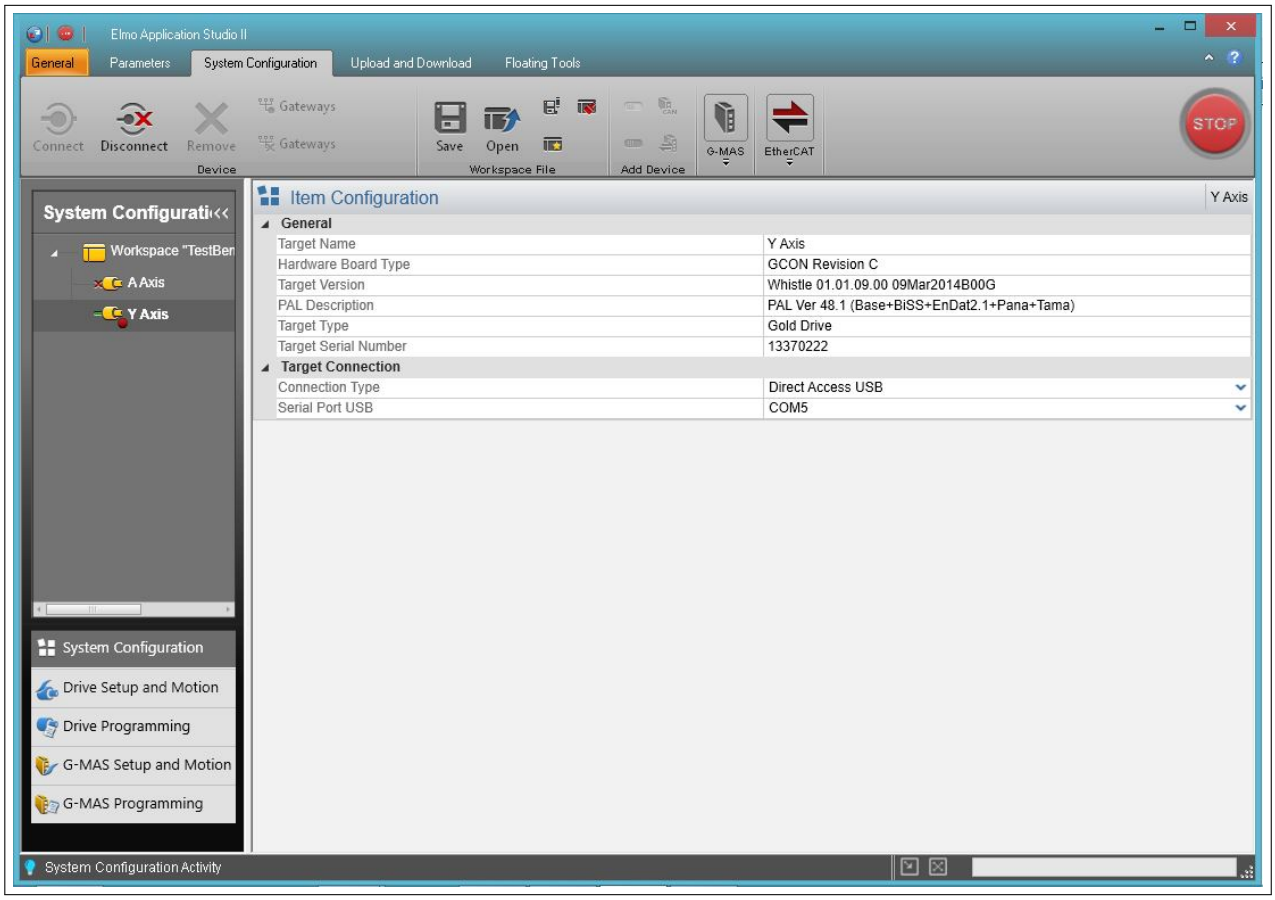

Figure A.36: EASII Setup 1-3: Once installed, open EASII and create a new workspace in the System Configuration Tab section. Connect the drive via USB. Add a drive in the left-hand column by right clicking the workspace, and enter the drive's connectivity information ("Target Connnection"). Click "Connect".

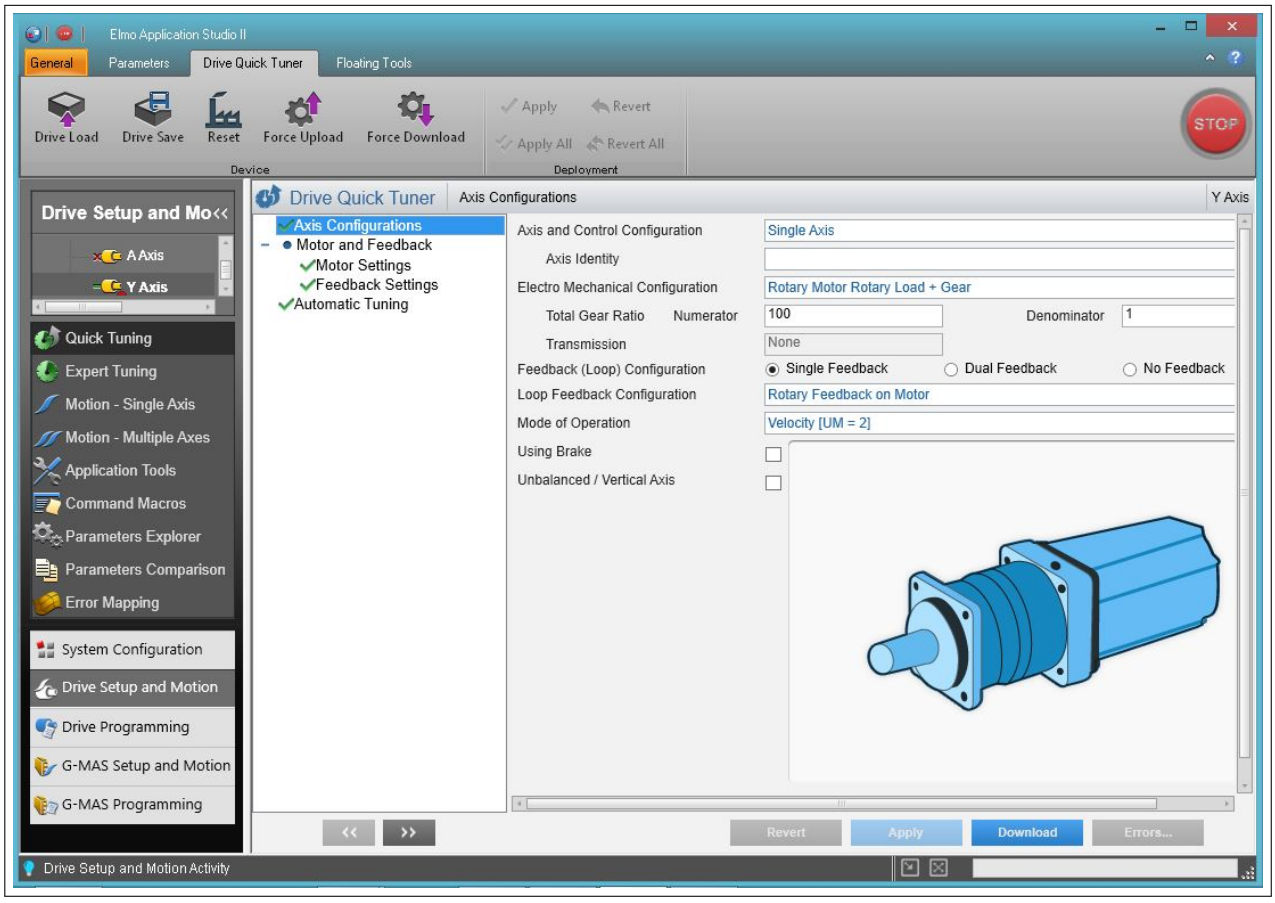

Figure A.37: EASII Setup 4: Now that the drive is connected. Click the "Drive Setup and Motion" tab on the left-hand side, and navigate to "Quick Tuning". This will now present the above display. Enter the parameters for the motor you are controlling. Shown is the Y-Axis or the Mobile Base axis.

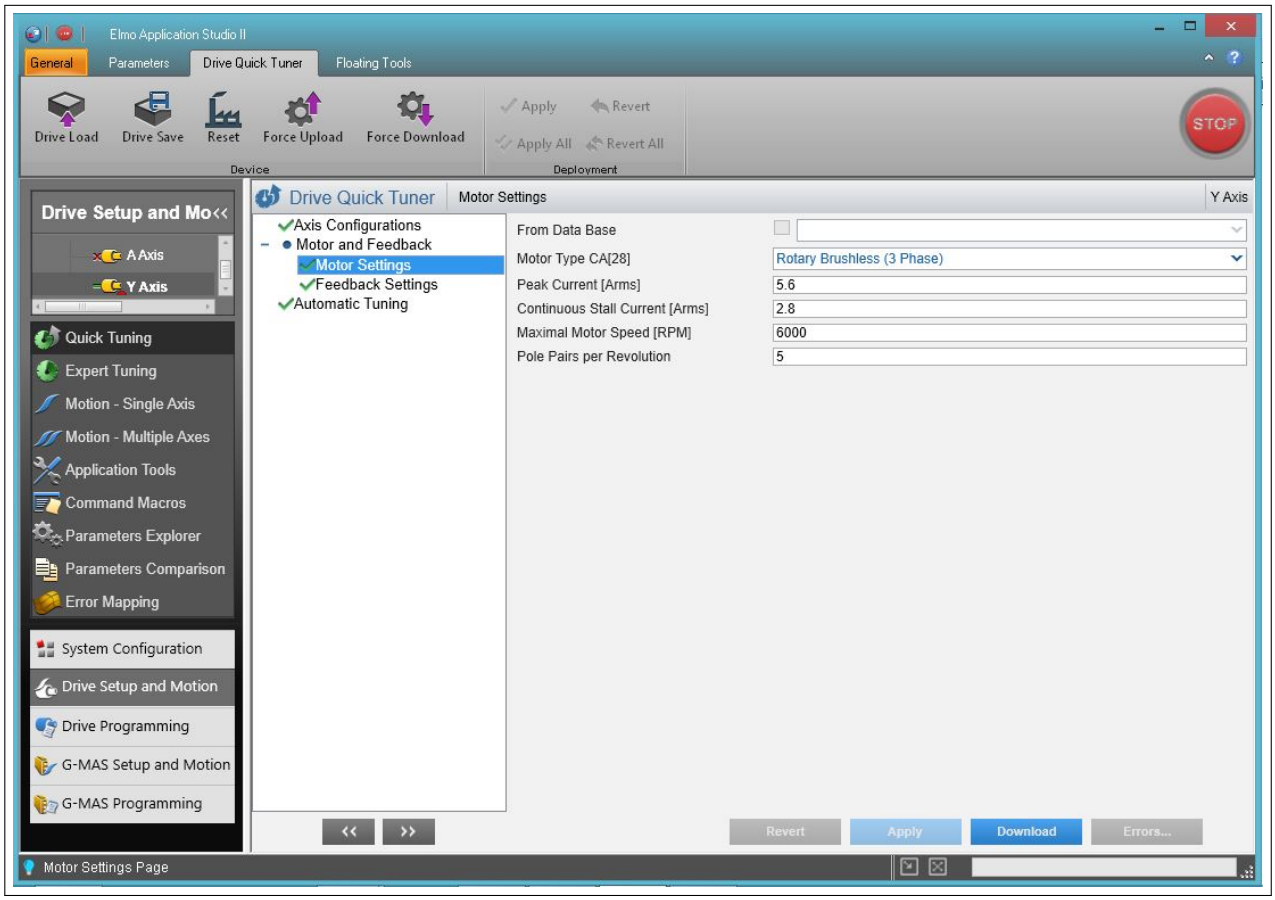

Figure A.38: EASII Setup 4: Continue to enter the motors parameters.

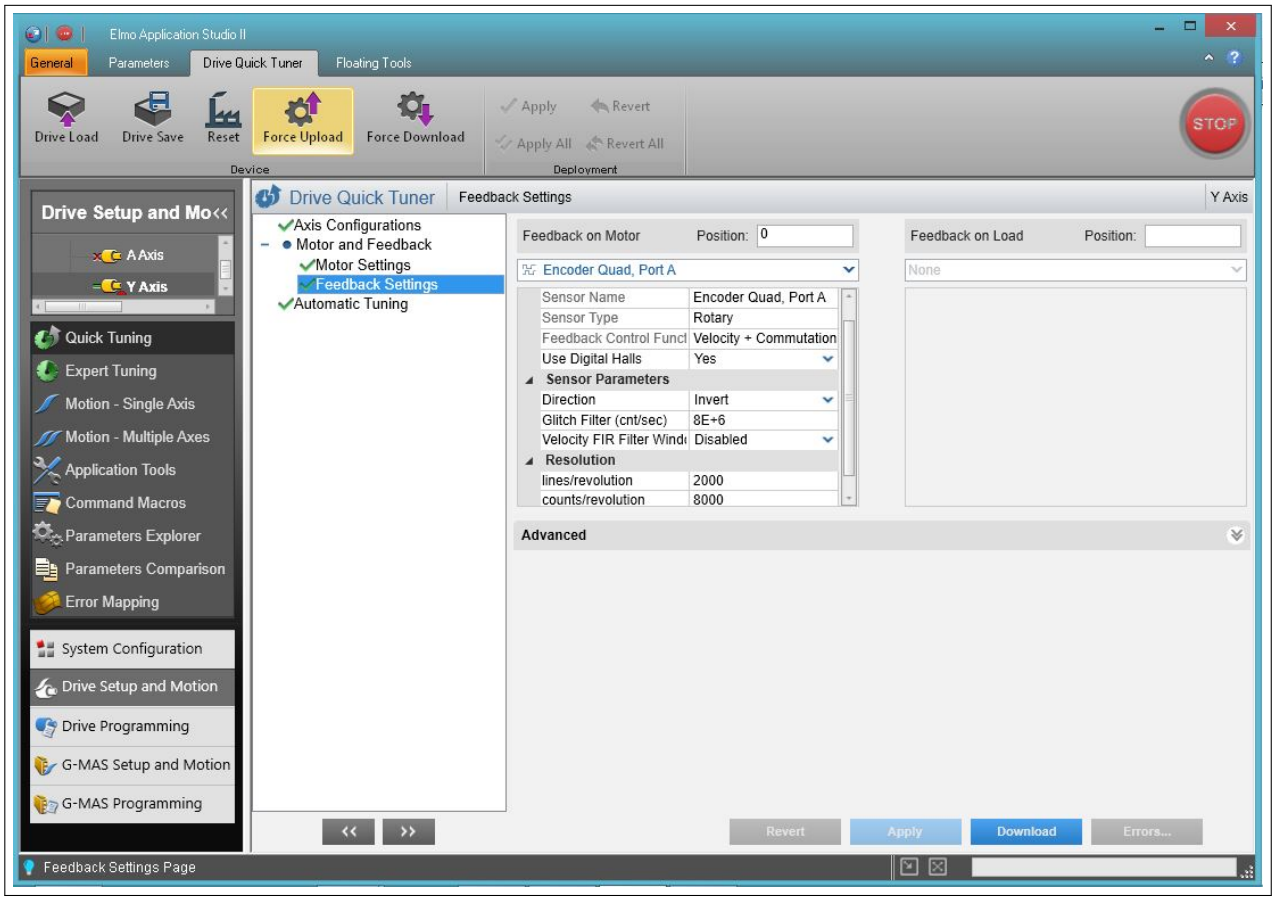

Figure A.39: EASII Setup 5: Enter the feedback information available to the motor and used for control.

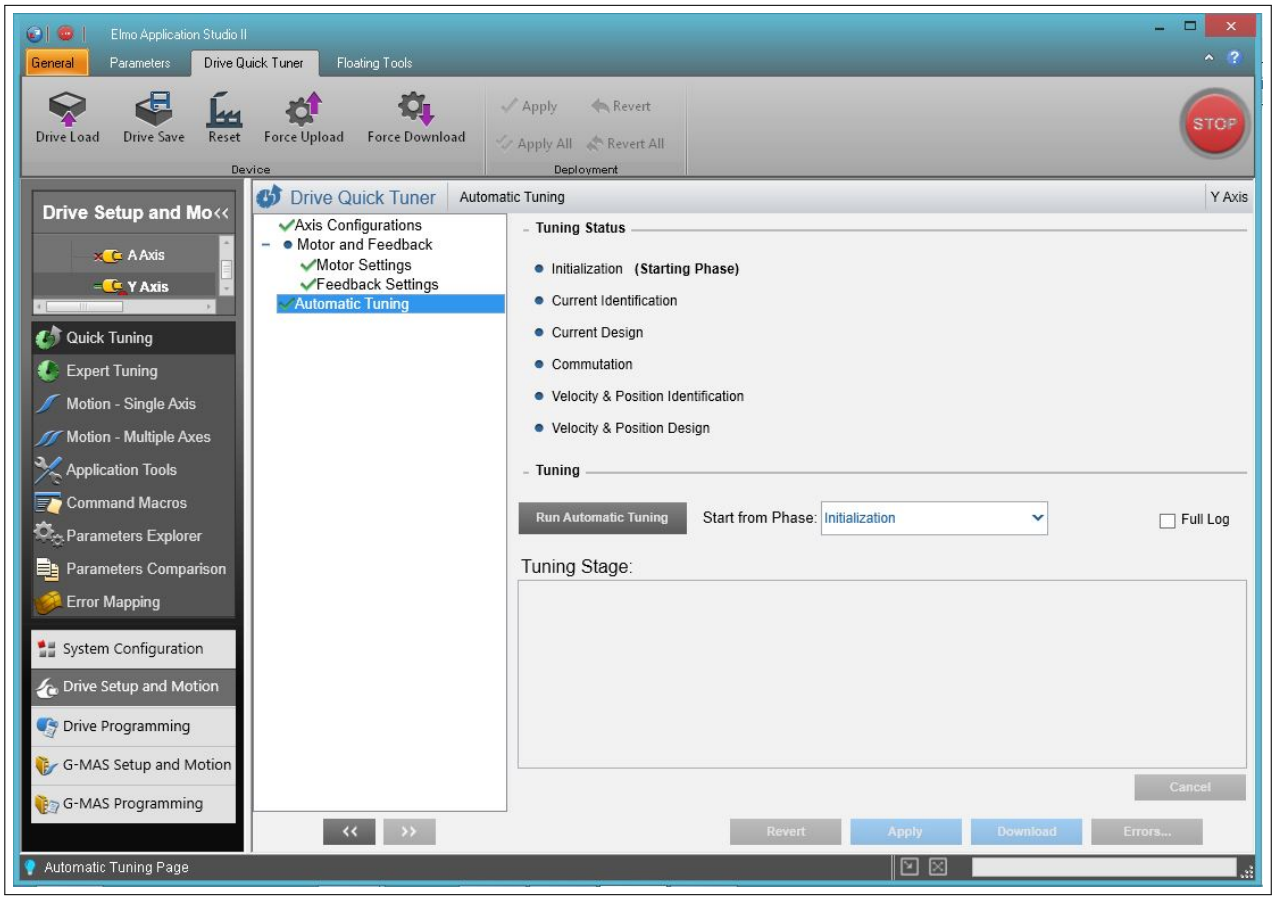

Figure A.40: EASII Setup 6: Once all the information is entered the software will now attempt to tune the motor using the control indicated in step 4. Be sure the motor is fully installed in the application, the power to the motor's drive is on, and any STO or emergency stop circuit is allowing for motor movement.

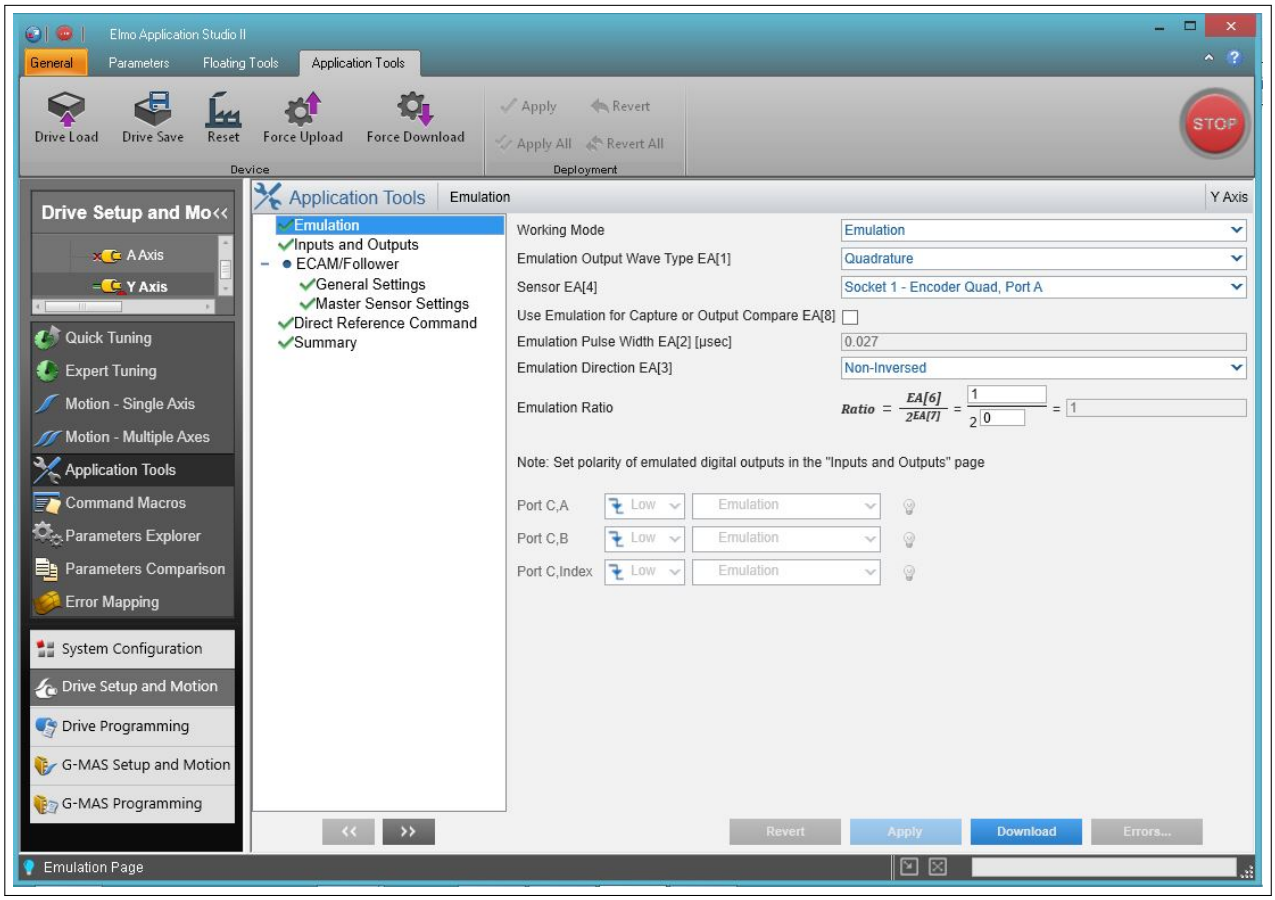

Figure A.41: EASII Setup 7: Now that the motor is tuned, selecting the "Application Tools" section on the left-hand side in order to setup inputs and outputs. For this application, "Emulation" is desired to output encoder quadrature to the myRIO, therefore the above setting will output this signal on Port A. See Wiring Diagram Section for more information.

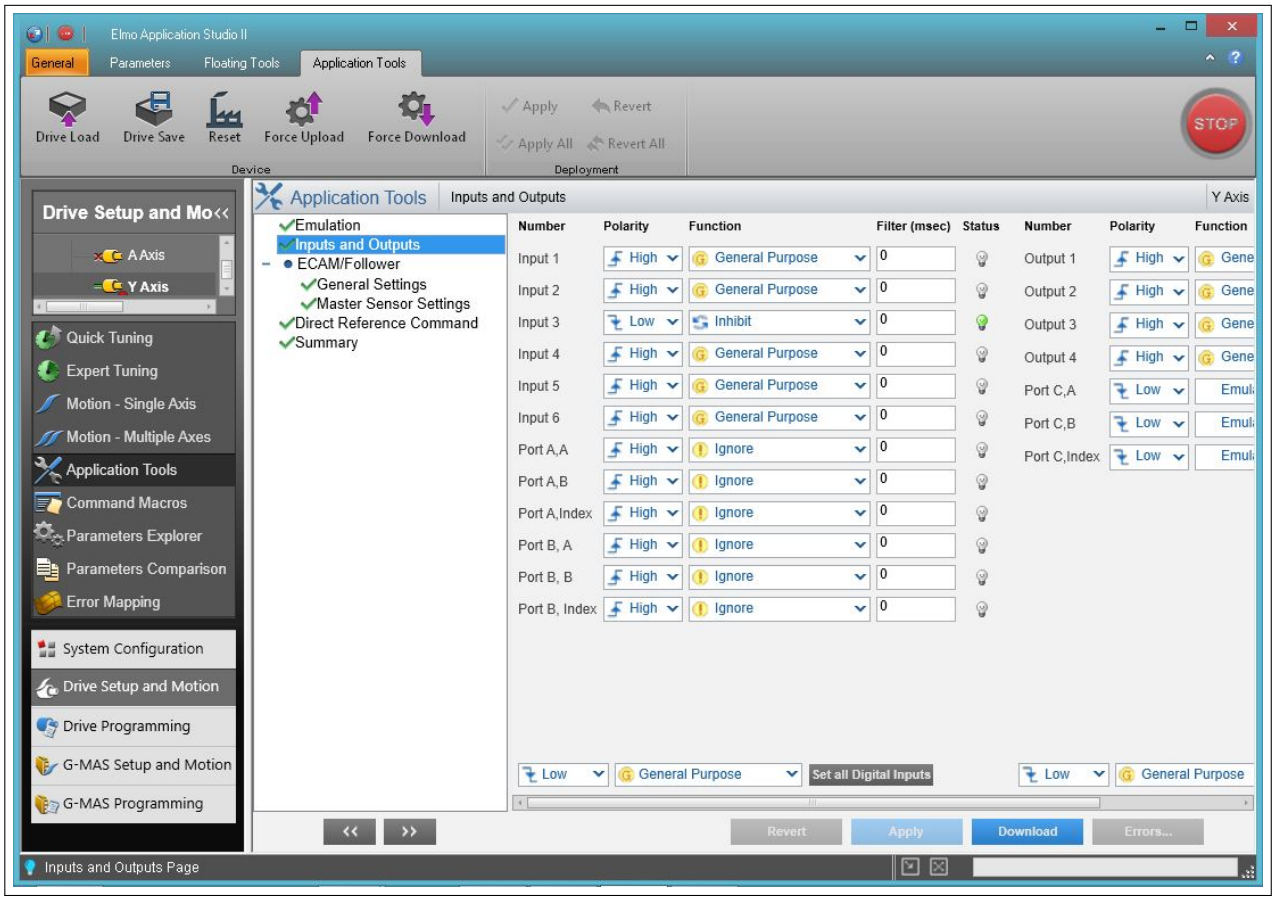

Figure A.42: EASII Setup 8: Selecting "Inputs and Outputs" will allow setting an inhibit pin to control motor enable/disable. This is normally set low, instead of high, because we want the motor to be disabled when no signal/power is received, or inhibit when low.

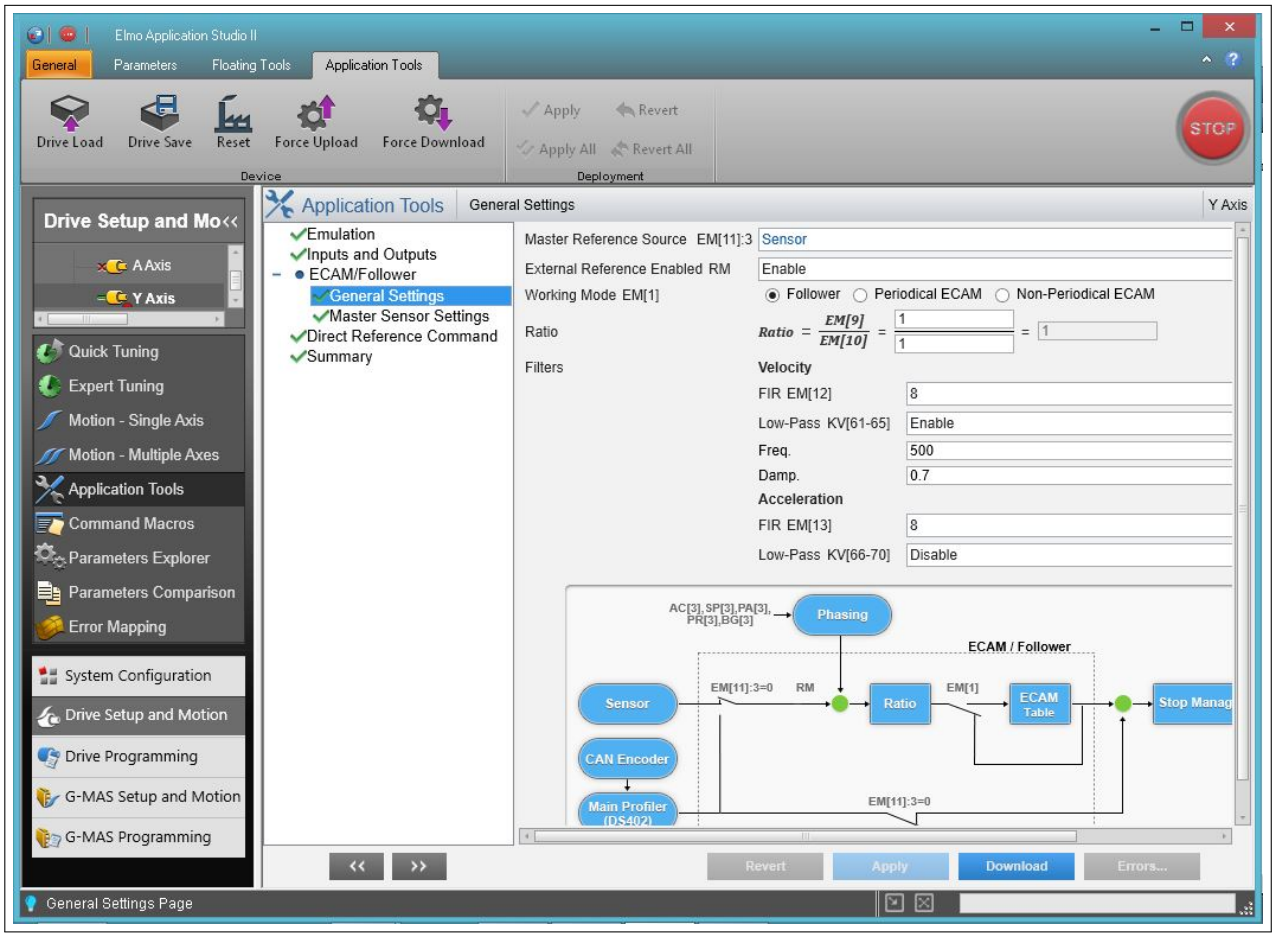

Figure A.43: EASII Setup 9: While not explicit programmed, the ECAM/Follower section plays a role in the Direct Reference Command through the EASII software which we will want in the next step. Allow for the above settings in order to continue.

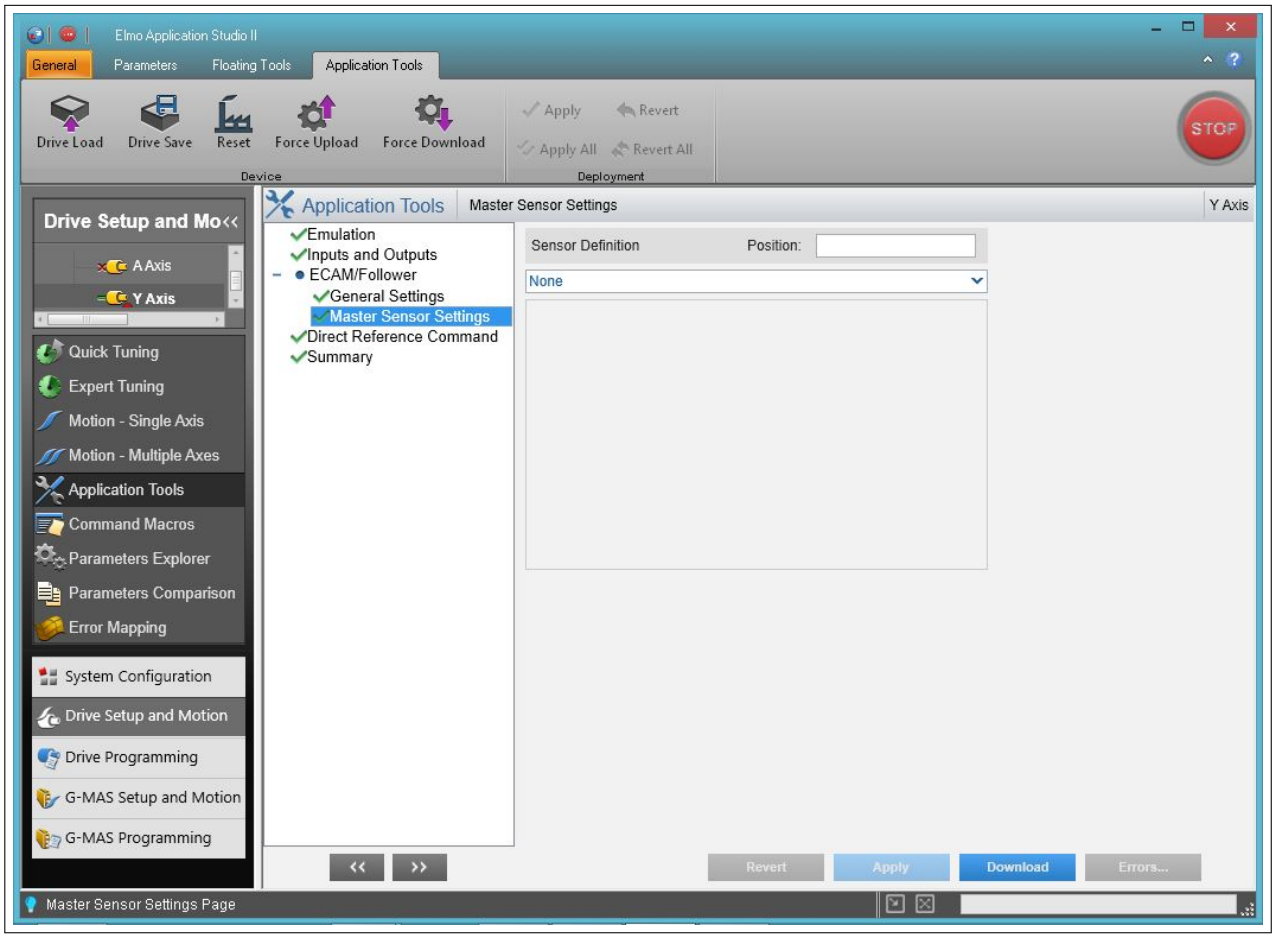

Figure A.44: EASII Setup 9 Cont.: While not explicit programmed, the ECAM/Follower section plays a role in the Direct Reference Command through the EASII software which we will want in the next step. Allow for the above settings in order to continue.

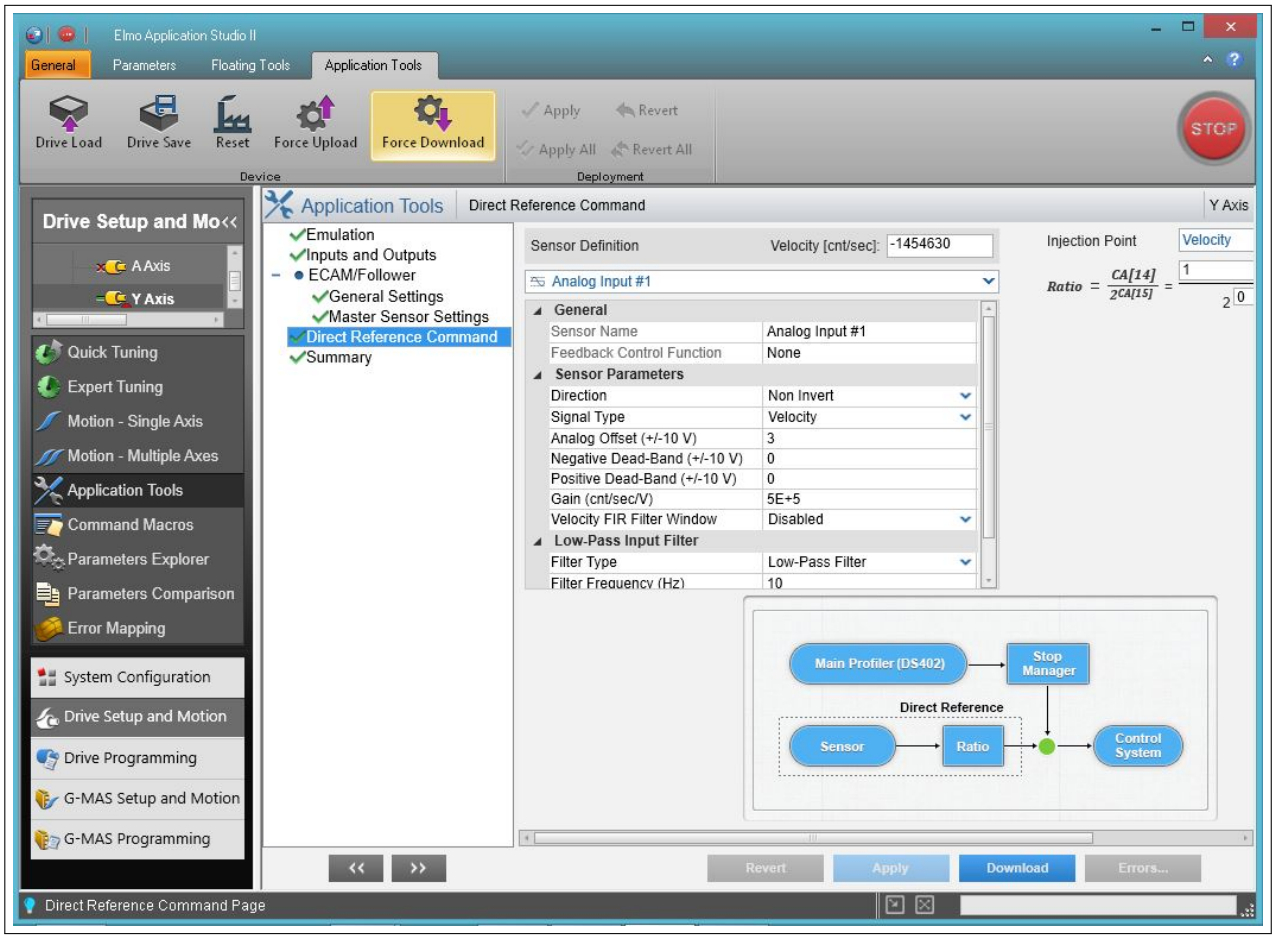

Figure A.45: EASII Setup 9 Cont.: The direct reference command is how the motor will be commanded in velocity mode as an analog voltage signal from the myRIO. Shown above the Analog Input #1 is selected as the source, and the settings below show the 3V offset and the gain per volt received in order to scale the incoming signal properly to velocity. Note the "Ratio" in the upper right hand corner, this is an additional gain on the commanded velocity, and for most cases should be equal to 1 as shown above. A low pass filter was not enabled for the experiments, but can be applied for better signal quality on this command input.

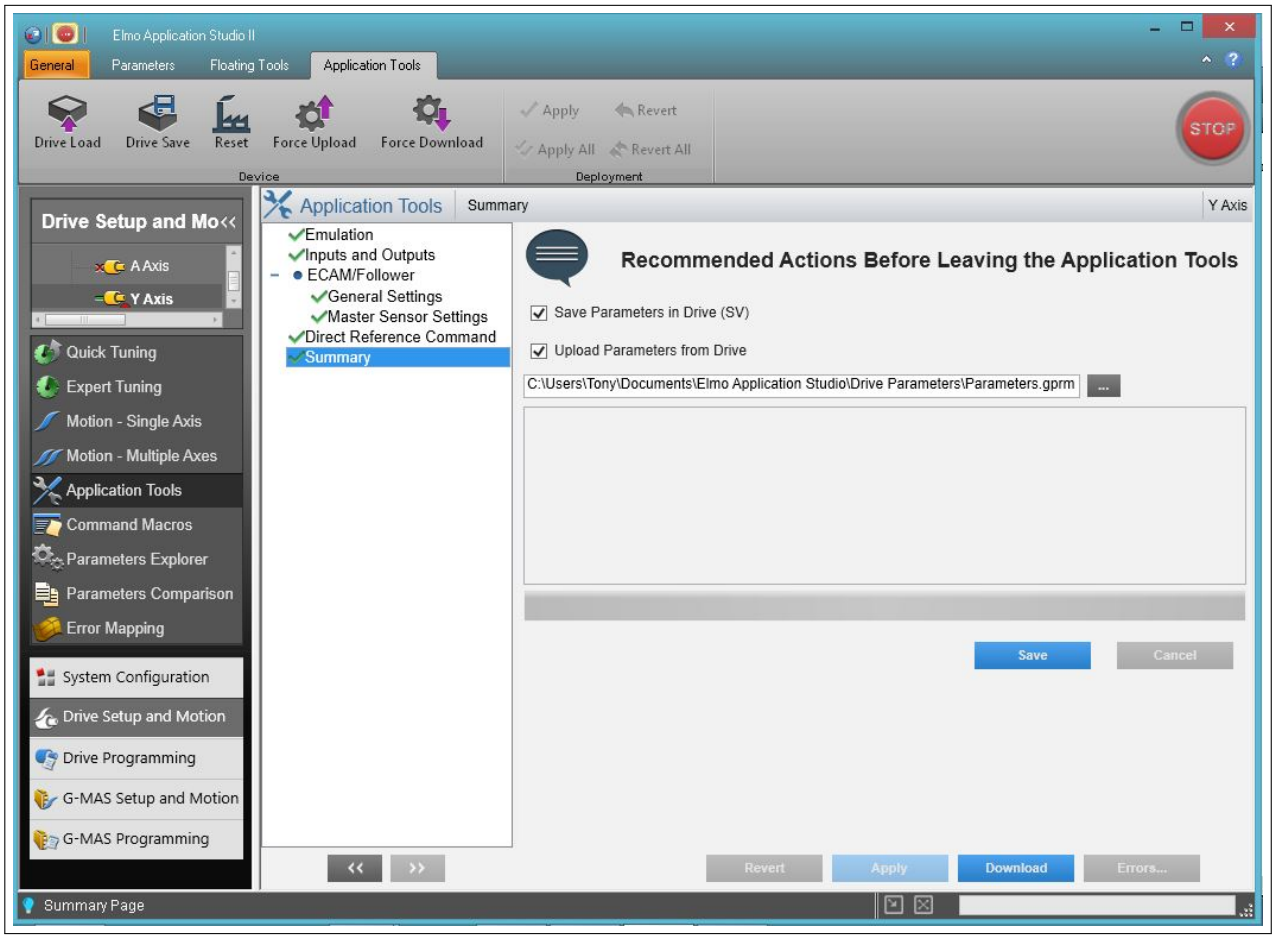

Figure A.46: EASII Setup 10: Before leaving this section, it is necessary to save the parameters of the setup to the drive. The "Summary" portion of this setup will save parameters and copy them to the drive for you. Continue only after this is complete. The drive will need to be restarted in order to begin receiving and executing commands from the voltage signal.

Appendix B

IMPEDANCE CONTROL STRUCTURE

B.1 Force Command Control

To alter the apparent impedance of our system dynamics, namely,

$$F_h(t) = M\dot{v}(t) + Bv(t), \tag{B.1}$$

where the applied human force input, F_h, acts on a system with mass, M, and damping, B, generating a velocity, $v(t)$, we add a motor force, F_m. This motor force, F_m, is added to the force input side of the equation as

$$F_h(t) + F_m(t) = M\dot{v}(t) + Bv(t), \tag{B.2}$$

and will facilitate an impedance change in (B.1). It follows that the motor force, F_m, should yield the change in system mass and damping

$$F_m(t) = \Delta M\dot{v}(t) + \Delta Bv(t), \tag{B.3}$$

and substituting it into (B.1),

$$F_h(t) + [\Delta Mv(t) + \Delta Bv(t)] = Mv(t) + Bv(t). \tag{B.4}$$

Rearranging (B.4), the preferred system dynamics can be described as having desired mass, M_d, and damping, B_d,

$$F_h(t) = M_d\dot{v}(t) + B_dv(t) \tag{B.5}$$

where

$$M_d = M - \Delta M \tag{B.6}$$

$$B_d = B - \Delta B. \tag{B.7}$$

Solving equation (B.5) for $\dot{v}(t)$ and substituting it into equation (B.3), we can define our motor force, F_m, as

$$F_m(t) = \left(\frac{\Delta M}{Md}\right) F_h(t) + \frac{\Delta B \cdot M_d - \Delta M \cdot B_d}{M_d} v(t). \tag{B.8}$$
$$F_m(t) = f\left(F_h(t), M, B, M_d, B_d, v(t)\right) = f\left(F_h(t), v(t)\right)$$

assuming we know the actual mass, M, and damping, B, as well as user set desired mass, M_d, and desired damping, B_d, the motor force, F_m, is now only a function of human force input, F_h, and system velocity, $v(t)$. Once the necessary force from the motor, F_m, is calculated, the motor drive proportional-integral (PI) control loop will regulate current to output the calculated force. Fig. B.1 expresses this control law.

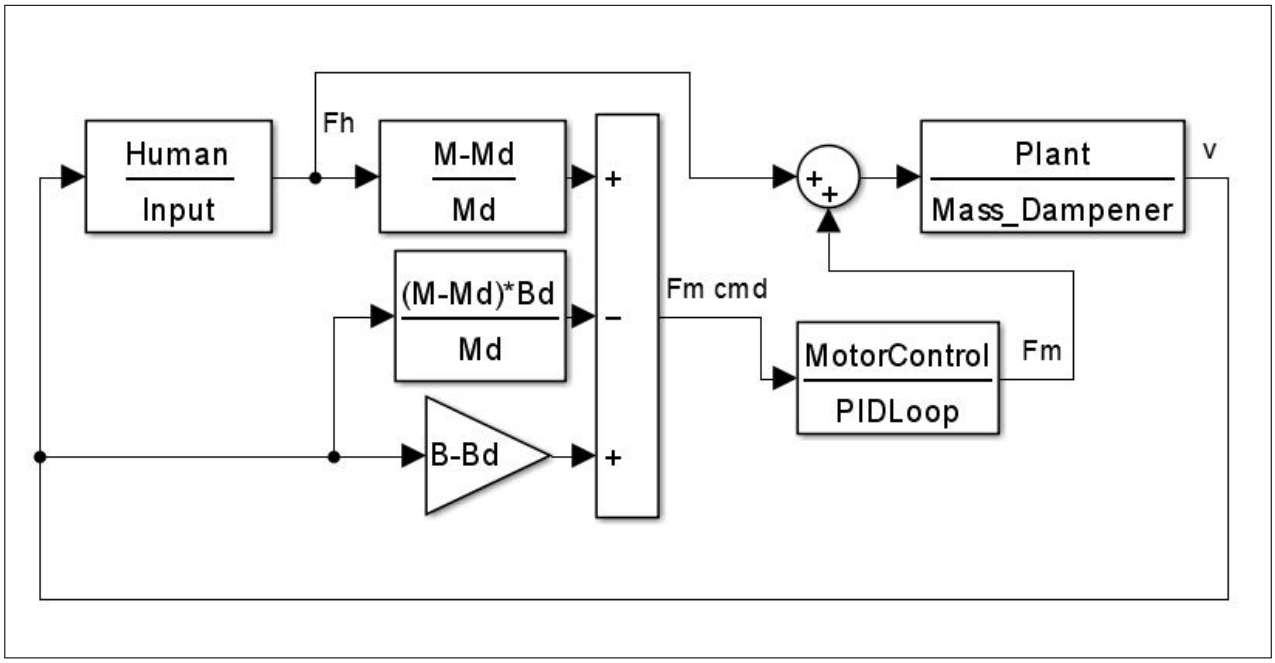

Figure B.1: Torque Commanded Impedance Control Loop. Block diagram expressing the force from the motor, F_m, with the definition of from (B.8).

B.2 Velocity Command Control

Recall, to modify the apparent impedance of a system, a motor force, F_m, must resist or assist the human force input, F_h. Previously, the motor force, F_m, was prescribed based on knowledge of the actual system dynamics. This can lead to errors due to an inaccurate system model and non-linearities. Alternatively, a velocity command can be generated from desired model dynamics and used in combination with the motor's PI loop in order to produce said desired dynamics on the real system. To do this, we need only to solve the desired dynamic system

$$F_h(t) = M_d\dot{v}(t) + B_d v(t) \tag{B.9}$$

for velocity, $v(t)$, and subsequently command it to the motor, as shown in Fig. B.2.

The benefit of velocity commanded control is that the actual mass, M, and damping, B, of the system do not appear explicitly in the calculated control, rather the actual system is governed by a motor-plant velocity loop controller. By avoiding system identification we circumvent troublesome issues by relying on the motor's controller to govern how much force the true system requires in order to produce the necessary velocity of the desired system.

Note that limitations of motor control over the actual system will only allow for certain range of desired mass, M_d, and damping, B_d, parameters; e.g. if the actual mass, M, is too large and desired mass, M_d, too small, the motor force, F_m, required to assist in accelerations may not fall within the motor's range.

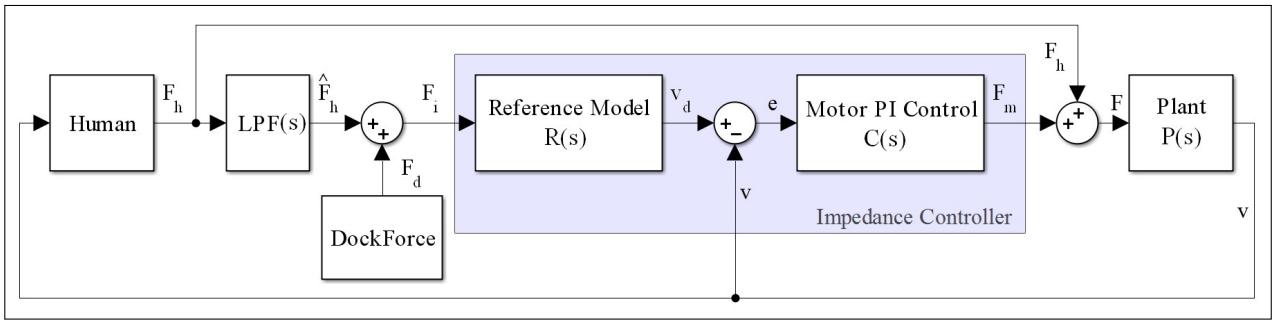

Figure B.2: Block diagram of impedance controller creating the desired plant dynamics from human force input, F_h, using a reference model with custom set mass, M_d, and damping, B_d, parameters. The human force input, F_h, is put through a low pass filter (LPF), the filtered human force input, $\hat{F}_h$, is then added to dock force, F_d, to yield force input, F_i, that drives the reference model. This model estimates ideal system dynamics and outputs desired velocity, v_d, commands to the motor controller. The motor's proportional-integral (PI) controller then works on the error, e, between desired velocity, v_d, and actual plant velocity, v, in order to produce motor force, F_m. By the design of the application the human force input, F_h, is also applied directly on the fixture/plant. This will be treated as a disturbance force attempting to disrupt the reference tracking of the motor's PI loop.

Appendix C

PARAMETER SELECTION EXPERIMENTATION

C.1 Free Space Manipulation Experiment

One goal for the controller is to accurately position a fixture. An experiment was conducted to test the user's ability to position the test bed mobile base to a goal approximately 0.1 m away from a start position with a variety of apparent system dynamics, or desired mass, M_d, and desired damping, B_d. A visual indicator shown in Fig. A.3 was used to display the mobile base location to the user and while the Y-Axis motor's encoder collected the position data. Fig. C.1 and C.2 show the start and end locations, respectively.

For each trial, a randomized assignment of mass and damping was used, and the operator would begin to test by commanding a velocity towards the goal with the intent on placing the indicator within the goal area, and completed via a mouse click when satisfied in positioning the mobile base. Once a trial was complete, to ensure consistent starting position and blind assignment of control parameters, the code automatically drove the test bed back to zero and assigned a new combination of desired mass, M_d, and desired damping, B_d, for the tester to evaluate.

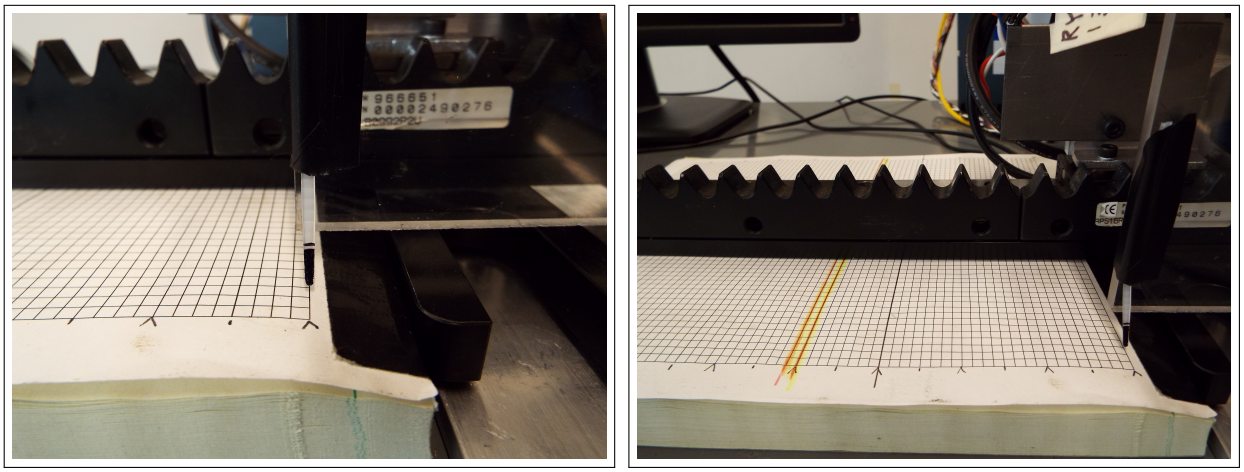

Figure C.1: Position Test Starting Location. Graph paper showing a 1/8" grid. Test evaluated the user moving the mobile base 4.0625" ($\approx$ 0.1m) from the starting location. *Left*: Position test start location zoomed in. *Right*: Position test start location zoomed out.

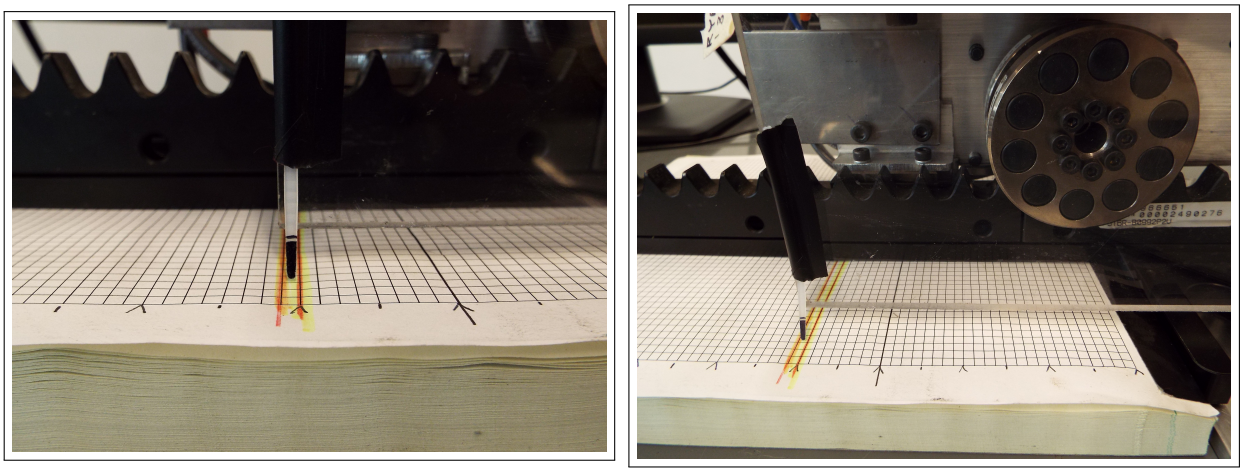

Figure C.2: Position Test End Location. Graph paper showing a 1/8" grid. Test evaluated the user moving the mobile base 4.0625" ($\approx$ 0.1m) from the starting location. *Left*: Position test end location zoomed in. *Right*: Position test end location zoomed out.

The investigation used 300 trials, 10 runs of 30 permutations of each the following desired mass, M_d, with each desired damping, B_d:

Desired Mass, M_d (kg)	Desired Damping, B_d $(N-s/m)$
10	30
30	65
50	100
75	150
100	200
	300

The trail's position vs time data was collected and used to determine performance factors of percent overshoot, the settling time, and the steady state error, defined as,

$$\%OS = \begin{cases} \left(\frac{x_{max}}{x_g} - 1\right) 100 & \text{if } x_{max} > x_g \\ 0 & \text{if } x_{max} \leq x_g \end{cases} \tag{C.1}$$

$$T_s = t_{\pm 2\%} - t_0 \tag{C.2}$$

$$e_{ss} = |x_{final} - x_g| \tag{C.3}$$

where $\%OS$ is percent overshoot, x_{max} is the maximum position reached away from the start position, x_g is the goal position (0.1 m), T_s is settle time, $t_{\pm 2\%}$ is the time it takes to reach and stay within $\pm 2\%$ of the goal, t_0 is the time when the fixture was first moved from the start position, e_{ss} is steady state error, x_{final} is the final position of the fixture when the trail is completed.

C.1.1 MATLAB Code - Free Space Manipulation Evaluation

To process the data, the file type for each trail was a tab delimited data text (*.txt) file. Fig. C.3 is an example of one of these data sets.

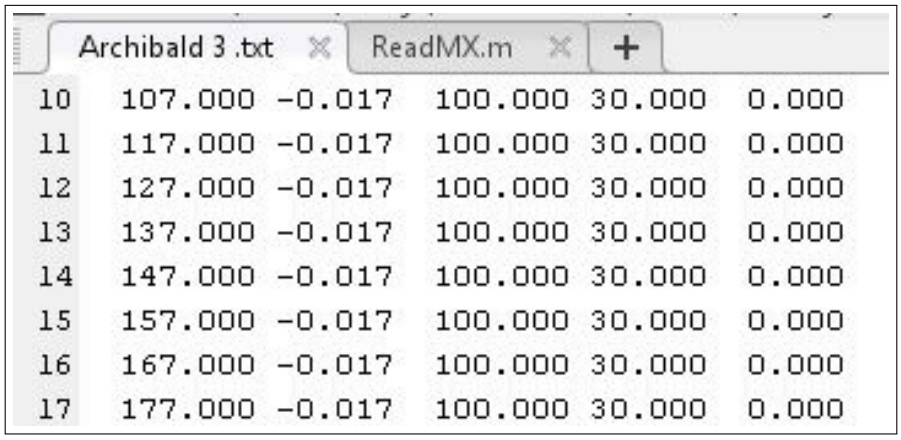

Figure C.3: Example data file for position test. Note the columns are from left to right as follows: Time (ms); Position (in); Desired Mass (kg); Desired Damping (N-s/m); Velocity (in/s).

The following code was used in order to process the trial data:

Table of Contents


```
% Read and Process Test Bench Data
% Tony Piaskowy
% 8-12-2015
% BARC Research Positioning Test Results Evaluation

clear all; clc; close all;
```

Import Data

Allow the user to select the folder with all the trail data in

```
FilterSpec = '*.txt';
current_path=cd;
[FileName,PathName,FilterIndex] = uigetfile(FilterSpec);
cd(PathName)

s = dir('*.txt');                   % s is structure array with field
 name
file_list = {s.name};               % convert the name field from the
 elements
                                    % of the structure array into a
 cell array
                                    % of strings.

file_list'                          % Display Folder Contents

for wi=1:length(file_list)          % Import every file and collect
 data

FileName=file_list{wi};             % Find the next file name
A=importdata(FileName);             % Import the data
disp(strcat('Imported: ',FileName));% Display the file being imported
T=A(:,1);                           % Time (ms)
P=A(:,2);                           % Position (in)
M=A(1,3);                           % Desired Mass (kg)
B=A(1,4);                           % Desired Damping (N-s/m)
V=A(:,5);                           % Velocity (in/s)
```

Resize and Set Goal

Settling Time Adjustment

```
ct=1;
for L=2:length(T)                    % Search for the last point that
 is outside of +/-2%
    if abs(P(L))<=0.02
        ct=ct+1;
    end
end

% Time adjustment (Zero the time when the user begins motion)
T=T(ct:end)-T(ct);
P=P(ct:end);
V=V(ct:end);
Target=(4+1/16);
Goal=(T-T)+Target;
MXIN=length(P);
```

Find %OS

```
MV=max(P);
if MV<=Target
    POS=0;
else
POS=(MV/Target-1)*100;
end
```

Find Settling Time

```
L=0;
for L=1:MXIN-1
    if abs(P(MXIN-L))>=Target*(1.02)
        ST=length(P)-L;
        break
    elseif abs(P(MXIN-L))<=Target*(0.98)
        ST=length(P)-L;
        break
    end
end
ST=(T(ST)-T(1))/1000;
```

Find Steady State Error

```
SSE=P(end)-Target;

% Plot Trial
% figure
% % subplot(211)
% plot(T,P,T,Goal,'r--')
% xlabel('Time (ms)')
```

```
% ylabel('Position (m)')
% % ylim([-1 5])
% title(strcat('Mass/Damp Accuracy:',FileName,'; M=',num2str(M),'_
 B=',num2str(B),'_ Goal=',num2str(Goal(end))))
%
% % subplot(212)
% % plot(T,V)
% % xlabel('Time (ms)')
% % ylabel('Velocity (m/s)')
```

Store Variables and Results

```
% Aquire Index
D = strsplit(FileName,'.');
C = strsplit(D{1},' ');
TrialIndex=str2num(C{2});

% % Write Data
AkData(wi,:)=[TrialIndex,M(1),B(1),POS,ST,SSE];
% TData(TrialIndex,:)=T;
% PData(TrialIndex,:)=P;
% VData(TrialIndex,:)=V;
% GData(TrialIndex,:)=Goal;

end

SData=sortrows(abs(AkData),[2,3]);

% Averaging Data
ct=1;
rdg=1;
Tot(ct,:)=SData(1,2:6);
Chng=0;
ChngI=1;
for MT=2:size(SData,1);
    if SData(MT-1,2)==SData(MT,2)              %if M1 = M2
        if SData(MT-1,3)==SData(MT,3)          %if B1 = B2
            Tot(ct,:)=Tot(ct,:)+SData(MT,2:6); %Add All Metrics
            rdg=rdg+1;                         %Increase Total by 1
            if MT==size(SData,1);              %Check If Last Entry
                Tot(ct,:)=Tot(ct,:)./rdg;      %Divide Total by # of
 entries
            end
        else                                   %If B1~= B2
            Tot(ct,:)=Tot(ct,:)./rdg;          %Divide Total by # of
 entries
            rdg=1;                             %Set total summed to 1
            ct=ct+1;                           %Index to a new
 permutation row
            if MT~=size(SData,1);              %Check If Last Entry
                Tot(ct,:)=SData(MT,2:6);       %Start Next Mass Row
 summation
            end
```

```
        end
    else                                        %if M1~=M2
        Tot(ct,:)=Tot(ct,:)./rdg;               %Divide Total
        rdg=1;                                  %Set total summed to 1
        Chng(ChngI)=ct;                         %Save the row when
 mass changes
        ct=ct+1;                                %Index Row
        ChngI=ChngI+1;                          %Index Change Matrix
 for next change
        if MT~=size(SData,1);                   %Check If Last Entry
            Tot(ct,:)=SData(MT,2:6);            %Set Next Row as
 starting total
        end

    end
end


%Storing The Averages into Mass vs Dampening Plots
Chng=[0 Chng length(Tot)];
for GH=1:(length(Chng)-1)
    POSZ(:,GH)=Tot(Chng(GH)+1:Chng(GH+1),3);
     STZ(:,GH)=Tot(Chng(GH)+1:Chng(GH+1),4)';
    SSEZ(:,GH)=Tot(Chng(GH)+1:Chng(GH+1),5)';
end
Chng=Chng(1:(length(Chng)-1))+1;

%Storing Our Tested Parameters
XC=Tot(Chng,1)';
YC=Tot(1:Chng(2)-1,2);

% %Save Finished Data to SpreadSheet
% CurrentDIR=cd;
% cd('C:\Users\Tony\Documents\BARC\Buddy Robot
\TestBenchMandBAccuracyTest\Results');
% datatype={'POS' 'ST' 'SSE'};
% dataFinal=[POSZ;STZ;SSEZ];
% HD=size(POSZ,1);
% for dstore=1:3
%     F=(dstore-1)*HD+1;
%     L=(dstore)*HD;
%     xlswrite(strcat(C{1},'Results',datatype{dstore}),[[0 XC];[YC
 dataFinal(F:L,:)] ])
% end
% cd(CurrentDIR);

DateNTime=datetime('now','Format','MM_dd_yyyy''_T_''HH_mm_ss');
DNTStr=datestr(DateNTime,'mm_dd_yyyy_T_HH_MM_SS');
```

2D Plot of Results

```
figure('position', [0, 0, 2000, 450])
```

```
subplot(131)
contourf(XC,YC,POSZ);colormap(gray);colorbar;
title('Overshoot (%) Average')
xlabel('Desired Mass, M_d (kg)');ylabel('Desired Damping(N-s/m)')

% figure
subplot(132)
contourf(XC,YC,STZ);colormap(gray);colorbar;
title('Settling Time (s) Average')
xlabel('Desired Mass, M_d (kg)');ylabel('Desired Damping(N-s/m)')

%%Metric Results
% figure
subplot(133)
contourf(XC,YC,SSEZ.*0.0254);colormap(gray);colorbar;
title('|Steady State Error| (m) Average')
xlabel('Desired Mass, M_d (kg)');ylabel('Desired Damping(N-s/m)')

% % Preference
% hold on
% plot(30,150,'wo')
% subplot(312);hold on; plot(30,150,'wo')
% subplot(311);hold on; plot(30,150,'wo')

% %Save Plots
% CurrentDIR=cd;
% cd('C:\Users\Tony\Documents\BARC\Buddy Robot
\TestBenchMandBAccuracyTest\Results');
% hgexport(gcf, strcat(C{1},'AllPlots',num2str(wi),'_',DNTStr),
 hgexport('factorystyle'), 'Format', 'tiff')
% cd(CurrentDIR);
```

SURF - 3D plot, Color Map

figure surf(XC,YC,POSZ);colormap(jet);colorbar; title('Overshoot (%) Average') xlabel('Mass(kg)');ylabel('Dampening(N/m/s)')

figure surf(XC,YC,STZ);colormap(jet);colorbar; title('%Settling Time (s) Average') xlabel('Mass(kg)');ylabel('Dampening(N/m/s)')

figure surf(XC,YC,SSEZ);colormap(jet);colorbar; title('Steady State Error (in) Average') xlabel('Mass(kg)');ylabel('Dampening(N/m/s)')

Calculate and Plot Ratio Data

```
% TimeConstants
TCs = XC'*diag(inv(diag(YC)))';
TCs = reshape(TCs,[30,1]);              % Turn Matrix into one column
 to plot
POSZ = reshape(POSZ,[30,1]);            % Turn Matrix into one column
 to plot
STZ = reshape(STZ,[30,1]);              % Turn Matrix into one column
 to plot
```

```
SSEZ =  reshape(SSEZ,[30,1]);           % Turn Matrix into one column
 to plot

figure
subplot(131)
semilogx(TCs,POSZ,'bo');xlabel('\tau = M_d/B_d (s)');ylabel('Percent
 Overshoot [%]');grid on
subplot(132)
semilogx(TCs,STZ,'ro');xlabel('\tau = M_d/B_d (s)');ylabel('Settling
 Time [s]');grid on
title('Time Constant, \tau, vs. Performance')
subplot(133)
semilogx(TCs,SSEZ.*0.0254,'go');xlabel('\tau = M_d/B_d
 (s)');ylabel('Steady-State Error [m]');grid on
```

Published with MATLAB® R2015b

C.1.2 Results - Free Space Manipulation Evaluation

Fig. C.4 shows the results of percent overshoot, settling time, and steady state error in free space manipulation. These results varied from data set to data set, but the idea of a preferred mass and damping for manipulation was becoming clear. Further testing would be required to generate enough data to yield "best fit" for free space manipulation using this type of impedance control. Fig. C.5 attempted to capture any trends in performance based on the time constant, $\tau = M_d/B_d$, of the trial. These results were seemingly inconclusive, yet more testing is desired in order to rule out the intuition that with a smaller time constant our deice should come to a halt faster and therefore for small adjustments, quick application and removal of human input, should yield more dexterous manipulation performance.

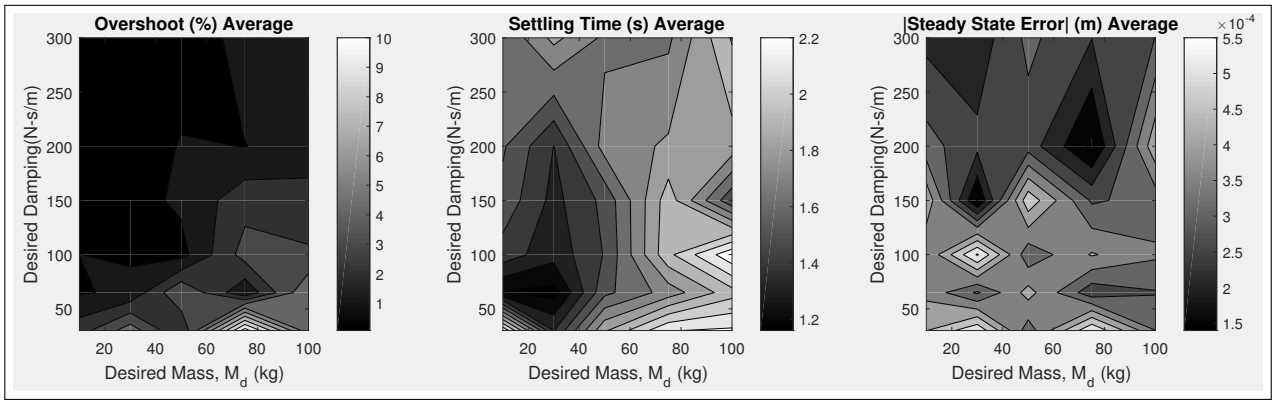

Figure C.4: Example of the results from a user after 300 trials of various desired masses and damping parameters in free space manipulation to a goal position $\approx$ 0.1m away from the starting location. Showing the percent overshoot, settling time, and steady state error of the user's positioning control over the mobile base versus Desired Mass, M_d, and Desired Damping, B_d, using this impedance control.

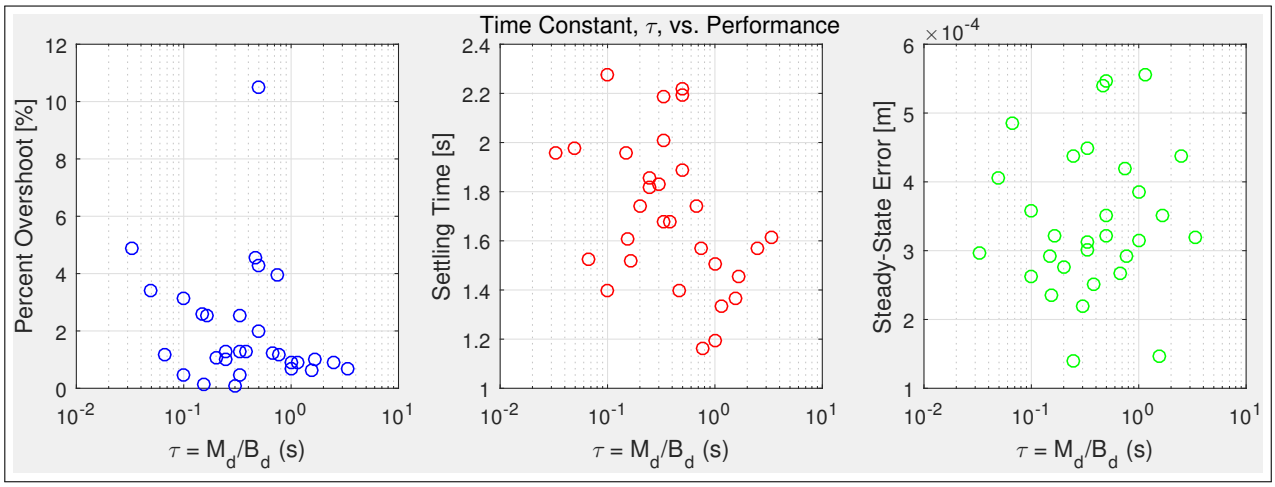

Figure C.5: Example of the results from a user after 300 trials of various desired masses and damping parameters in free space manipulation to a goal position $\approx$ 0.1m away from the starting location. Showing time constant, τ, versus manipulation performance.

C.2 Dock Experiment - Variable Damping

The proposed controller must also be able to prevent contact instabilities, which arise from contact force inputs into our system. The solution attempted was to increase the damping of the system in order to mitigate the input effects of the contact generated forces and stably dock the fixture with the structure. This contact instability, or bouncing effect, is illustrated with Fig. C.6 below.

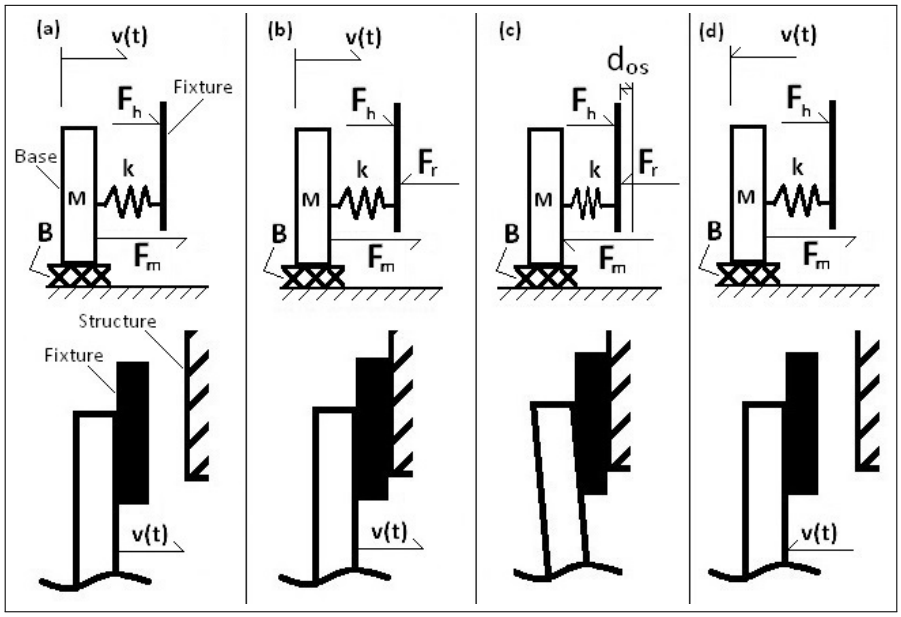

Figure C.6: Diagram of dock rebound due to the reaction force from the structure once the fixture makes contact. Assuming the fixture is a massless device, with a constant human operator force, F_h, applied to it, no dock force, $F_d = 0$, and is attached to a base by some stiffness, k. The fixture's base has mass, M, damping, B, and motor force, $F_m(t)$, applied to it. **(a)** Before contact: the fixture of mass, M, is traveling at steady state velocity $v(t) = \hat{F}_h/B_d$. **(b)** Contact: The fixture makes contact with structure, deflecting the fixture, and generating a reaction force, F_r, canceling human force input, F_h, and commanding an opposing acceleration from the reference model causing the motor to decelerate the fixture mass, M. **(c)** Docked: The mass, M, is at zero velocity and the fixture is in contact with the structure, however energy may have been stored in the fixture stiffness, k, due to the mobile base overshooting the fixture-structure contact position by some distance, d_{os}, resulting in a residual force, F_r. **(d)** Rebound: when in fixture-structure contact the reaction force, F_r, will be greater than or equal to human force input, F_h, and commands a velocity away from the structure. Once separated from the structure, the reaction force, F_r, becomes zero and the human force input, F_h, once again commands the base towards the structure.

The variable damping takes place in the near-regime, seen in Fig. C.7, when the fixture-structure proximity is small enough where contact is possible, and the new applied damping will take the shape of the modified logistic function, shown below,

$$B_m(\tilde{x}) = \begin{cases} B_d, & \tilde{x} \geq x_n \\ \left(\dfrac{2\left[(B_m)_{max} - B_d\right]}{1 + e^{[\tilde{x} - x_{ns}]/r_B}} \right) + B_d, & x_{ns} \leq \tilde{x} < x_n \\ (B_m)_{max}, & \tilde{x} < x_{ns}. \end{cases} \tag{C.4}$$

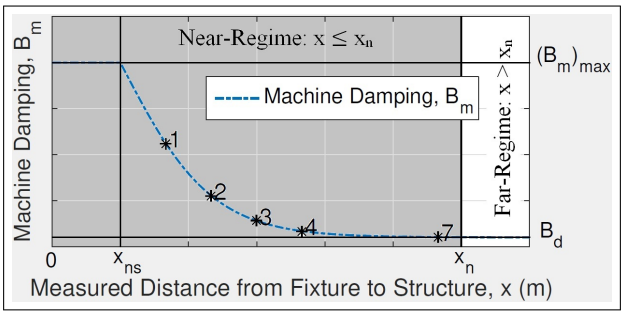

Figure C.7: Operating regimes defined as a function of distance from structure, x. At or below x_n, the optical sensors become reliable and fixture-structure proximity, $\tilde{x}(t)$, acts on system damping. This defines the near-regime. Within the near-regime, a saturation damping occurs when the measured distance $\tilde{x}(t)$ is below x_{ns}. Overlaid is an illustration of the machine damping, B_m. Highlighted design parameters: $(B_m)_{max}$, the maximum damping set, B_d, the desired damping set by operator, $x_n = 0.030m$, the maximum distance of near-regime, and $x_{ns} = 0.005m$, the damping saturation distance set to include potential fasteners. Not explicitly shown, but used in demonstrating the shape is the machine damping distance constant, $r_B = 0.0033m$. Points, $*^n$, where $(\tilde{x} - x_{ns}) = nr_B$, n-multiples of the distance constant, r_B, demonstrate the exponential transition between maximum machine damping, $(B_m)_{max}$, and desired damping, B_d. When the fixture is n distance constants, r_B, away from the saturation point, x_{ns}, the transition completion is: 46.2%, 76.2%, 90.5%, 96.4%, and 99.8% at $n = 1, 2, 3, 4,$ & 7, respectively.

This function of machine damping, B_m, can be adjusted in order to generate the desired dock behavior. An experiment was conducted varying the maximum machine damping, $(B_m)_{max}$, and recording the ability to mitigate contact instabilities with a constant force applied towards the structure. Fig. A.2 shows the fixture and structure.

The test began with the mobile base and structure at 0.035m apart, further than the near-regime (0.030m width), in order to capture the full transition of damping. The force sensor supporting the fixture was then given a 5N force bias towards the structure generating a velocity - this simulated a constant force applied to the fixture. As the fixture approached the structure, the fixture's optical sensors fed back proximity distance information and altered the damping as this gap was closed.

In total four maximum machine damping, $(B_m)_{max}$, were tested and the docking behavior, position versus time, was recorded. A constant desired mass, M_d, of 30 kg and desired damping, B_d, of 150 $N - s/m$ was used with the maximum machine damping, $(B_m)_{max}$, of:

Trial	$(B_m)_{max}$
1	150
2	300
3	600
4	1200

Fig. C.8 shows the results of the trials, illustrating the behavior of contact between the fixture-base assembly and the structure with varying maximum machine damping, $(B_m)_{max}$. The coupled system dynamics depend on the stiffness and damping of each the fixture-base assembly and structure. Further research into how to select the maximum machine damping, $(B_m)_{max}$, can be done in order to allow for the best contact relationship and manipulation of the fixture.

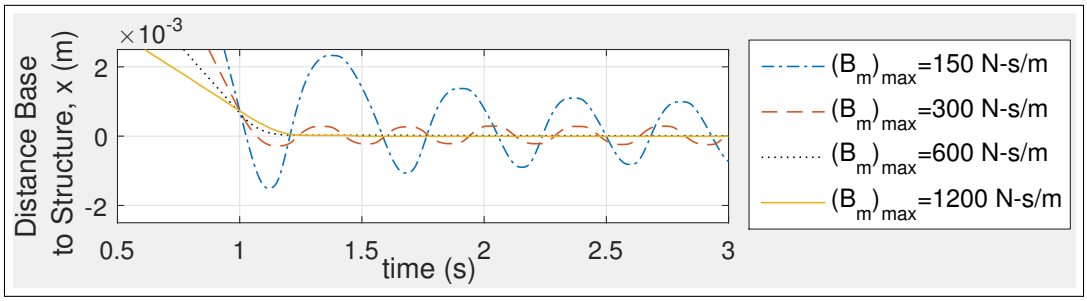

Figure C.8: Dock attempts with a constant user input force, $F_h = -5\ N$, desired mass, $M_d = 30\ kg$, desired damping, $B_d = 150$ N-s/m, machine damping distance constant, $r_B = 0.0036m$, and varying maximum machine damping, $(B_m)_{max}$. Note: Times have been altered to collocate the point of contact.

VITA

Walter Tony Piaskowy is a graduate research assistant at the University of Washington (UW) and produced this work at the Boeing Advanced Research Center (BARC) on campus. This work has been in partial fulfillment of a Master's of Science in Mechanical Engineering (MSME), after which he plans to continue the research as a PhD student at UW starting Spring 2016.

Tony is originally from Lemont, Illinois, a suburb just outside of Chicago, and previously attended the University of Illinois Champaign-Urbana where he completed a Bachelors degree in Engineering Mechanics (formerly Theoretical and Applied Mechanics), specializing in Fluid Mechanics.

He welcomes your comments to `apiasko2@uw.edu`.